STRUCTURAL VIBRATION ANALYSIS OF SINGLE WALLED CARBON NANOTUBES WITH ATOM-VACANCIES

A THESIS SUBMITTED TO
THE GRADUATE SCHOOL OF NATURAL AND APPLIED SCIENCES
OF
MIDDLE EAST TECHNICAL UNIVERSITY

BY

İBRAHİM ONUR DOĞAN

IN PARTIAL FULLFILLMENT OF THE REQUIREMENTS
FOR
THE DEGREE OF MASTER OF SCIENCE
IN
MECHANICAL ENGINEERING

FEBRUARY 2010

Approval of the thesis:

STRUCTURAL VIBRATION ANALYSIS OF SINGLE WALLED CARBON NANOTUBES WITH ATOM -VACANCIES

submitted by **İBRAHİM ONUR DOĞAN** in partial fulfillment of the requirements for the degree of **Master of Science in Mechanical Engineering Department, Middle East Technical University** by,

Prof. Dr. Canan Özgen _____
Dean, Graduate School of **Natural and Applied Sciences**

Prof. Dr. Suha Oral _____
Head of Department, **Mechanical Engineering Dept., METU**

Asst. Prof. Dr. Yiğit Yazıcıoğlu _____
Supervisor, **Mechanical Engineering Dept., METU**

Assoc. Prof. Dr. Kahraman Güçlü Köprülü _____
Co-Supervisor, **Electrical and Electronics Eng. Dept., TOBB ETU**

Examining Committee Members:

Asst. Prof. Dr Cüneyt Sert _____
Mechanical Engineering Dept., METU

Asst. Prof. Dr. Yiğit Yazıcıoğlu _____
Mechanical Engineering Dept., METU

Assoc. Prof. Dr. Kahraman Güçlü Köprülü _____
Electrical and Electronics Eng. Dept., TOBB ETU

Asst. Prof. Dr. Ender Ciğeroğlu _____
Mechanical Engineering Dept., METU

Prof. Dr. Şakir Erkoç _____
Physics Dept., METU

Date: 02/02/2010

I hereby declare that all information in this document has been obtained and presented in accordance with academic rules and ethical conduct. I also declare that, as required by these rules and conduct, I have fully cited and referenced all material and results that are not original to this work.

Name, Last Name : İbrahim Onur DOĞAN

Signature :

ABSTRACT

STRUCTURAL VIBRATION ANALYSIS OF SINGLE WALLED CARBON NANOTUBES WITH ATOM-VACANCIES

Doğan, İbrahim Onur
M.Sc., Department of Mechanical Engineering
Supervisor : Asst. Prof. Dr. Yiğit Yazıcıoğlu
Co-Supervisor : Assoc. Prof. Dr. Güçlü Köprülü

February 2010,131 pages

Recent investigations in nanotechnology show that carbon nanotubes (CNT) have one of the most significant mechanical, electrical and optical properties. Interactions between those areas like electrical, optical and mechanical properties are also very promising in both research and industrial fields. Those unique characteristics are built by mainly the atomistic structure of the carbon nanotubes.

In this thesis, the effects of vacant atoms on single walled carbon nanotubes (SWCNT) are investigated using matrix stiffness method. In order to use this technique a linkage between structural mechanics and molecular mechanics is established. A code has been developed to construct the SWCNT with the desired chirality, extracting the vacant atoms with the corresponding atomic bonds between the neighbor nodes and calculating the effect of those vacancies on its vibrational properties. A finite element software is also utilized for validation of the code and results.

In order to investigate the convergence of the effect of those vacant nodes a numerous number of analyses have been carried out with randomly positioned vacant atoms. Also consecutive vacant nodes have been positioned in order to investigate the effect on the structural properties through the length of a CNT.

In addition to those, as a case study, the reduction in Young's modulus property because of the vacancies has also been investigated and the effects are tabulated in the report.

It is concluded in this study that the any amount of vacant atoms have substantial effect on modal frequencies and Young's modulus. Chirality and the position of the vacancies are the main parameters determining the structural properties of a CNT.

Keywords: Matrix stiffness method, CNT, Atom-Vacancy, Vibration, Modulus of Elasticity

ÖZ

ATOM BOŞLUKLU TEK DUVARLI KARBON NANOTÜPLERİN YAPISAL TİTREŞİM ANALİZİ

Doğan, İbrahim Onur
Yüksek Lisans, Makine Mühendisliği Bölümü
Tez Yöneticisi : Y. Doç. Dr. Yiğit Yazıcıoğlu
Ortak Tez Yöneticisi : Doç. Dr. Güçlü Köprülü

Şubat 2010, 131 Sayfa

Nano teknoloji alanında yapılan son araştırmalar karbon nanotüplerin çok önemli mekanik, elektriksel ve optik özellikler taşıdığını göstermektedir. Elektrik, optik ve mekanik alanlar arasındaki etkileşimler de araştırma ve endüstriyel alanlarda gelecek vaat etmektedir. Bütün bu benzersiz özellikler başlıca karbon nanotüplerin atomistik yapısı sebebiyle oluşmaktadır.

Bu tezde atom boşluklarının tek duvarlı karbon nanotüplere etkisi direngenlik matrisi metodu kullanılarak incelenmiştir. Bu metodu kullanmak için yapısal ve moleküler mekanik arasında bağlantı kurulmuştur. Geliştirilen kod sayesinde istenen kiralitede oluşturulabilen tek duvarlı karbon nanotüp içinden atom ve ilgili yan atomlarla kurulan bağlar çıkarılmış ve bu boşlukların titreşimsel özelliklere etkisi hesaplanmıştır. Bir sonlu elemanlar analizi programı kullanılarak kodun ve sonuçların doğrulaması yapılmıştır.

Eksik atomların etkisinin yakınsamasını incelemek için rastgele pozisyonlandırılan atomlarla çok sayıda analiz yapılmıştır. Ayrıca peş peşe yerleştirilen atom boşlukları kullanılarak bu etkinin bir karbon nanotüp boyunca etkisi araştırılmıştır.

Bunlara ilaveten bir yan çalışma olarak, atom boşluklarının elastik modüle etkisi araştırılmıştır.

Bu tezde herhangi miktarda atom boşluklarının titreşim modu frekanslarına ve elastik modülüne önemli etkisi olduğu saptanmıştır. Kiralite ve atom boşluklarının pozisyonu karbon nanotüplerin yapısal özelliklerini etkileyen başlıca parametreler olduğu belirlenmiştir.

Anahtar Kelimeler: Direngenlik Matrisi Metodu, Karbon Nanotüp, Atom boşlukları, Titreşim, Elastik Modül

To My Fiancée

ACKNOWLEDGMENTS

I would like to express my sincere appreciation to my supervisor, Dr. Yiğit YAZICIOĞLU for his boundless help, excellent supervision and leading guidance from beginning to end of thesis work.

I would also like to express my sincere gratitude to my co-supervisor, Dr. Güçlü KÖPRÜLÜ, for his invaluable guidance throughout this study.

I would like to express my special thanks to Kaan DOĞAN, Murat HALİSÇELİK and Ahmet Levent AVŞAR for their discussions throughout this work.

I would like to thank my fiancée and family for their endless love and support throughout my life.

My special thanks go to my colleagues and friends Kamil M. Çakar, Cem Gözükara, Güvenç Canbaloğlu, Kaan Özsoy, Berkan Büyükdağlıoğlu, Gökhan Cüylan, Devrim Anıl and Koray Atılgan for their support and encouragement.

Also I would like to thank to ASELSAN for giving me the opportunity to use the computational capabilities.

I would like to thank also to TÜBİTAK for giving me the financial support throughout this work.

TABLE OF CONTENTS

LIST OF TABLES

TABLES

LIST OF FIGURES

FIGURES

LIST OF SYMBOLS

f : Generalized Forcing Vector

i : Unit Imaginary Number

$[K]$: Stiffness Matrix

$[k^e]$: Elemental Stiffness Matrix in Local Coordinate System

$[K^e]$: Elemental Stiffness Matrix in Local Global System

$[M]$: Mass matrix

$\left[m^e\right]$: Elemental Mass Matrix in Local System

$\left[M^e\right]$: Elemental Mass Matrix in Global System

$[H]$: Structural Damping Matrix

x : Generalized Displacement Vector

ω : Frequency

u : Displacement Vector

a_{c-c} : Carbon to Carbon Distance

C_h : Chirality Vector

n : Chirality Vector Parameter

m : Chirality Vector Parameter

D : Diameter of CNT

q : Displacements

A : Cross-sectional Area of the Bonds/Frames

E : Young's Modulus

L : Length of Bonds/Frames

G : Shear Modulus of Elasticity

J : Polar Moment of Inertia

I : Area Moment of Inertia

ρ : Density of the Frame Element

λ : Transformation Matrix

k_r : Bond Stretching Force Field Constant

k_θ : Bond Bending Force Field Constant

k_τ : Bond Torsional Resistance Constant

U_r : Bond Stretching Energy

U_θ : Bond Bending Energy

U_τ : Bond Torsional Energy

U_A : Strain Energy under Axial Tension

U_M : Strain Energy under Bending Moment

U_T : Strain Energy under Pure Torsion

CHAPTER 1

INTRODUCTION

1.1 Introduction

Ever since Iijima [1] reported the new kind of long and slender types of fullerene, carbon nanotubes opened promising research opportunities. Regarding their potentially unique mechanical opportunities and availability to be produced in variety, nanoscience began to investigate deeply that new coming material. In this work Iijima [1] presented the preparation of needle-like tubes using an arc-discharge evaporation method. First discovery was made by producing multi-walled carbon nanotubes in which the number of coaxial sheets of graphite may vary from 2 to 50. Iijima reported that at any SWCNT or any layer of a MWCNT the carbon atoms are positioned in hexagonal pattern.

Following, Iijima and Ichihashi [2] presented that while a variety length and diameter of MWCNT are produced in arc-discharge method, another unique form, SWCNT is existing in the gas phase.

An additional method laser ablation was developed by Guo and Nikolaev [3] which uses a pulsed laser that vaporizes a graphite target in a high temperature reactor filled with inert gas. The method was valuable since addition of cobalt and nickel leads a production of majorly SWCNT with controllable diameter which can be done by tuning the temperature of the reactor.

Latest but the still developing production mechanism is named as Chemical Vapor Deposition (CVD) which was utilized in the production of CNT by Yacaman and Yoshida et.al. [4]. In this method a process gas like ammonia or nitrogen and a carbon containing gas like methane or ethanol are bled into a chamber where a metal catalyst substrate is heated up to 700°C. Nanotubes are grown on the edges of metal catalyst. Size of the CNT can be controlled by etching the metal substrate or using plasma laser by aligning the nanotubes.

Since the discovery of carbon nanotubes, much attention has been given to the investigation of their exceptional physical properties. From [5-8]; mechanical attributes of nanotubes can be tabulated as in Table 1.1;

Table 1.1 Mechanical Properties of CNT

Material	Young's Modulus [TPa]	Tensile Strength[GPa]
Armchair SWNT	0,94	126
Zigzag SWNT	0,92	94
MWNT	0,8-0,9	150
Stainless Steel	0,2	0.65-3
Kevlar	0,15	3,5

In addition to those, hardness of the new material seemed to be noteworthy. Popov [9] reported his experimental data on producing a super hard phase of single wall carbon nanotubes by applying shear deformation in a high pressure chamber. Using nano indentation technique he showed that the new hard phase of SWCNT exhibits higher bulk modulus of 462-546 GPa than diamond which is around 420 GPa. Also the hardness is found to be up to 152 GPa which attributes the SWNT to the class of super hard materials.

Many studies have been conducted regarding the electrical properties of carbon nanotubes. Hong and Myung [10] reported that the metallic carbon nanotubes can

carry an electrical current density of 4x10^9 A/cm^2 which is about 1000 times greater than copper.

Another considerable topic is the investigation of thermal properties of CNT. Pop and Mann [11] reported that the conductivity of a SWCNT of length 2.6μm and diameter 1.7nm, is around 3500W/ (m K) at room temperature. The experiment has been carried out by producing an individual SWCNT in bridged configuration between two platinum supports. Fortunately the experiment exhibits a surprising result that CNT have the highest conductivity around room temperature (300K) and then decreasing exponentially down to 1000 W/(m K) around 800K which allows that kind of conductor to be used in even commercial products. In another study Kim and Shi [12] reported their experiment which indicates that the thermal conductivity of Multi walled carbon nanotubes is around 3000 W/(m K) and again having peak around 320 K.

In addition to these, CNT have significant optical properties. Hence many studies have been carried out. Yang and Ci [13] reported that an array of SWCNT is acting as an ideal black material which absorbs light perfectly at all angles and over all wavelengths. That makes the CNT a perfect candidate as using as a blackbody which should ideally have an absorbance or emissivity of 1.0. Authors indicated that the "forests" of SWCNT can have an absorbance of 0.98-0.99 covering from far-ultraviolet (200nm) to far-infrared (200μm) wavelengths. The reasoning why these nanotubes are much-like a black body is explained as the different types of chirality covers full spectrum of wavelength and light might be trapped in the array of CNT due to multiple reflections.

Interactions between these three fields; mechanical, electrical and optical have been reported. These nanomaterials are being widely used and started to be commercial as sensors. Hierold [14] reported his experiments utilizing a SWCNT in as a force sensor. Growing the SWCNT in a bridged configuration on gold supports, he was

able to plot the resistance versus deformation graph of the CNT and showed that since very large length over diameter aspect ratio can be obtained, nanotubes are good choice to build high resolution displacement sensors.

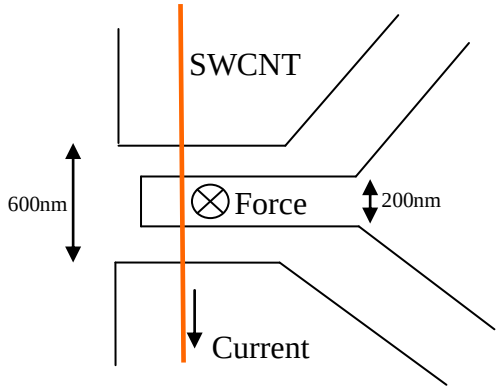

Figure 1.1 Schematic for Usage of CNT as a Force Sensor [14]

Baughman [15] reported that he generated artificial muscles that are assembled from large planes of individual carbon nanotubes like as in natural muscles. Under low operational voltage, the planes of CNT exhibit large strains which make it more efficient against conventional ferro-electric actuators.

As another example, Kim and Lieber [16] studied on the nanoscale electromechanical systems which they call nanotweezers based on carbon nanotubes. They managed to attach two electrically conductive and mechanically robust CNT to independent electrodes of glass micropipettes. Applying voltage, they observed that the free ends of CNT are closed and opened. They utilize this capability of CNT to grab or manipulate nanoscale materials and nanowires.

At a later study in Berkeley, Fennimore [17] developed rotational actuators from single individual CNT. Since miniaturization is the most valuable attribute in any field like electronic devices, computation, manufacturing or medical, they focused on

construction and operation of a nanoscale electromechanical actuator with a rotatable metal plate which a MWCNT serves as motion-enabling actuator shaft.

Another demonstration of CNT based sensor was achieved by Nishio [18]. Author reported an application which utilizes the oscillation amplitude of a nanotube cantilever to detect nanoscale mass particles. The oscillations were measured using a focused electron beam of a scanning electron microscope. The great achievement is obtained as they can measure the mass of the particle at around 100 zeptogram where the limitation is the measurement resolution of the equipment not the nanotubes.

An example of electrical input-optical output was achieved by Chen and Prebeinos [19]. They used the high local electric fields on supported single carbon nanotube molecules to produce bright infrared emission. To demonstrate the reverse interaction, the study of Steward and Leonard [20] can be given. In their optoelectronic setup, they manage to change the current-voltage of an illuminated nanotube by photon inducing.

Another promising development is achieved by Xu [21] by utilizing these nanotubes as IR detectors. Author reported that a dense uniform array of CNT, can give proper output voltages when exposed to infrared radiation. Also usage of CNT enables to cover a broad range of spectral response from 1 to 10μm by only tuning the diameter of the individual tubes. Besides the detection area is not limited to flat, wafer-size plane, hence curved detection areas can be produced with low manufacturing cost. In addition to these he reported that the dense structure of such a detector suppresses the random thermal noise.

Usage of an individual carbon nanotube as circuit elements and transistors was demonstrated by Tans and Verschueren [22]. In their study they developed three terminal switching devices that consist of one semiconducting SWCNT connected to two metal electrodes. By applying voltage, the nanotube can be switched from a

conducting state to an insulating stage. They reported that the prototype was operable in room temperature conditions which obviously enable the nanoscale device to be used in wider areas.

These studies show that understanding these extraordinary attributes of nanotubes has great importance for nanoscience to manipulate and grow them accordingly. So both experimental and theoretical studies were conducted to investigate individual behaviors of nanotube. In one research Demczyk and Wang [23] manage to make pulling and bending tests on MWCNT in bridged configuration and achieve a tensile strength of 0.15 TPa using an atomic force microscope. Noting that nanotubes exhibit highly flexible behavior up to fracture, they suggest CNT are good candidates as reinforcement fibers in structural materials.

Wong [24] presented his experimental results which indicates that SWCNT have higher ultimate strengths than MWCNT, where as MWCNT are uniquely tough and energy-absorbing material. The method is to pin the nanotubes into a molybdenum disulfide surface and the bending force at the tip of an atomic force microscope is measured to reach the desired mechanical properties.

Theoretical studies in investigation of CNT properties are governed by mainly two approaches. The former is the predictive method by modeling the CNT as continuum models. Tersoff [25] conducted simple calculations of energies of the nanostructures based on the deformation of the graphene sheet, treated as an elastic continuum. He concluded that the results can be used to predict the elastic strain energy of nanotubes.

In a later study, Ru [26] followed this continuum shell model to investigate the buckling of CNT subjected to axial compression. He found the critical pressure is about 1.8 GPa for a 1.3 nm diameter SWCNT. Even though this continuum approach is beneficial to predict the structural and dynamic mechanical properties of

nanotubes, method neglects the detailed characteristics of nanotube chirality and does not take the interatomic forces acting.

Lu and Liu [27] developed another continuum model for the Van der Waals interactions between CNT walls. Previous models for those bonds involved many assumptions and using Lennard-Jones potential functions to model these Van der Waals forces showed that the critical buckling pressure is much smaller than those analyses involving assumptions.

The other main approach in theoretical studies is the atomistic discrete models. In these techniques the most important step is to model the bonds between carbon atoms both in walls of a SWCNT or the interlayer interactions between coaxial tubes of a MWCNT. Lier and Alsenoy [28] carried out an ab initio study to measure the Young's modulus of a number of closed single walled nanotubes. The method ab initio is detailed approach which deals with even electrons of each atom. One major difference of ab initio is that it doesn't use any kind of empirical data that is obtained from an experimental study or observation. Interestingly it is widely used to model any kind of atomic structure and is the one that gives the closest result to any experimental data. In the CNT case, authors presented that the modulus of elasticity is higher than 1 TPa which agrees with experimental and previous theoretical studies. They reported that the calculated Young's modulus for a graphene layer is found to be smaller than for its (5, 5) nanotube counterpart.

In one study Duan and Wang [29] utilized different approaches to model the carbon nanotube fracture. The tensile strength, fracture strain and fracture angle under tension were reviewed using Morse potential and reactive empirical bond-order potential. These enabled to simulate the nonlinear behavior of the bonds between C-C but the computational workload is the limitation of the size of CNT modeled.
A linear-elastic model has been developed by Li and Chou [30] in which every bond in a CNT is treated as beams and the atoms are treated as joints of the related load-

bearing beam members. Since in this method the beam's sectional parameters are needed, authors suggested a linkage between force field constant in molecular mechanics and sectional parameters in structural mechanics. After obtaining those parameters Li and Chou validated their approach and results of a graphene sheet extracted from their method was checked with the experimentally data. They reported the linear relation between tube diameter and modulus of elasticity. Also findings pointed that the helicity is another critical parameter affecting the modulus of elasticity.

In another study Li and Chou [31] modeled the Van der Waal forces between C atoms of interacting coaxial tubes by treating them as beams in MWCNT. The sectional parameters were derived with similar approach. As an additional result they reported that number of tube layers have some noticeable effects of elastic properties of MWCNT. Also they reported that inner nested tubes can be deformed only if they carry the tensile or shear forces directly, which implies those Van der Waals forces are not transmitting the forces significantly. Authors widen their approach [32], [33] to investigate the fundamental frequencies of both SWCNT and MWCNT. The additional work was to construct the mass matrix of the whole system in order to obtain system's equation of motion of free vibration for undamped structures. Using direct stiffness method, elemental stiffness and mass matrices are assembled into global matrices. They pointed that the fundamental cantilevered and bridged frequencies can reach up to 1.5 THz.

In another study Li and Chou [34], used same analogy to predict the tensile strength of CNT by utilizing the C-C bonds' breaking energy. They developed a criterion involving the bond length before and after tensile force applied on the ends of the carbon nanotube. Findings show that the tensile strength of defect-free carbon nanotubes are in the range of 50-60 GPa, besides armchair nanotubes show higher strength.

Tserpes and Papanikos [35] utilized that linkage to develop a three-dimensional finite element model for single-walled carbon nanotubes. A commercial software is used to locate the atoms and beams to represent the whole carbon nanotube. Tensile force is applied to calculate the deformation of the end nodes from which the nanotube's modulus of elasticity is obtained. Authors conducted a study of the effect of the thickness of the bonds to the Young's modulus since a variety of values have been both developed and measured using atomic force microscopes. Tserpes and Papanikos pointed out that the selection of bond thickness has significant effect on the calculation of system's mechanical properties.

Up to this point, given properties makes CNT a unique material in any field. During the production stage of carbon nanotubes, those materials may contain defects or vacancies. Studies were reported that any kind of imperfection changes mechanical, electrical and optical characteristics. Defect may occur in form of Stone-Wales defect which changes the hexagonal network into a pentagon and heptagon by rearranging bonding pairs locally which also designates this defect as 5-7-7-5 defect in literature. Since the tensile strength is dominated by the weakest bond in the whole structure, the strength of the rearranged bond will become the maximum strength of the chain. Lu and Bhattacharya [36] studied the effect of randomly occurring 5-7-7-5 defects on mechanical properties of CNT using the atomistic simulation technique. They reported that the fracture invariably started from the vacancy whereas for a defect-free tube the starting point is randomly positioned. The almost linear effect of number of vacancies on stiffness, ultimate strength and ultimate strain is tabulated in their report.

Another form of defects is the atom-vacancies which can appear in nanotubes when purification made in the production stage or as a result of irradiation exposure. The latter mechanism is the collisions of energetic particles which force the C atoms to displace from their original positions in the nanotube network.

Mielke and Troya [37] established a quantum mechanical model using density functional theory to investigate the nanotubes under axial tension. The results were in agreement with previous studies and they reported around % 26 reductions for failure stresses in existence of one or two atom-vacancies. Also large holes which are introduced via oxidative purification processes reduce the strength significantly.

The theoretical models govern mostly two approaches which use reconstruction of the vacancy or not. Sammalkorpi and Krasheninnikov [38] conducted a study by employing molecular dynamics simulation and continuum theory to predict the mechanism of the reconstruction. They succeeded to plot the ratio of Young's modulus of CNT before over after vacancy versus defect concentration. Interestingly the non reconstructed bonding is also simulated and the discrepancies between two models can apart up to only around %5.

A non reconstructed model was studied by Pirmoradian [39] which employs the linear elastic model of Li and Chou [30], to investigate the effect of vacancies on the fundamental frequencies of carbon nanotubes. This recent study and conclusions were published in 2008 and Pirmoradian only focused on the effect of one atom vacancy on CNT's first cantilevered modal frequency. They reported the frequency variation is insensitive to the nanotube diameter.

The investigation conducted in this report covers the first five natural frequencies of both bridged and cantilevered support configuration. Also increasing percentages of vacancies were induced with being randomly positioned. In addition to these the effect of vacancy on the vibration plane and as a case study the reductions in Young's Modulus were investigated in this thesis.

More studies have been concentrated on modeling the imperfections in both SWCNT and MWCNT since interesting findings besides the reduction in mechanical

properties, were reported about interactions or behavioral change in such as electrical, thermal conductivity.

Gomez-Navarro and Pablo [40] published their work on tuning the conductance of SWCNT by ion irradiated atomically vacant carbon nanotubes. Defects are known to modify the electrical resistance of carbon nanotubes. In their work consecutive Argon irradiation doses were applied to SWCNT to produce a uniform density of defects. Consecutive measurements were taken and resistance of nanotube versus defect amount dependence was plotted. They reported %0.03 of vacancy amount increases the resistance of CNT about %0.1.

To summarize, researches show that a defect-free carbon nanotube is the cutting-edge nanomaterial to build nanoscale devices, sensors or one of the most effective strengthening material to be used in composites. On the other hand, the complications or the uncontrolled parameters in the growing stage may result in imperfections in these materials. Both the experimental and theoretical studies show that any amount of imperfection significantly disturbs the characteristics of carbon nanotube. The understanding of the results of those vacancies/defects needs to be in great consideration.

1.2 Objective

The objective of this thesis is to obtain the dynamic characteristics of various types of SWCNT with atom-vacancies existing in the atomistic structure. This is accomplished by using matrix stiffness method to interpret the whole stiffness and mass matrices of the CNT which uses the linkage between molecular and structural mechanics. Effect of different percentage of vacancies is investigated on changing length, diameter and chirality of CNT. It is also aimed to use a commercial finite element program to verify the code developed and the elements that are used to

construct the truss-beam model. As a case study, relation between modulus of elasticity and the amount of imperfections of the SWCNT is also in concern.

1.3 Scope of the Thesis

In Chapter 2, firstly brief information about CNT will be presented. Following that, theory of matrix stiffness method will be explained with the elements used, elemental forces, stiffness matrices and globalization of local matrices. Also linkage between structural and molecular mechanics will be established. The approaches that are used to construct the CNT geometry, apply the boundary constraints and implementation of vacancies will be identified.

In Chapter 3, the methodology of the case study will be described. The investigation is focused on the effect of vacancies on Young's Modulus of CNT.

In Chapter 4, the verification method will be presented. Also the interaction between the source code and the commercial software ANSYS will be established.

In Chapter 5, results obtained with the source code will be presented. Firstly effects of randomly placed different percentages of vacancies will be shown. Then the maximum and minimum amount of variations will be shown. Next, the effect of position of the vacancies will be plotted. The results of the case study will be given at the end of this section.

In Chapter 6, the discussion, conclusions and recommendations for future work will be given.

CHAPTER 2

THEORY

2.1 Basics of Carbon Nanotubes

Carbon nanotubes are cylindrically shaped nanostructures which can be produced with length over diameter ratio up to 28000000:1 [41]. These nanostructures can be illustrated as rolled-up cylinders of graphene sheets of sp^2 bonded carbon atoms for single walled carbon nanotubes. For both graphene sheets and carbon nanotubes the geometry of the hybridized orbital is trigonal planar. This is the reason why each carbon atom has three nearest neighbors within the graphite sheets or CNT. This bonding structure with sp^2 network provides the molecules with their unique strength as compared to sp^3 network diamonds.

The most important parameter of these structures is the chirality and this parameter shapes the helicity of the nanotube. Depending on the angle of the roll-up vector, the nanotubes are named to be zigzag or armchair at extremities. Any configuration in between are named as chiral nanotubes. Some critical geometrical parameters derived and tabulated in the study of Dresselhaus et al. [42] and will to be used in this report.

In general, this chiral vector C_h is defined with integers in form of (n,m) and the basis vectors a_1 and a_2 in Figure 2.1.

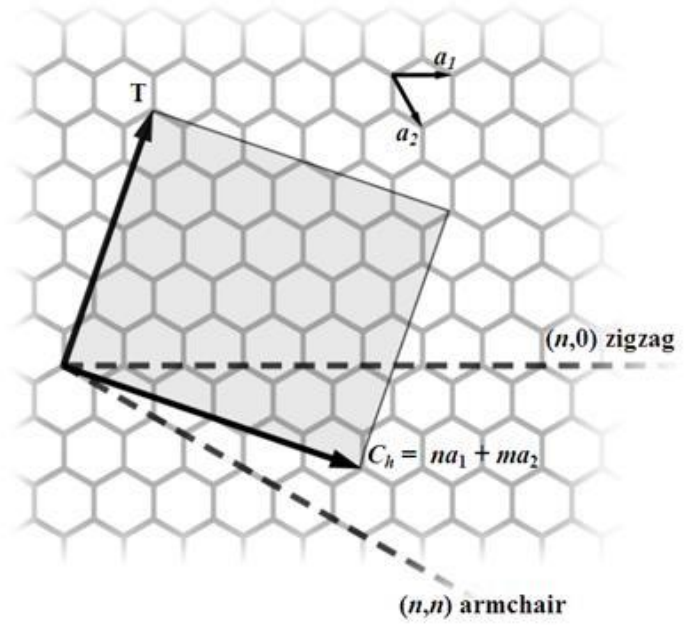

Figure 2.1 Chirality Vector of CNT [42]

Carbon to carbon atom distance in nanotubes;

$$a_{c-c} = 1.421\,\text{Å} \tag{2.1}$$

Circumferential length of a nanotube;

$$L_C = |C_h| = \sqrt{3}a_{c-c}\sqrt{n^2 + m^2 + nm} \tag{2.2}$$

Diameter of an individual nanotube;

$$D = \frac{L_C}{\pi} = \frac{\sqrt{n^2 + m^2 + nm}}{\pi}\sqrt{3}a_{c-c} \tag{2.3}$$

As can be seen the major parameters that define the diameter of CNT and helicity are the elements of the chiral vector. Not only chirality determines the positions of C-C atoms with respect to the axis of CNT, but also chirality identify whether the CNT is conductor or not. (See Figure 2.2)

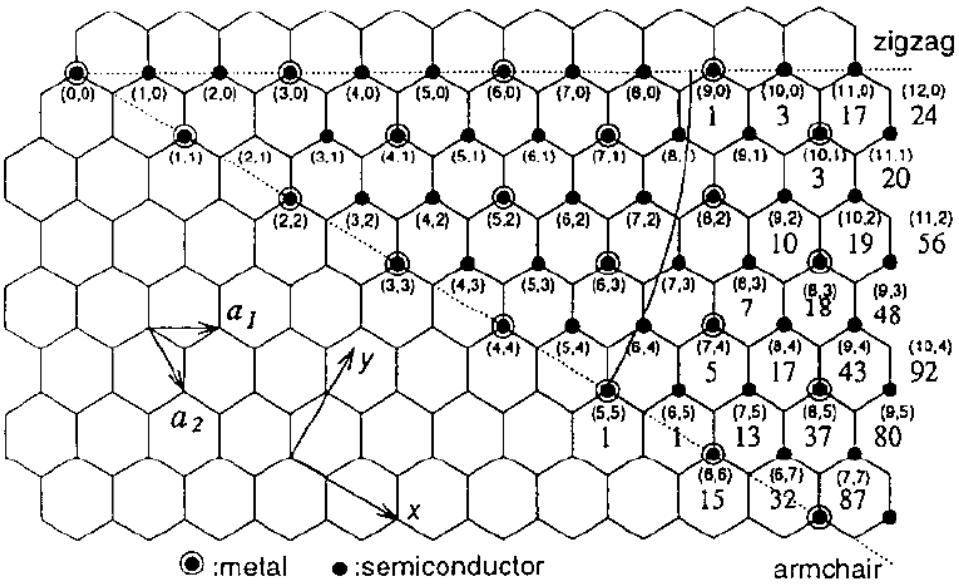

Figure 2.2 Conductivity Behavior of CNT [42]

Even though basically multiwalled nanotubes are concentrically located single walled nanotubes, their mechanical and geometric properties are comparatively worthy to analyze. A MWNT can be illustrated as "Russian Doll" model. For instance the inner most NT has a chirality of (8,0) whereas the second coaxial tube is (10,0). The intralayer distance was measured to be around 3.4 Å as in the same as planar graphene sheets.

This situation is not just a geometrical difference but also many characteristics differ from SWNT. To open up, the chemical resistance is significantly improved than

SWNT. On the other hand the conductivity of SWNT is more unique and MWNT does not exhibit this property that significantly.

2.2 Matrix Stiffness Method

In structural analysis, various kinds of modeling techniques are utilized to obtain the total or directional deformations under certain axial, bending or torsional forces and moments. Among these techniques, MSM, also known as displacement method or direct stiffness method is particularly used in computerized analysis of complex discrete models including statically indeterminate ones. It is a matrix oriented method that uses the individual members' stiffness to find the member forces and displacements in structures.

A direct application of this model is commonly preferred in finite element analysis of structures. Before obtaining necessary matrices, the system should be properly defined into a set of simpler, idealized elements at interconnected at the nodes. After this discretization, the material stiffness properties of these individual members are to be globalized with respect to global coordinates and a proper set of equations governing the behavior of the entire structure is obtained. With the given forces/moments the displacements with respect to global coordinates can be obtained by solving these equations. For any set of given forces/moments the globalized set of equations should be obtained in form of;

$$K \; u \; = \; f \qquad (2.4)$$

where u and f are the displacement and force vectors respectively. In u , the first three components are the translational displacements and next three are the rotational displacements. The second set of six variables is again translational and rotational displacements but designate for the j node. In f , the first three

components are the force components in x, y and z directions and next three are the bending moments in three planes displacements. The second set of six variables is again forces and moments but designates for the j node.

$$u = \begin{bmatrix} u_{xi} \\ u_{yi} \\ u_{zi} \\ \theta_{xi} \\ \theta_{yi} \\ \theta_{zi} \\ u_{xj} \\ u_{yj} \\ u_{zj} \\ \theta_{xj} \\ \theta_{yj} \\ \theta_{zj} \end{bmatrix} \quad (2.5) \qquad f = \begin{bmatrix} f_{xi} \\ f_{yi} \\ f_{zi} \\ m_{xi} \\ m_{yi} \\ m_{zi} \\ f_{xj} \\ f_{yj} \\ f_{zj} \\ m_{xj} \\ m_{yj} \\ m_{zj} \end{bmatrix} \quad (2.6)$$

A system of simultaneous linear equations should be transformed in these forms and the given set of forces and the boundary condition of the nodal displacements should be implemented into these vectors. After inserting the known value for each DOF, master stiffness equation is complete and ready to be evaluated by the available methods like matrix inversion or Cholesky decomposition.

In this thesis, as a case study, matrix stiffness method is utilized to find the modulus of elasticity of various SWNT with or without atom vacancies by finding the z-axis displacements of the end nodes.

Also since the basis of this thesis is to investigate the fundamental frequencies of the SWNT, the main study is focused on the equation of motion for harmonic forcing which is;

$$[M]\ \ddot{x} + i[H]\ x + [K]\ x = f \tag{2.7}$$

where $[M]$, $[H]$, $[K]$ are mass, structural damping and stiffness matrices of the structure respectively, x is the vector of generalized coordinates, f is the generalized forcing vector and i is the unit imaginary number. In the frequency domain it can be expressed as;

$$[K] - \omega^2[M] + i[H] \quad x = f \tag{2.8}$$

In this study, no damping is included and only the natural frequencies are investigated since all the applications of CNT in literature are based on free vibration of CNT. Hence the corresponding and reduced form of (2.8) becomes;

$$[K] - \omega^2[M] \quad x = 0 \tag{2.9}$$

This is referred as an eigenvalue problem in mathematics and can be transformed into a standard form by multiplying by $[M]^{-1}$ which leads;

$$[M]^{-1}[K] - \omega^2[M]^{-1}[M] \quad x = 0 \tag{2.10}$$

If necessary designations are used, the equation will be in form of;

$$\left[\ A - \lambda[I]\right]\ x = 0 \tag{2.11}$$

where $[M]^{-1}[K] = A$ and $\lambda = \omega^2$

The solution of this equation results in N number of eigenvalues; $\omega_1^2, \omega_2^2, \omega_3^2 \ldots . \omega_N^2$ where N corresponds to the number of degrees of freedom. The resulting eigenvalues extracted from the equation provide the natural frequencies of the system. If these eigenvalues are substituted back into the original set of equations, the values of x vector correspond to eigenvectors of that specific natural frequency. These vectors are mode shapes of the system and contain unitless displacements for every DOF. The natural frequencies and mode shapes are found using MATLAB's *eig* function. Resulting set of matrices will contain 6N mode shape vectors and N number eigenvalues which square root of those, are natural frequencies of the system. (See App A)

For natural frequencies, *sort* function is used to have the frequencies in ascending order. Using that order, the mode shape matrices rearranged to draw the first five fundamental frequencies. It is beneficial to draw to mode shapes for both defectless and defected nanotubes and investigate the effect of vacancies on the preferred mode shapes. The methodology is to use the x, y, z displacements in the eigenvector to add them to the initial coordinates of atoms. At that point, a scaling factor is utilized in order to have larger displacements which ease to identify the effects when visualizing.

Therefore elemental and global mass matrices should also be constructed for the whole structure in order to solve for the fundamental frequencies and the mode shapes of the nanotubes. In order to construct the elemental and global stiffness and mass matrices, firstly the type of element namely space frame should be explained.

2.2.1 Space Frame Element

The appropriate element used to model the bonding between carbon atoms in a SWCNT is space frame element. Detailed explanations and derivations are explained in Singiresu [43]. It is a straight bar of uniform cross section that is capable of carrying axial forces and bending moments about the two principal axes in the plane of its cross section and twisting moment about its centroidal axis. The corresponding displacement degrees of freedom are shown in Figure 2.3.

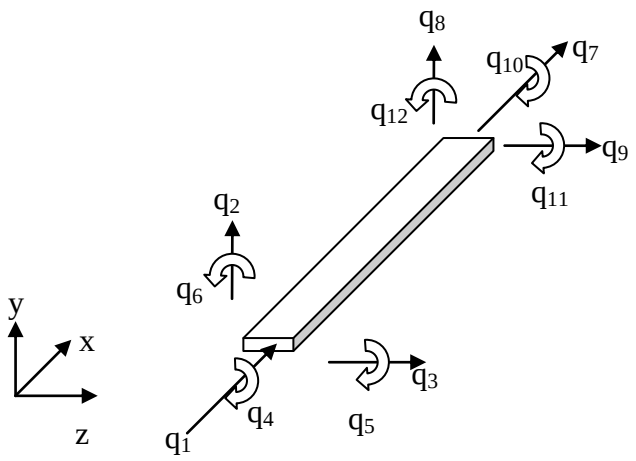

Figure 2.3 Degrees of Freedom of a Space Frame Element [43]

It can be seen that a stiffness matrix of a frame element should be of order 12x12. A space frame element has twelve degrees of freedom since there are three displacements and three rotations DOF at each of two nodes. If the local axes are chosen to coincide with the principal axes of the cross-section, it is possible to construct the 12x12 stiffness matrix from 2x2 and 4x4 sub matrices. So the displacements can be separated into four groups, each of which can be considered independently of the others. If the local xyz coordinate system is chosen to be coincided with the principle axes of the cross section and with the x axis representing

the centroidal axis of the frame, the bending displacements and forces in xy and xz planes can be considered to be independent of each other. In any other arbitrary selection calculations will not be that clear. For instance the bending displacements in xy plane q_2, q_6, q_8 and q_{12} depend not only on the bending forces acting in that plane like shear forces in y direction and bending moments acting in the xy plane, but also bending forces acting in the plane xz.

2.2.1.1 Axial Displacements

According to the engineering theory of bending and torsion of beams, q_1 and q_7, the axial displacements, depend only to the axial forces. (See Figure 2.4)

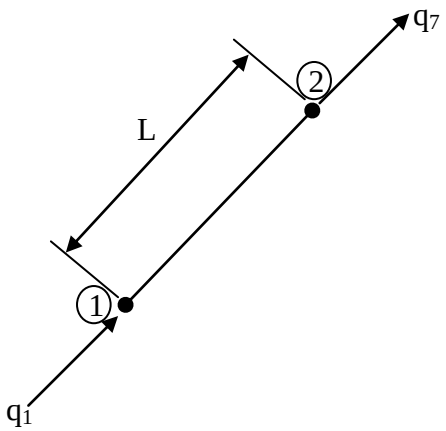

Figure 2.4 Axial Displacements of a Space Frame Element [43]

Nodal displacements are q_1 and q_7 and a linear displacement model leads to the stiffness matrix, that corresponds to the axial displacement is derived as;

$$\begin{matrix} & q_1 & q_7 \end{matrix}$$

$$\left[k_a{}^e\right] = \frac{AE}{L}\begin{bmatrix} 1 & -1 \\ -1 & 1 \end{bmatrix}\begin{matrix} q_1 \\ q_7 \end{matrix} \qquad (2.12)$$

where *E* is modulus of elasticity, *A* is the cross-sectional area and L is the length of the element [43]. For the sake of clarification, identification of the degrees of freedom is placed at the top and right hand side of the matrix.

2.2.1.2 Torsional Displacements

According to the engineering theory of bending and torsion of beams, q_4 and q_{10}, are the torsional displacements and depend only on the torsional moments. (See Figure 2.5)

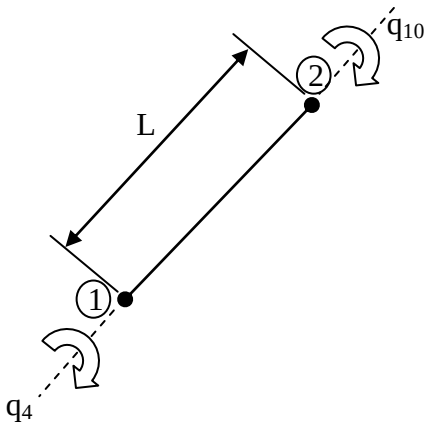

Figure 2.5 Torsional Displacement of a Space Frame Element [43]

As can be reviewed from Singiresu [43] the stiffness matrix that corresponds to torsional displacements for a circular cross sectional frame can be expressed as;

$$\begin{matrix} & q_4 & q_{10} \end{matrix}$$

$$\left[k_t{}^e\right] = \frac{GJ}{L}\begin{bmatrix} 1 & -1 \\ -1 & 1 \end{bmatrix}\begin{matrix} q_4 \\ q_{10} \end{matrix} \qquad (2.13)$$

where $\frac{GJ}{L}$ is called the torsional stiffness of the frame element. G and J are shear modulus of elasticity, polar moment of inertia respectively.

2.2.1.3 Bending Displacements in the Plane xy

Four bending DOF are $q_{2,}$ $q_{6,}$ q_8 and q_{12} (See Figure 2.6) and the corresponding stiffness matrix [43] can be shown as;

$$\begin{matrix} & q_2 & q_6 & q_8 & q_{12} & \\ \left[k_{xy}{}^{e} \right] = \frac{EI_z}{L^3} & \begin{bmatrix} 12 & 6L & -12 & 6L \\ 6L & 4L^2 & -6L & 2L^2 \\ -12 & -6L & 12 & -6L \\ 6L & 2L^2 & -6L & 4L^2 \end{bmatrix} & \begin{matrix} q_2 \\ q_6 \\ q_8 \\ q_{12} \end{matrix} \end{matrix} \qquad (2.14)$$

where I_z is the area moment of inertia of the cross section about the z axis.

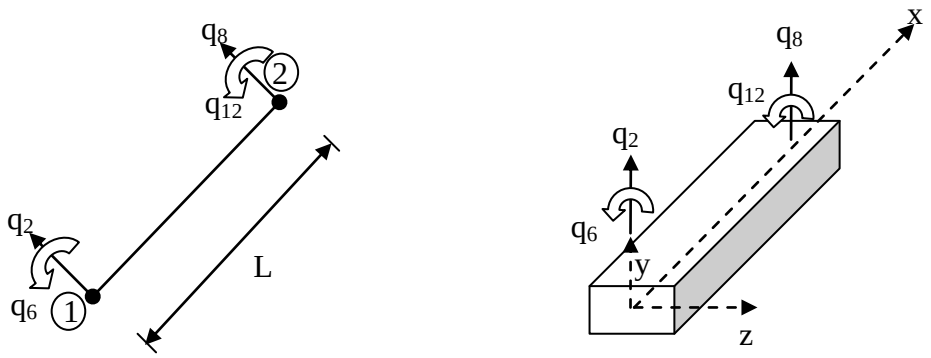

Figure 2.6 Bending Displacements of a Space Frame Element in xy Plane [43]

2.2.1.4 Bending Displacements in the Plane xz

In this case the bending of the element takes place in the xz plane. Four bending DOF are q_3, q_5, q_9 and q_{11} (See Figure 2.7) and the corresponding stiffness matrix [43] can be shown as;

$$\begin{matrix} & q_3 & q_5 & q_9 & q_{11} \end{matrix}$$

$$\left[k_{xz}{}^{e} \right] = \frac{EI_y}{L^3} \begin{bmatrix} 12 & 6L & -12 & 6L \\ 6L & 4L^2 & -6L & 2L^2 \\ -12 & -6L & 12 & -6L \\ 6L & 2L^2 & -6L & 4L^2 \end{bmatrix} \begin{matrix} q_3 \\ q_5 \\ q_9 \\ q_{11} \end{matrix} \qquad (2.15)$$

where I_y is the area moment of inertia of the cross section about the y axis.

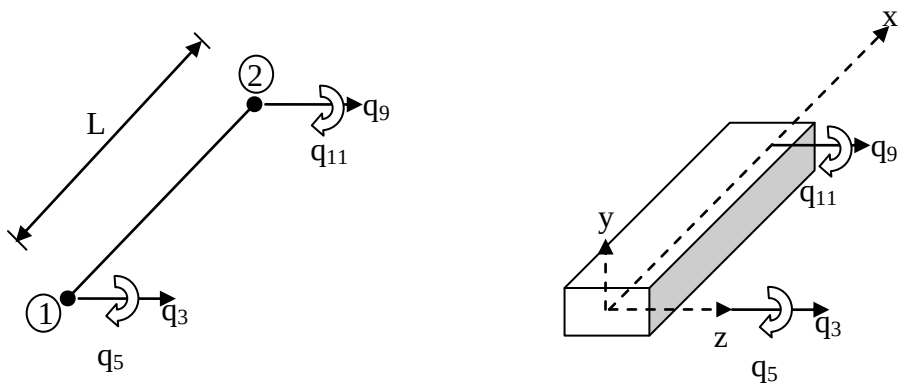

Figure 2.7 Bending Displacements of a Space Frame Element in xz Plane [43]

2.2.1.5 Total Element Stiffness Matrix

Superposition of these derived different sets of independent displacements gives the overall stiffness matrix of the frame element;

$$\left[\underset{12X12}{k^{(e)}} \right] = \begin{bmatrix} k_{ii} & k_{ij} \\ k_{ij}^{\ T} & k_{jj} \end{bmatrix} \tag{2.16}$$

$$k_{ii} = \begin{bmatrix} \frac{EA}{L} & 0 & 0 & 0 & 0 & 0 \\ 0 & \frac{12EI_z}{L^3} & 0 & 0 & 0 & \frac{6EI_Z}{L^2} \\ 0 & 0 & \frac{12EI_y}{L^3} & 0 & -\frac{6EI_y}{L^2} & 0 \\ 0 & 0 & 0 & \frac{GJ}{L} & 0 & 0 \\ 0 & 0 & -\frac{6EI_y}{L^2} & 0 & \frac{4EI_y}{L} & 0 \\ 0 & \frac{6EI_z}{L^2} & 0 & 0 & 0 & \frac{4EI_z}{L} \end{bmatrix} \tag{2.17}$$

$$k_{ij} = \begin{bmatrix} -\frac{EA}{L} & 0 & 0 & 0 & 0 & 0 \\ 0 & -\frac{12EI_z}{L^3} & 0 & 0 & 0 & \frac{6EI_Z}{L^2} \\ 0 & 0 & -\frac{12EI_y}{L^3} & 0 & -\frac{6EI_y}{L^2} & 0 \\ 0 & 0 & 0 & -\frac{GJ}{L} & 0 & 0 \\ 0 & 0 & -\frac{6EI_y}{L^2} & 0 & \frac{2EI_y}{L} & 0 \\ 0 & -\frac{6EI_z}{L^2} & 0 & 0 & 0 & \frac{2EI_z}{L} \end{bmatrix} \tag{2.18}$$

$$k_{jj} = \begin{bmatrix} \frac{EA}{L} & 0 & 0 & 0 & 0 & 0 \\ 0 & \frac{12EI_z}{L^3} & 0 & 0 & 0 & -\frac{6EI_Z}{L^2} \\ 0 & 0 & \frac{12EI_y}{L^3} & 0 & \frac{6EI_y}{L^2} & 0 \\ 0 & 0 & 0 & \frac{GJ}{L} & 0 & 0 \\ 0 & 0 & \frac{6EI_y}{L^2} & 0 & \frac{4EI_y}{L} & 0 \\ 0 & -\frac{6EI_z}{L^2} & 0 & 0 & 0 & \frac{4EI_z}{L} \end{bmatrix} \qquad (2.19)$$

Again with the identification of the displacement DOF positioned at the top and right hand side, the overall matrix [46] can be expressed as below;

$$\begin{array}{c} \begin{matrix} q_1 & q_2 & q_3 & q_4 & q_5 & q_6 & q_7 & q_8 & q_9 & q_{10} & q_{11} & q_{12} \end{matrix} \\ \left[k^e\right] = \begin{bmatrix} \frac{EA}{L} & 0 & 0 & 0 & 0 & 0 & -\frac{EA}{L} & 0 & 0 & 0 & 0 & 0 \\ 0 & \frac{12EI_z}{L^3} & 0 & 0 & 0 & \frac{6EI_Z}{L^2} & 0 & -\frac{12EI_z}{L^3} & 0 & 0 & 0 & \frac{6EI_Z}{L^2} \\ 0 & 0 & \frac{12EI_y}{L^3} & 0 & -\frac{6EI_y}{L^2} & 0 & 0 & 0 & -\frac{12EI_y}{L^3} & 0 & -\frac{6EI_y}{L^2} & 0 \\ 0 & 0 & 0 & \frac{GJ}{L} & 0 & 0 & 0 & 0 & 0 & -\frac{GJ}{L} & 0 & 0 \\ 0 & 0 & -\frac{6EI_y}{L^2} & 0 & \frac{4EI_y}{L} & 0 & 0 & 0 & \frac{6EI_y}{L^2} & 0 & \frac{2EI_y}{L} & 0 \\ 0 & \frac{6EI_z}{L^2} & 0 & 0 & 0 & \frac{4EI_z}{L} & 0 & -\frac{6EI_z}{L^2} & 0 & 0 & 0 & \frac{2EI_x}{L} \\ -\frac{EA}{L} & 0 & 0 & 0 & 0 & 0 & \frac{EA}{L} & 0 & 0 & 0 & 0 & 0 \\ 0 & -\frac{12EI_z}{L^3} & 0 & 0 & 0 & -\frac{6EI_z}{L^2} & 0 & \frac{12EI_z}{L^3} & 0 & 0 & 0 & -\frac{6EI_Z}{L^2} \\ 0 & 0 & -\frac{12EI_y}{L^3} & 0 & \frac{6EI_y}{L^2} & 0 & 0 & 0 & \frac{12EI_y}{L^3} & 0 & \frac{6EI_y}{L^2} & 0 \\ 0 & 0 & 0 & -\frac{GJ}{L} & 0 & 0 & 0 & 0 & 0 & \frac{GJ}{L} & 0 & 0 \\ 0 & 0 & -\frac{6EI_y}{L^2} & 0 & \frac{2EI_y}{L} & 0 & 0 & 0 & \frac{6EI_y}{L^2} & 0 & \frac{4EI_y}{L} & 0 \\ 0 & \frac{6EI_Z}{L^2} & 0 & 0 & 0 & \frac{2EI_z}{L} & 0 & -\frac{6EI_z}{L^2} & 0 & 0 & 0 & \frac{4EI_z}{L} \end{bmatrix} \begin{matrix} q_1 \\ q_2 \\ q_3 \\ q_4 \\ q_5 \\ q_6 \\ q_7 \\ q_8 \\ q_9 \\ q_{10} \\ q_{11} \\ q_{12} \end{matrix} \end{array}$$

(2.20)

2.2.2 Global Stiffness Matrix and Assemble

The 12x12 stiffness matrix given in Eq(2.20) is with respect to the local xyz coordinate system where q and Q stand for DOF with respect to local and global coordinate system, respectively.

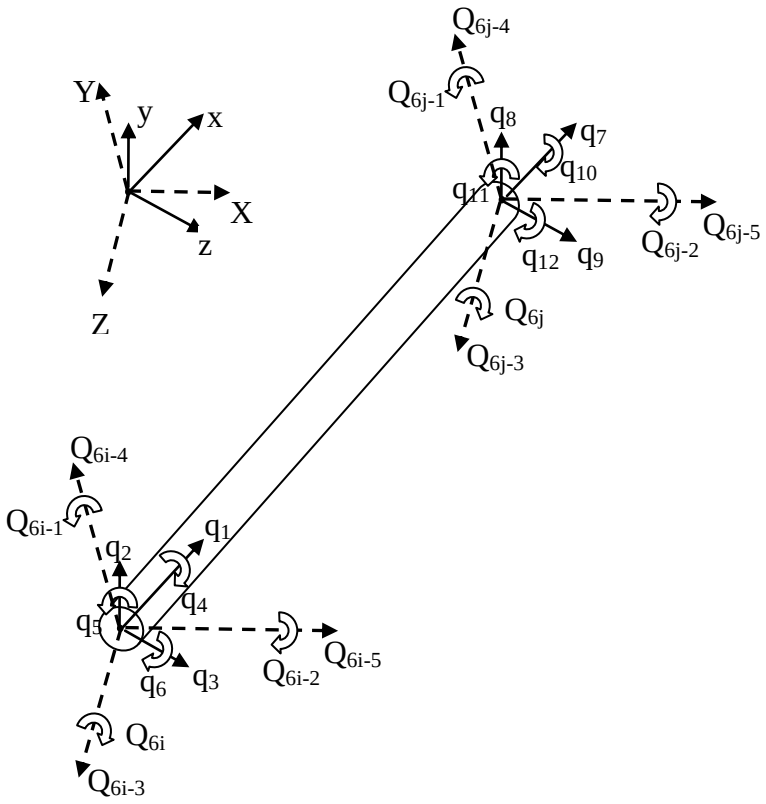

Figure 2.8 Symbolic Orientation of Local Coordinate System with respect to Global Coordinate System [43]

The nodal displacements in local and global coordinate systems are related by the relation given in Figure 2.8. And the transformation matrix is found to be as given in(2.21).

$$\begin{Bmatrix} q_1 \\ q_2 \\ q_3 \\ q_4 \\ q_5 \\ q_6 \\ q_7 \\ q_8 \\ q_9 \\ q_{10} \\ q_{11} \\ q_{12} \end{Bmatrix} = \begin{bmatrix} l_{ox} & m_{ox} & n_{ox} & 0 & 0 & 0 & 0 & 0 & 0 & 0 & 0 & 0 \\ l_{oy} & m_{oy} & n_{oy} & 0 & 0 & 0 & 0 & 0 & 0 & 0 & 0 & 0 \\ l_{oz} & m_{oz} & n_{oz} & 0 & 0 & 0 & 0 & 0 & 0 & 0 & 0 & 0 \\ 0 & 0 & 0 & l_{ox} & m_{ox} & n_{ox} & 0 & 0 & 0 & 0 & 0 & 0 \\ 0 & 0 & 0 & l_{oy} & m_{oy} & n_{oy} & 0 & 0 & 0 & 0 & 0 & 0 \\ 0 & 0 & 0 & l_{oz} & m_{oz} & n_{oz} & 0 & 0 & 0 & 0 & 0 & 0 \\ 0 & 0 & 0 & 0 & 0 & 0 & l_{ox} & m_{ox} & n_{ox} & 0 & 0 & 0 \\ 0 & 0 & 0 & 0 & 0 & 0 & l_{oy} & m_{oy} & n_{oy} & 0 & 0 & 0 \\ 0 & 0 & 0 & 0 & 0 & 0 & l_{oz} & m_{oz} & n_{oz} & 0 & 0 & 0 \\ 0 & 0 & 0 & 0 & 0 & 0 & 0 & 0 & 0 & l_{ox} & m_{ox} & n_{ox} \\ 0 & 0 & 0 & 0 & 0 & 0 & 0 & 0 & 0 & l_{oy} & m_{oy} & n_{oy} \\ 0 & 0 & 0 & 0 & 0 & 0 & 0 & 0 & 0 & l_{oz} & m_{oz} & n_{oz} \end{bmatrix} \begin{Bmatrix} Q_{6i-5} \\ Q_{6i-4} \\ Q_{6i-3} \\ Q_{6i-2} \\ Q_{6i-1} \\ Q_{6i} \\ Q_{6j-5} \\ Q_{6j-4} \\ Q_{6j-3} \\ Q_{6j-2} \\ Q_{6j-1} \\ Q_{6j} \end{Bmatrix} \tag{2.21}$$

where λ can be expressed as;

$$\underset{12x12}{\lambda} = \begin{bmatrix} \underline{\lambda} & 0 & 0 & 0 \\ 0 & \underline{\lambda} & 0 & 0 \\ 0 & 0 & \underline{\lambda} & 0 \\ 0 & 0 & 0 & \underline{\lambda} \end{bmatrix} \tag{2.22}$$

in which;

$$\underset{3x3}{\underline{\lambda}} = \begin{bmatrix} l_{ox} & m_{ox} & n_{ox} \\ l_{oy} & m_{oy} & n_{oy} \\ l_{oz} & m_{oz} & n_{oz} \end{bmatrix} \tag{2.23}$$

Here l_{ox}, m_{ox} and n_{ox} stand for the direction cosines of the x axis. Likewise l_{oy}, m_{oy} and n_{oy} represent for the y axis and l_{oz}, m_{oz} and n_{oz} represent for the z axis with respect to the global X, Y, Z axes. Since the axis of the local element is chosen to be coincident with the local x axis, finding the direction cosines of x axis is clearly straight forward as;

$$l_{ox} = \frac{X_j - X_i}{L} \tag{2.24}$$

$$m_{ox} = \frac{Y_j - Y_i}{L} \tag{2.25}$$

$$n_{ox} = \frac{Z_j - Z_i}{L} \tag{2.26}$$

Where the parameters X_j, X_i, Y_j, Y_i, Z_j, Z_i are the coordinates of nodes i and j in the global system. In addition to these, the derivation of other direction cosines can be expressed as;

$$l_{oy} = \frac{-m_{ox}}{\sqrt{l_{ox}^{\,2} + m_{ox}^{\,2}}} \tag{2.27}$$

$$m_{oy} = \frac{l_{ox}}{\sqrt{l_{ox}^{\,2} + m_{ox}^{\,2}}} \tag{2.28}$$

$$n_{oy} = 0 \tag{2.29}$$

$$l_{oz} = \frac{-l_{ox} n_{ox}}{\sqrt{l_{ox}^{\,2} + m_{ox}^{\,2}}} \tag{2.30}$$

$$m_{oz} = \frac{-m_{ox} n_{ox}}{\sqrt{l_{ox}^{\ 2} + m_{ox}^{\ 2}}} \tag{2.31}$$

$$n_{oz} = \sqrt{l_{ox}^{\ 2} + m_{ox}^{\ 2}} \tag{2.32}$$

Finally using the transformation matrix, the stiffness matrix of the element with reference to the global coordinate system [46] can be obtained as;

$$\left[K^e \right] = \lambda^{\ T} \left[k^e \right] \lambda \tag{2.33}$$

2.2.3 Consistent and Lumped Mass Matrices

In order to find the system's modal frequencies, system mass matrix should be obtained. First individual elemental mass matrices should be constructed. In literature there are two approaches; namely consistent and lumped mass matrices.

Former is called consistent because the same derivation used in elemental stiffness matrix construction was utilized to construct the elemental mass matrix. Usually it is preferable to transform this consistent mass matrix in to simpler form to solve several dynamic problems in literature. The simplest form of these matrices can be obtained by placing concentrated masses at node point at which the degrees of freedom of the element are placed. In that case the concentrated masses refer to translational and rotational inertia of the element and are calculated by assuming the dynamic coupling that exists between the element displacements are excluded. Hence the resulting mass matrix is purely diagonal and is called a lumped mass matrix.

This reduction method leads to nearly exact results if the masses placed at the nodes are small in volume. Since the lumped mass matrix of the element is diagonal, the

overall assembled mass matrix of the structure requires less effort and storage than any consistent mass matrix model.

The element chosen to model the bonding between C-C atoms is the space frame element as presented earlier. So the given consistent mass matrix for a space frame element [43] can be given as;

$$\left[m^e\right] = \rho AL \begin{bmatrix} \frac{1}{3} & 0 & 0 & 0 & 0 & 0 & \frac{1}{6} & 0 & 0 & 0 & 0 & 0 \\ 0 & \frac{13}{35} & 0 & 0 & 0 & \frac{11L}{210} & 0 & \frac{9}{70} & 0 & 0 & 0 & \frac{-13L}{420} \\ 0 & 0 & \frac{13}{35} & 0 & -\frac{11L}{210} & 0 & 0 & \frac{9}{70} & 0 & 0 & \frac{13L}{420} & 0 \\ 0 & 0 & 0 & \frac{J}{3A} & 0 & 0 & 0 & 0 & 0 & \frac{J}{6A} & 0 & 0 \\ 0 & 0 & -\frac{11L}{210} & 0 & \frac{L^2}{105} & 0 & 0 & 0 & -\frac{13L}{420} & 0 & -\frac{L^2}{140} & 0 \\ 0 & \frac{11L}{210} & 0 & 0 & 0 & \frac{L^2}{105} & 0 & \frac{13L}{420} & 0 & 0 & 0 & -\frac{L^2}{140} \\ \frac{1}{6} & 0 & 0 & 0 & 0 & 0 & \frac{1}{3} & 0 & 0 & 0 & 0 & 0 \\ 0 & \frac{9}{70} & 0 & 0 & 0 & \frac{13L}{420} & 0 & \frac{13}{35} & 0 & 0 & 0 & -\frac{11L}{210} \\ 0 & 0 & \frac{9}{70} & 0 & -\frac{13L}{420} & 0 & 0 & 0 & \frac{13}{35} & 0 & \frac{11L}{210} & 0 \\ 0 & 0 & 0 & \frac{J}{6A} & 0 & 0 & 0 & 0 & 0 & \frac{J}{3A} & 0 & 0 \\ 0 & 0 & \frac{13L}{420} & 0 & -\frac{L^2}{140} & 0 & 0 & 0 & \frac{11L}{210} & 0 & \frac{L^2}{105} & 0 \\ 0 & \frac{-13L}{420} & 0 & 0 & 0 & -\frac{L^2}{140} & 0 & -\frac{11L}{210} & 0 & 0 & 0 & \frac{L^2}{105} \end{bmatrix} \tag{2.34}$$

where ρ is the density of the frame element.

On the other hand for a space frame element, in a lumped mass matrix model total mass is concentrated at two nodes namely i and j, and the elemental mass matrix can be constructed as;

$$\left[m^e\right] = \frac{\rho AL}{2}\begin{bmatrix} 1 & 0 & 0 & 0 & 0 & 0 & 0 & 0 & 0 & 0 & 0 & 0 \\ 0 & 1 & 0 & 0 & 0 & 0 & 0 & 0 & 0 & 0 & 0 & 0 \\ 0 & 0 & 1 & 0 & 0 & 0 & 0 & 0 & 0 & 0 & 0 & 0 \\ 0 & 0 & 0 & 0 & 0 & 0 & 0 & 0 & 0 & 0 & 0 & 0 \\ 0 & 0 & 0 & 0 & 0 & 0 & 0 & 0 & 0 & 0 & 0 & 0 \\ 0 & 0 & 0 & 0 & 0 & 0 & 0 & 0 & 0 & 0 & 0 & 0 \\ 0 & 0 & 0 & 0 & 0 & 0 & 1 & 0 & 0 & 0 & 0 & 0 \\ 0 & 0 & 0 & 0 & 0 & 0 & 0 & 1 & 0 & 0 & 0 & 0 \\ 0 & 0 & 0 & 0 & 0 & 0 & 0 & 0 & 1 & 0 & 0 & 0 \\ 0 & 0 & 0 & 0 & 0 & 0 & 0 & 0 & 0 & 0 & 0 & 0 \\ 0 & 0 & 0 & 0 & 0 & 0 & 0 & 0 & 0 & 0 & 0 & 0 \\ 0 & 0 & 0 & 0 & 0 & 0 & 0 & 0 & 0 & 0 & 0 & 0 \end{bmatrix} \tag{2.35}$$

As mentioned before this elemental mass matrix is constructed with respect to local xyz coordinates. So same transformation matrices are used to reorient the elemental matrix with respect to global XYZ coordinates as;

$$\left[M^e\right] = \lambda^T \left[m^e\right] \lambda \tag{2.36}$$

In structural analysis of a CNT, stiffness of the bonds will be represented by the space frame element of which the cross sectional parameters should be known. The method used to establish those parameters will be explained later.

Investigating the natural frequencies of these structures, the mass matrix should also be constructed and in that analogy it is obvious and fortunate that the lumped mass matrix model is perfectly fitting for the role of the carbon atoms located at the “joints” of the frames.

2.3 Linkage between Molecular and Structural Mechanics

In the structural network of the carbon nanotube, each carbon atom has three sp^2 bonding with its neighbors and forms hexagons on the wall of the tube. Each of these covalent bonds has characteristic bond lengths and bond angles. In molecular mechanics the total potential energy of a bond network is composed of both bonded and non-bonded interactions [30] as;

$$U = \sum U_r + \sum U_\theta + \sum U_\phi + \sum U_\omega + \sum U_{vdw} \tag{2.37}$$

where U_r is for bond stretch energy, U_θ is for a bond angle bending , U_ϕ is for a dihedral angle torsion, U_ω is for a out of plane torsion and U_{vdw} is for a non-bonded Van der Waals interaction.(See Figure 2.9)

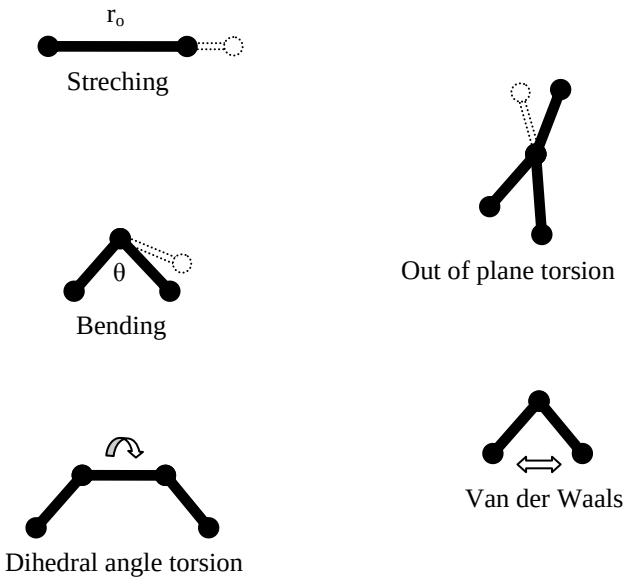

Figure 2.9 Bond interactions in Molecular Mechanics [30]

Li and Chou [30] presented that main contribution is done by mainly the first four components. For the sake of simplicity, the dihedral angle torsion and out of plane torsion are merged into a single equivalent term and can be expressed as follows;

$$U_r = \frac{1}{2}k_r(r - r_0)^2 = \frac{1}{2}k_r(\Delta r)^2 \tag{2.38}$$

$$U_\theta = \frac{1}{2}k_\theta(\theta - \theta_0)^2 = \frac{1}{2}k_\theta(\Delta\theta)^2 \tag{2.39}$$

$$U_\tau = \sum U_\phi + \sum U_\omega = \frac{1}{2}k_\tau(\Delta\phi)^2 \tag{2.40}$$

In which k_r k_θ k_τ are the bond stretching force constant, bond angle bending force constant and torsional resistance constant respectively. Also Δr, $\Delta\theta$, $\Delta\phi$ are the bond stretching increment, bond angle change and the twisting angle change of the bond.

Secondly, according to the classical structural mechanics, the strain energy of a uniform cross sectioned beam of length L is governed by the forces shown in Figure 2.10.

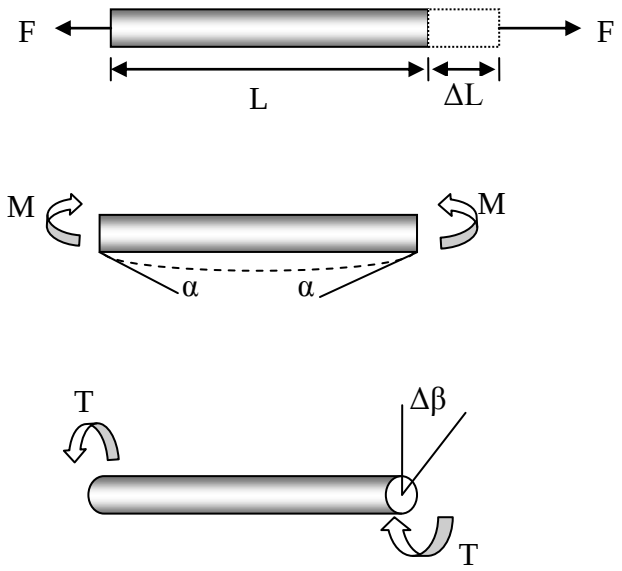

Figure 2.10 Axial, Bending and Torsional Deformations of a Frame Element [30]

The strain energy of a uniform beam of length L subjected to pure axial force of F is;

$$U_A = \frac{1}{2}\int_0^L \frac{F^2}{EA}dL = \frac{1}{2}\frac{F^2 L}{EA} = \frac{1}{2}\frac{EA}{L}(\Delta L)^2 \qquad (2.41)$$

where ΔL is the axial deformation.

The strain energy of a uniform beam of length L subjected to pure bending moment of M;

$$U_M = \frac{1}{2}\int_0^L \frac{M^2}{EI}dL = \frac{2EI}{L}\alpha^2 = \frac{1}{2}\frac{EI}{L}(2\alpha)^2 \qquad (2.42)$$

where α is the rotational angle at the ends of the beam. The strain energy of a uniform beam with circular cross section under pure torsion T is;

$$U_T = \frac{1}{2}\int_0^L \frac{T^2}{GJ}dL = \frac{1}{2}\frac{T^2 L}{GJ} = \frac{1}{2}\frac{GJ}{L}(\Delta\beta)^2 \tag{2.43}$$

where $\Delta\beta$ is the relative rotation between the ends of the beam.

So as Li and Chou [30] suggests both U_r and U_A represents the stretching energy, both U_θ and U_M represents the bending energy and both U_τ and U_T represent the torsional energy.

Comparing these equations, a direct linkage can be established between molecular mechanics parameters k_r, k_θ, k_τ and structural mechanics parameters $\frac{EA}{L}$, $\frac{EI}{L}$, $\frac{GJ}{L}$ as follows;

$$\frac{EA}{L} = k_r \tag{2.44}$$

$$\frac{EI}{L} = k_\theta \tag{2.45}$$

$$\frac{GJ}{L} = k_\tau \tag{2.46}$$

Fortunately, since the force constants k_r, k_θ, k_τ are known, equations (2.44), (2.45), (2.46) enable to obtain the necessary sectional stiffness parameters which will be substituted directly into elemental matrices in the source code. A number of studies focused on determining the cross sectional area of the bonds between C-C atoms. Tserpes and Papanikos [44] conducted a finite element model based analysis for CNT with different values of diameter for the bonds. A thickness of 0.340 nm gave

very close results to experimental studies. Obtaining the cross sectional area based on that value, necessary arrangements can be made to obtain the desired parameters as;

$$E = k_r \frac{L}{A} \tag{2.47}$$

$$I = \frac{k_\theta A}{k_r} \tag{2.48}$$

$$J = 2I \tag{2.49}$$

$$G = \frac{k_\tau L}{J} \tag{2.50}$$

Noteworthy that, these sectional parameters are the parameters of the bonds between carbon atoms and that are going to be used to find the natural frequencies and the modulus of elasticity of the whole nanotube.

2.4 Construction of CNT Geometry

In order to investigate the structural properties of nanotubes, first step is to build the truss-beam model. Since the aim is to create different amount of atom-vacancies on different types of nanotube, a parametrical geometry builder was developed. In that process, the main input parameters used to define the structure, are chirality and the total number of layers in either zigzag or armchair configuration.

Investigating the geometries of a CNT defined by (n,m) parameters, it is seen that a pattern exists.

For a zigzag (n,0) configuration;

- There are always n number of atoms at each layer
- Since m=0, all atoms are located at a diameter of $D = \frac{n}{\pi}\sqrt{3}a_{c-c}$
- On each layer, atoms are located by $\frac{360}{n}$ degrees apart
- Consecutive layers in +z direction are distanced by a pattern of $a_{c-c}, \frac{a_{c-c}}{2}, a_{c-c}, \frac{a_{c-c}}{2} \ldots$
- Numbering is done such that first node of each layer is located with a $\frac{360}{2n}$ degrees of angular offset with respect to the first atom of the previous layer.

Using the number of layers as the second input, the number of atoms is calculated directly as;

# of Atoms=# of Layers x n

Finally, the zigzag CNT is constructed in memory and can be visualized using the *plot3* [45] command of MATLAB. A demonstration for a (6,0) with 20 layers and 120 atoms is given in Figure 2.11;

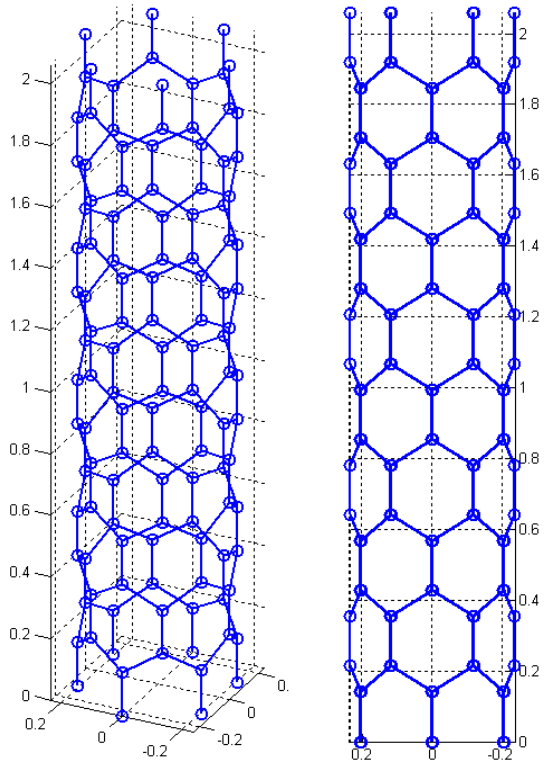

Figure 2.11 (6,0) 20 Layer Zigzag CNT Constructed with the Code

For an armchair (n,n) configuration;

- There are always 2n number of atoms at each layer
- All atoms are located at a diameter of $D = \frac{\sqrt{n^2 + m^2 + nm}}{\pi}\sqrt{3}a_{c-c}$
- Consecutive layers in +z direction are distanced by $\frac{\sqrt{3}}{2}a_{c-c}$
- Numbering is done such that first node of each layer is located with a $\frac{360}{3n}$ degrees of angular offset with respect to the first atom of the previous layer.

Finally the armchair CNT is constructed in memory and can be visualized using the *plot3* [45] command of MATLAB. A demonstration for a (6,6) with 10 layers and 120 atoms is given in Figure 2.12;

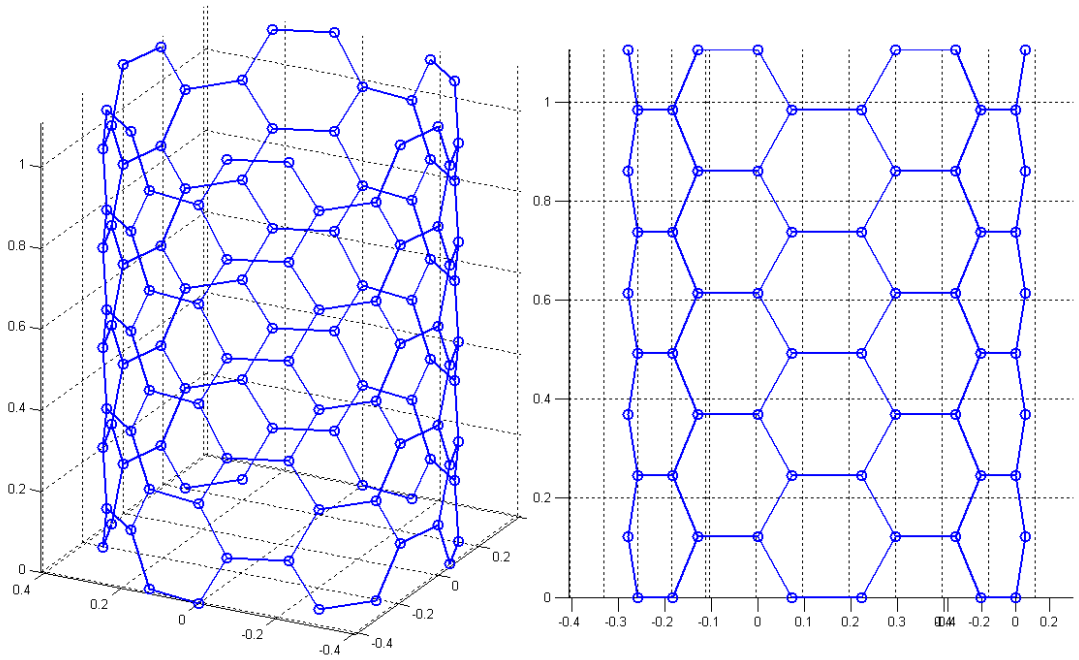

Figure 2.12 (6,6) 10 Layer Armchair CNT Constructed with the Code

In any case the methodology to locate the "beams" is to calculate the three dimensional distance of each atom with the whole atom cloud with the well-known equation;

$$Bondlength = \sqrt{x_i - x_j}^{\,2} + \sqrt{y_i - y_j}^{\,2} + \sqrt{z_i - z_j}^{\,2} \qquad (2.51)$$

A criterion was developed in this thesis to check if the two atoms at i and j are neighbor and bonding atoms.

$$0.95a_{c-c} \le Bondlength \le 1.05a_{c-c} \quad (2.52)$$

In this study %5 of tolerance is added, as a precaution, in order not to miss any bond because of any round off or truncation error of the coordinates stored in memory.
The output of the section is the connectivity matrix which identifies beams and its end point atoms. This is also used to plot the deformed/undeformed shapes and the vibration modes of the nanotubes in the post processing part.

2.5 Applying Boundary Conditions

Since the thesis focused on the practical use of CNT, it is inevitable to make the vibrational analysis in various constraint conditions. Common usages of CNT are mainly in cantilevered (fixed-free end configuration) and bridged (fixed-fixed end configuration) condition. In the developed algorithm partial extractions were made to free-free condition in free-free configuration in order to obtain the global mass and stiffness matrices of the restraint CNT in cantilevered or bridged configuration.

The methodology is such that for a cantilevered support CNT, the atoms at z=0 location have all degrees of freedom fixed. For instance for a (4,0) chirality nanotube, at z=0 there are 4 atoms which needs to be fixed. Nodes that are pointed with a black arrow in Figure 2.13 need to be restraint for a cantilevered boundary condition.

On the other hand for a bridged configuration, algorithm picks up the nodes at maximum +z direction and designate them the other end for the bridged configuration. Nodes that are pointed by red arrow in Figure 2.13 need to be restraint and the DOF correspond to these atoms should be zero. The arrows are used to point out the atoms that need to be constraint and does not represent any kind of force or moment in these figures.

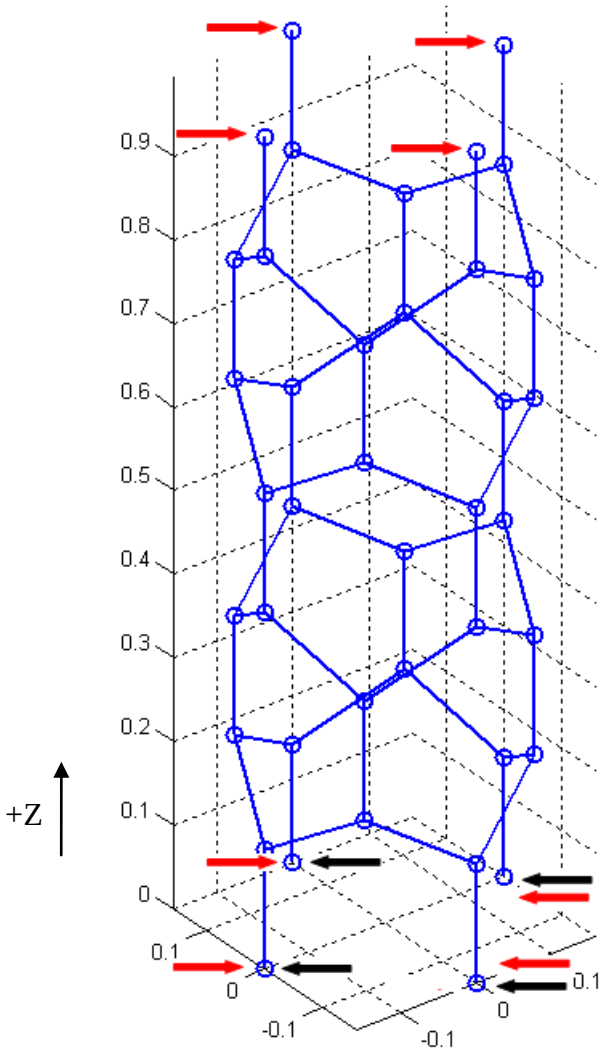

Figure 2.13 Application of Boundary Conditions in Cantilevered and Bridged Configurations for Zigzag Configuration

Secondly a similar approach was followed and for a zigzag configuration of (4,4) the network is such that there are 8 atoms on both ends. At z=0 there are 8 atoms which needs to be fixed. Atoms that are pointed by black arrow in Figure 2.14 need to be restraint for a cantilevered boundary condition. On the other hand for a bridged configuration, algorithm picks up the nodes at maximum +z direction and designates

them as the other end for the bridged configuration. The ones that are pointed by red arrow in need to be restraint and the DOF correspond to these atoms should be zero.

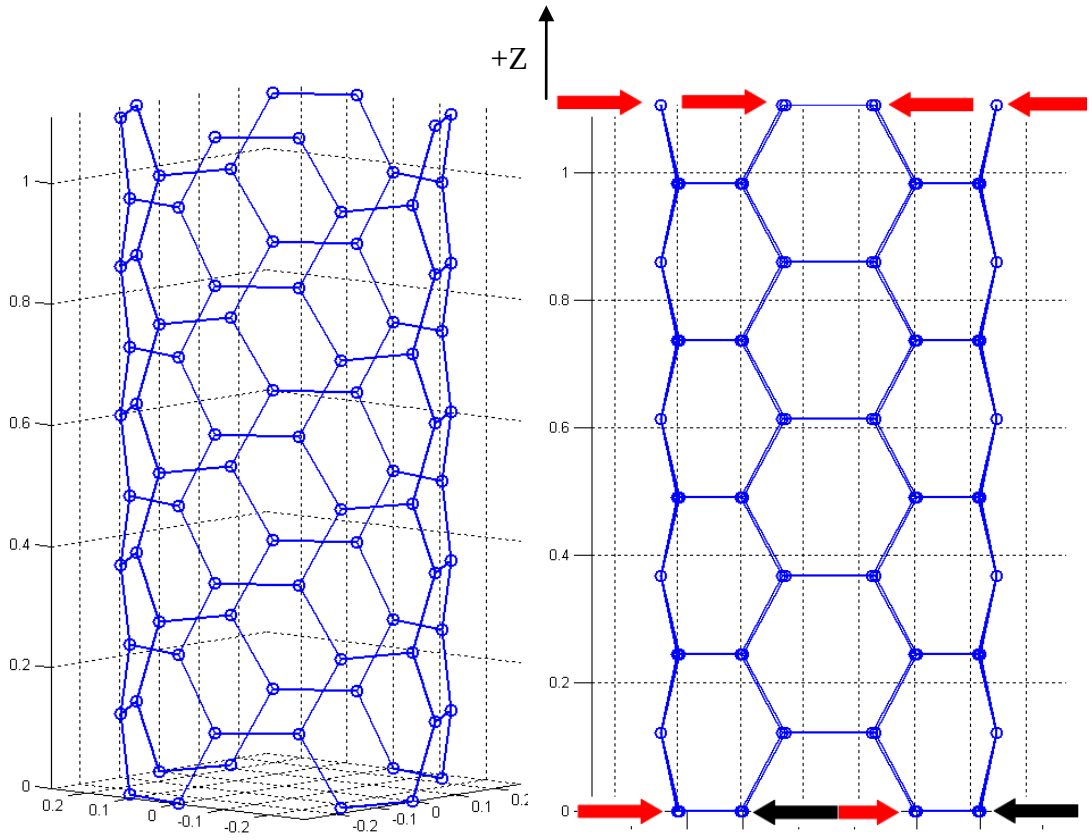

Figure 2.14 Isometric and Front View of an Armchair CNT and Application of Boundary Conditions on CNT

The first step is to obtain the free-free condition of the whole structure and previously described since the C-C are represented with space frame elements, for an N number of atoms, the size of the global stiffness and global mass matrices will be 6Nx6N as;

$$\underbrace{K_{GLOB}}_{6Nx6N}=\begin{pmatrix} k_{1,1} & \cdots & k_{1,6N} \\ \vdots & \ddots & \vdots \\ k_{6N,1} & \cdots & k_{6N,6N} \end{pmatrix} \tag{2.53}$$

$$\underbrace{M_{GLOB}}_{6Nx6N}=\begin{pmatrix} m_{1,1} & \cdots & m_{1,6N} \\ \vdots & \ddots & \vdots \\ m_{6N,1} & \cdots & m_{6N,6N} \end{pmatrix} \tag{2.54}$$

As explained, for a cantilevered zigzag nanotube of (n,0) with N number of atoms, since at z=0 there are n number of atoms, stiffness and mass matrices should be extracted from free –free matrices as;

$$\underbrace{K_{GLOB\_CANT}}_{6N-6nx6N-6n}=\begin{pmatrix} k_{1+6n,1+6n} & \cdots & k_{1+6n,6N} \\ \vdots & \ddots & \vdots \\ k_{6N,1+6n} & \cdots & k_{6N,6N} \end{pmatrix} \tag{2.55}$$

$$\underbrace{M_{GLOB\_CANT}}_{6N-6nx6N-6n}=\begin{pmatrix} m_{1+6n,1+6n} & \cdots & m_{1+6n,6N} \\ \vdots & \ddots & \vdots \\ m_{6N,1+6n} & \cdots & m_{6N,6N} \end{pmatrix} \tag{2.56}$$

For (n,0) since at z=0 and z_{max} locations there are n number of atoms, stiffness and mass matrices of bridged configuration should be as;

$$\underbrace{K_{GLOB\_BRID}}_{6N-12nx6N-12n}=\begin{pmatrix} k_{1+6n,1+6n} & \cdots & k_{1+6n,6N-6n} \\ \vdots & \ddots & \vdots \\ k_{6N-6n,1+6n} & \cdots & k_{6N-6n,6N-6n} \end{pmatrix} \tag{2.57}$$

$$\underbrace{M_{GLOB\_BRID}}_{6N-12nx6N-12n} = \begin{pmatrix} m_{1+6n,1+6n} & \cdots & m_{1+6n,6N-6n} \\ \vdots & \ddots & \vdots \\ m_{6N-6n,1+6n} & \cdots & m_{6N-6n,6N-6n} \end{pmatrix} \tag{2.58}$$

Secondly, for a cantilevered armchair nanotube of (n,n) with N number of atoms, since at z=0 there are 2n number of atoms, stiffness and mass matrices should be extracted from free–free matrices as;

$$\underbrace{K_{GLOB\_CANT}}_{6N-12nx6N-12n} = \begin{pmatrix} k_{1+12n,1+12n} & \cdots & k_{1+12n,6N} \\ \vdots & \ddots & \vdots \\ k_{6N,1+12n} & \cdots & k_{6N,6N} \end{pmatrix} \tag{2.59}$$

$$\underbrace{M_{GLOB\_CANT}}_{6N-12nx6N-12n} = \begin{pmatrix} m_{1+12n,1+12n} & \cdots & m_{1+12n,6N} \\ \vdots & \ddots & \vdots \\ m_{6N,1+12n} & \cdots & m_{6N,6N} \end{pmatrix} \tag{2.60}$$

For (n,n) armchair configuration since at z=0 and z_{max} locations there are 2n number of atoms each, stiffness and mass matrices of bridged configuration should be as;

$$\underbrace{K_{GLOB\_BRID}}_{6N-24nx6N-24n} = \begin{pmatrix} k_{1+12n,1+12n} & \cdots & k_{1+12n,6N-12n} \\ \vdots & \ddots & \vdots \\ k_{6N-12n,1+12n} & \cdots & k_{6N-12n,6N-12n} \end{pmatrix} \tag{2.61}$$

$$\underbrace{M_{GLOB\_BRID}}_{6N-24nx6N-24n} = \begin{pmatrix} m_{1+12n,1+12n} & \cdots & m_{1+12n,6N-12n} \\ \vdots & \ddots & \vdots \\ m_{6N-12n,1+12n} & \cdots & m_{6N-12n,6N-12n} \end{pmatrix} \tag{2.62}$$

2.6 Atomic-Vacancy Creation

A method is designed to create atomic-vacancies on the wall of any kind of carbon nanotube and compare the mechanical and vibrational attributes of the defect-free nanotubes and nanotubes with atom-vacancy type defects. Previous procedures were developed for defectless tubes and create nanotubes that are ready to solve for vibrational analysis.

Since the aim of this study is to investigate the effect of vacancies a methodology is developed to induce vacancies. As in the real case of atomic-vacancy creation by pulses of irradiation exposure, the idea is to remove randomly positioned or specifically selected atoms. In this thesis, different techniques for vacant atom selection were used. One of them is to have randomly positioned vacancies with increasing percentages of vacancies .The amount of vacant atoms is determined by an input given at the beginning of the code. The randomizer is modeled to be excluding defects at both ends of CNT in order not to violate the boundary conditions. MATLAB *rand* [45] function is used to randomly select the vacant atoms in the walls.

Also a part of the algorithm checks whether the randomly selection mechanism stored same value twice for a vacant atom. In that case that random selection is neglected and the randomizer runs again and replaces that vector of numbers for that particular analysis.

For each analysis, since the vacant atoms are stored, new numbering of nodes is done and for any missing node number the next node is stacked. By this way, the total number of nodes is reduced by the amount of vacant atoms. The connectivity matrix builder was utilized to rebuild the updated beam connectivity matrix and store it for later assemble process and visualization.

For the sake of clarification, Figure 2.15 is presented to visualize the final network of the nanotube. The vacancy position is shown with a red arrow.

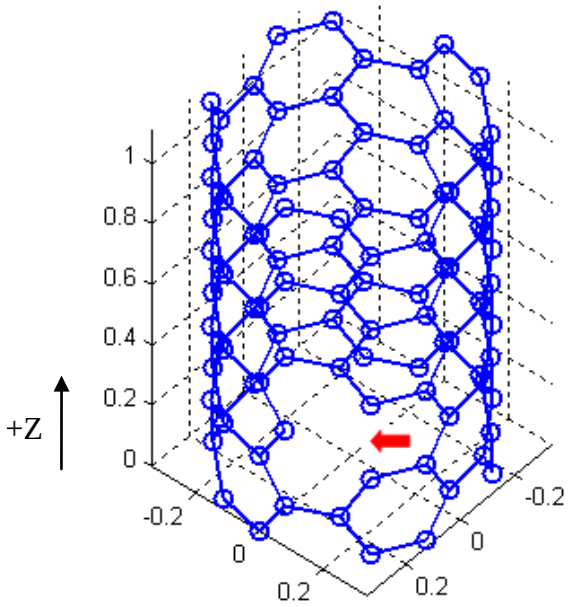

Figure 2.15 An Armchair Nanotube with One Atomic-Vacancy Implemented

Second type of analysis is utilized to determine the effect of the position of a vacant atom through all length of the CNT. By this way for varying kinds of equal length CNT, the effect of one vacant atom on the nanotubes first five cantilevered and bridged mode natural frequencies are plotted with a dimensionless position variable $\frac{Z}{L}$ where Z is the z coordinate of the atom extraction and L is the total length of that nanotube. The algorithm was designed to dislocate one atom in consecutive order, shown with red arrows in Figure 2.16 and the natural frequencies of the defected nanotubes were stored in memory.

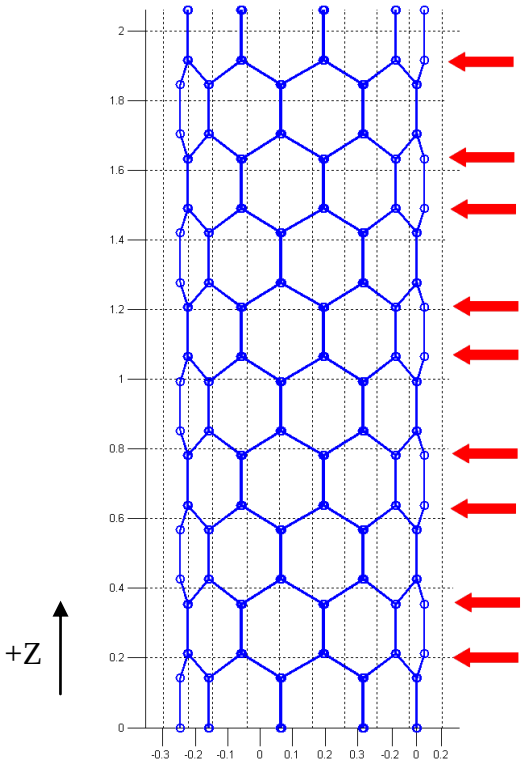

Figure 2.16 Atoms Extracted in the Analysis of Position of Vacancy

For any vacancy analysis, as can be interpreted, the total number of DOF is also reduced by an amount of 6 x #of vacant nodes. Hence all the new modified global K and M matrices for both cantilevered and bridged configurations are also reduced by the same amount.

One idea inevitably that comes to mind is that this kind of vacancy should create an instability in the network of the nanotube so the CNT shall need to rearrange C atoms. As proposed in [40] and [41], this kind of modeling tends to give very close and accurate results compared to a reconstructed model of C bonds. So with this assumption the bond lengths of the defected tube were not modified.

CHAPTER 3

A CASE STUDY ON EFFECT OF VACANCIES ON YOUNG'S MODULUS OF SWCNT

Even though this study mainly focused on the effect of vacancies on the vibrational properties of carbon nanotubes, the source code is written in such a way that it can easily be used to find the deformation of the nanotube under certain tension or compression forces. It is comparatively easier to find the deformed and repositioned coordinates of the nodes than finding the modal frequencies and shapes of the whole tube. The idea is simply based on the previously mentioned equation;

$$K \quad u \quad = \quad f \tag{3.1}$$

The aim is to have the cantilevered stiffness matrix of either the defectless or the vacancy-implemented nanotube. As explained earlier, the cantilevered nanotube stiffness matrix should be extracted in the size determined by the number of nodes and chirality.

For a zigzag configuration;

$$\underbrace{K_{GLOB\_CANT}}_{6N-6nx6N-6n} = \begin{pmatrix} k_{1+6n,1+6n} & \cdots & k_{1+6n,6N} \\ \vdots & \ddots & \vdots \\ k_{6N,1+6n} & \cdots & k_{6N,6N} \end{pmatrix} \tag{3.2}$$

where N is the number of nodes and n is the chirality parameter.

$$\underbrace{u}_{(6N-6n)x1} = \begin{Bmatrix} u_1 \\ u_2 \\ u_3 \\ . \\ . \\ . \\ u_{6(N-n)-2} \\ u_{6(N-n)-1} \\ u_{6(N-n)} \end{Bmatrix} \tag{3.3}$$

where $6\ N-n$ number of displacements components correspond to x,y,z displacements and rotation about x,y,z axes of each node respectively. As the third step, the generalized force vector should be constructed with a known magnitude of force in positive z direction, to be distributed at the n number of nodes on the free end of a zigzag nanotube as;

$$\underbrace{f}_{(6N-6n)x1} = \left\{ 0 \quad 0 \quad 0 \quad . \quad . \quad . \quad 0 \quad 0 \quad \frac{F_T}{n} \quad 0 \quad 0 \quad 0 \quad 0 \quad 0 \quad \frac{F_T}{n} \quad 0 \quad 0 \quad 0 \right\}^T \tag{3.4}$$

For an armchair configuration of (n,n) CNT, the matrices should be constructed as;

$$\underbrace{K_{GLOB\_CANT}}_{6N-12nx6N-12n} = \begin{pmatrix} k_{1+12n,1+12n} & \cdots & k_{1+12n,6N} \\ \vdots & \ddots & \vdots \\ k_{6N,1+12n} & \cdots & k_{6N,6N} \end{pmatrix} \tag{3.5}$$

where N is the number of nodes and n is the chirality parameter and there are 2n number of nodes on the fixed DOF side.

$$\underbrace{u}_{(6N-12n)x1} = \begin{Bmatrix} u_1 \\ u_2 \\ u_3 \\ . \\ . \\ . \\ u_{6(N-2n)-2} \\ u_{6(N-2n)-1} \\ u_{6(N-2n)} \end{Bmatrix} \tag{3.6}$$

This time, the generalized force vector should be constructed with a known force in positive z direction, to be distributed at the 2n number of nodes on the free end of a zigzag nanotube as;

$$\underbrace{f}_{(6N-12n)x1} = \left\{ 0 \quad 0 \quad 0 \quad . \quad . \quad . \quad 0 \quad 0 \quad \frac{F_T}{2n} \quad 0 \quad 0 \quad 0 \quad 0 \quad 0 \quad \frac{F_T}{2n} \quad 0 \quad 0 \quad 0 \right\}^T \tag{3.7}$$

At this point, having these matrices next step is to obtain the axial z axis displacements of nodes by simply multiplying both sides of the Eq(3.1) with the inverse of stiffness matrix as;

$$K^{-1} K \; u = K^{-1} \; f \tag{3.8}$$

From which displacements can be obtained as;

$$u = K^{-1} \; f \tag{3.9}$$

Using this data, the z-axis of the displacements of the end nodes are utilized to find and substitute for the elongation amount in the equation;

$$E = \frac{\frac{F_T}{A}}{\frac{\Delta L}{L}} \tag{3.10}$$

where E is the Young's Modulus, F_T is the total tension force applied on the nodes of free end of the tube, ΔL is the elongation and L is the total length of the tube.

In this case, A the cross-sectional area of the tube is found from a hollow tube approximation built by the thickness of the bonds and diameter of the nanotubes as shown in Figure 3.1.

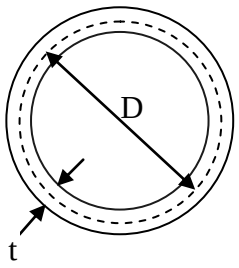

Figure 3.1 Area Cross-section of the CNT

So the area of cross-section can be taken as;

$$A = \pi\left(\left(\frac{D}{2} + \frac{t}{2}\right)^2 - \left(\frac{D}{2} - \frac{t}{2}\right)^2\right) \tag{3.11}$$

For the calculation of Young's Modulus of a defectless CNT, the ΔL is taken as one of the same values for the z-axis displacement of any end nodes. On the other hand, when a vacancy is implemented, the deformation on the end nodes differs because of

the structural asymmetry caused by the vacancy. Figure 3.2 can be beneficial to visualize a condition where the vacancy happens to be close to the end where tensile force is applied. Yellow arrow indicates the fixed end where green arrow pointing the vacancy and the blue one shows the differently elongated nodes. In this case taking one of the displacements may lead to an incorrect result.

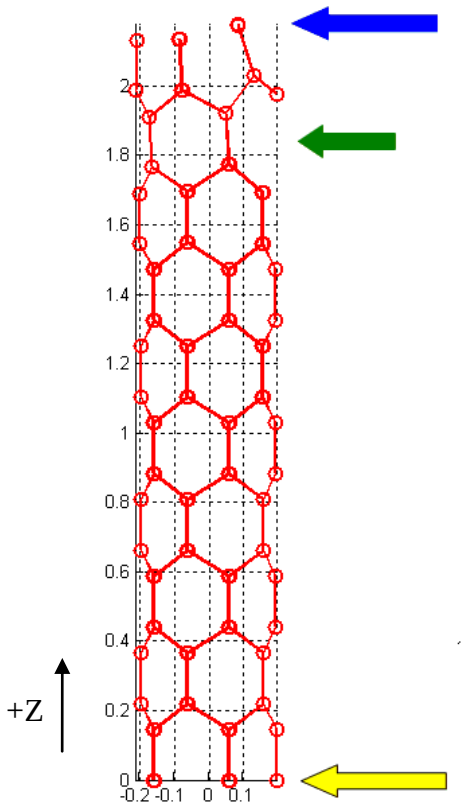

Figure 3.2 Vacancy Implemented Deformed CNT under Tensile Force

A concept is utilized in order not to have wrong conclusions for the effect of vacancies on Young's Modulus of Elasticity. The elongation term in Eq(3.10) is replaced with the average of the sum of all z-axis displacements of the end nodes.
For a zigzag configuration;

$$\Delta L = \frac{\sum_{0}^{n-1} u_{(N-n-3)-6n}}{n} \tag{3.12}$$

For an armchair configuration;

$$\Delta L = \frac{\sum_{0}^{2n-1} u_{(N-2n-3)-6n}}{2n} \tag{3.13}$$

The terms on the numerators are the z-axis displacement found from the matrix multiplication of Eq(3.1). In the results section, the effect of different amount of vacancies on the elastic modulus will be given.

CHAPTER 4

VERIFICATION

In this thesis a verification model was also developed in order to verify the cross-sectional parameters, elemental stiffness functions, assemble functions and the solver function in the code. A commercial FEA software, ANSYS 11 Classic, was used to model the carbon nanotubes with the xyz coordinates extracted from the code. The method is to create an input using the parameters of that particular analysis automatically that can be read by ANSYS to make a structural or vibrational analysis.

In order to construct the truss-beam model, BEAM4 and MASS 21 elements were selected to model the bonds and joints. All the parameters and the constants are transferred to the input file created by the source code. A shortened version is given in Appendix B.

The commands were used as input for both defect-free and atomically-vacant nanotubes, and a verification analysis could be made. (See App B) This input data file automatically creates the elements in ANSYS and locates the beams between “atom” nodes according to the connectivity matrix information

The selected element BEAM4 is a uni-axial element with tension, compression, torsion and bending capabilities. The element has six degrees of freedom at each node, translations in the nodal x, y and z directions and rotations about the nodal x, y and z axes. Parameters of the BEAM4 element are shown as;

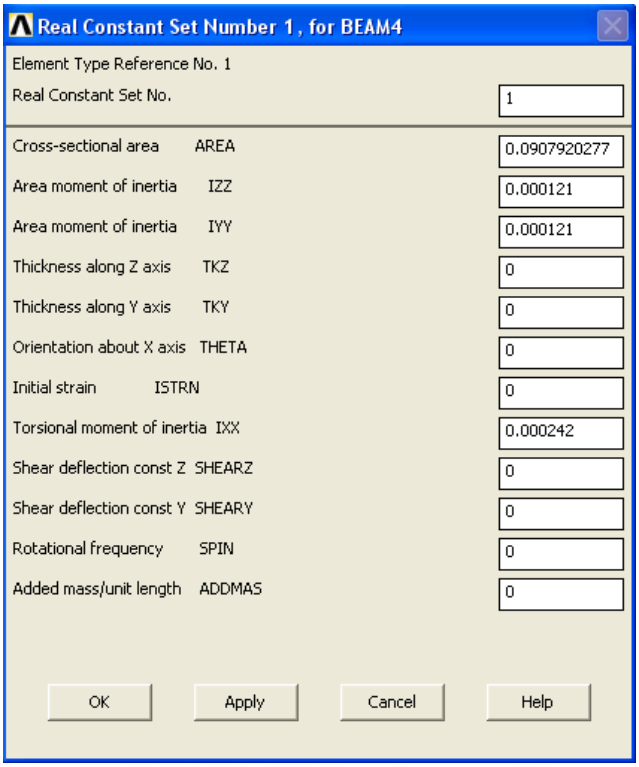

Figure 4.1 Cross-sectional Parameters of BEAM4 Element used in FE Analysis

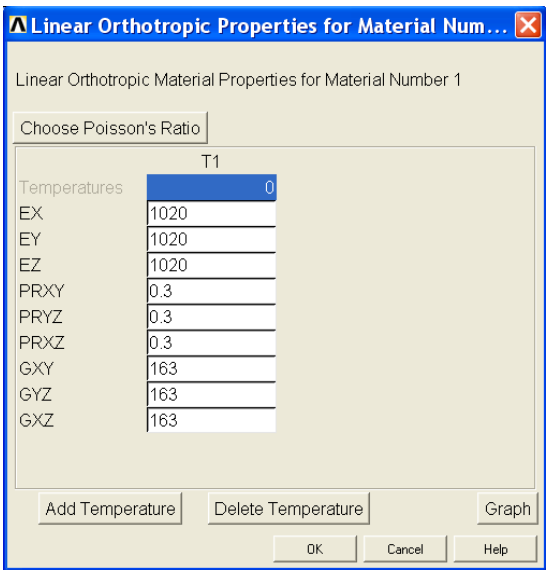

Figure 4.2 Material Properties of BEAM4 Element used in FE Analysis

Secondly MASS21 is a point element having up to six degrees of freedom: translations in the nodal x, y, z directions and rotations about x, y and z axes. Parameters of the MASS21 element can be shown in Figure 4.3.

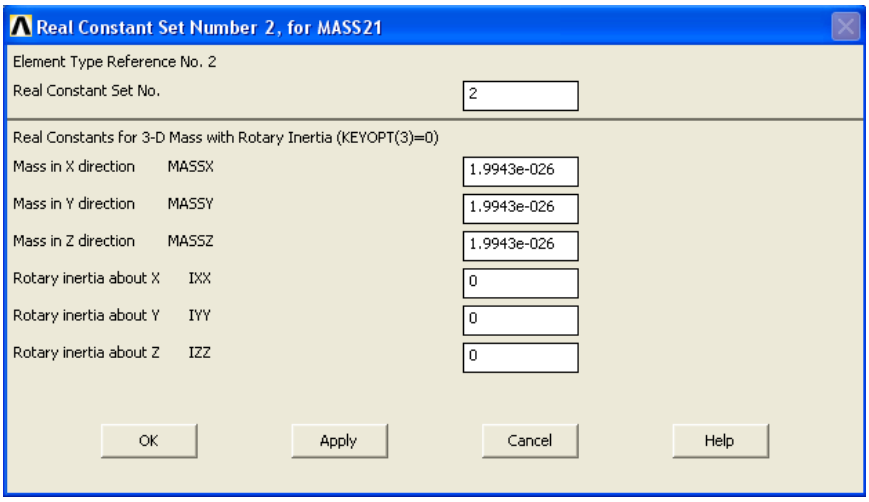

Figure 4.3 Mass Properties of MASS21 Element used in FEA

The boundary conditions of cantilevered or bridged were also implemented on the FEA model and can be seen as;

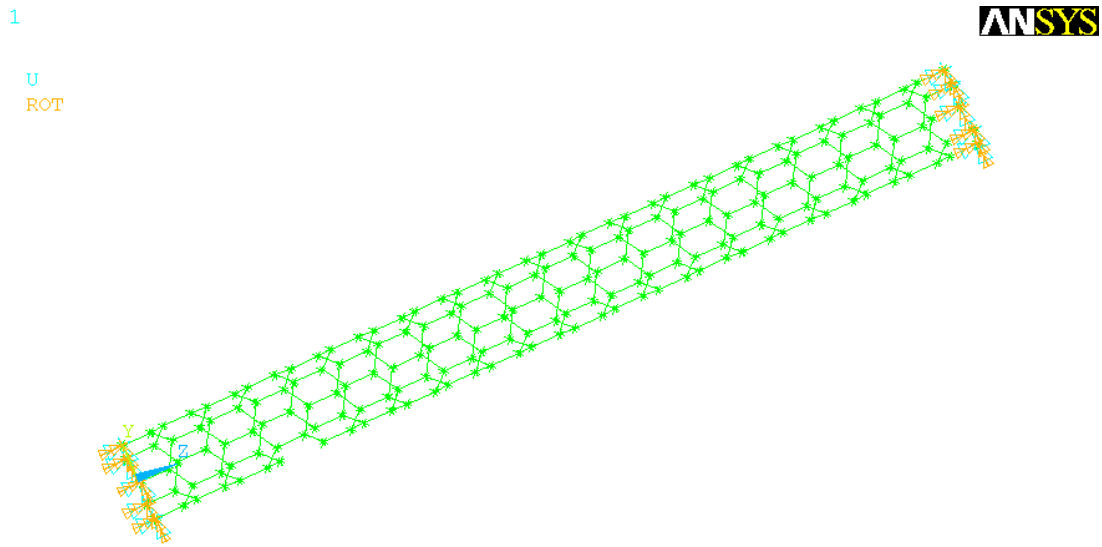

Figure 4.4 Boundary Condition Implemented CNT

Mode shapes and natural frequencies could be verified using ANSYS post processing capabilities.

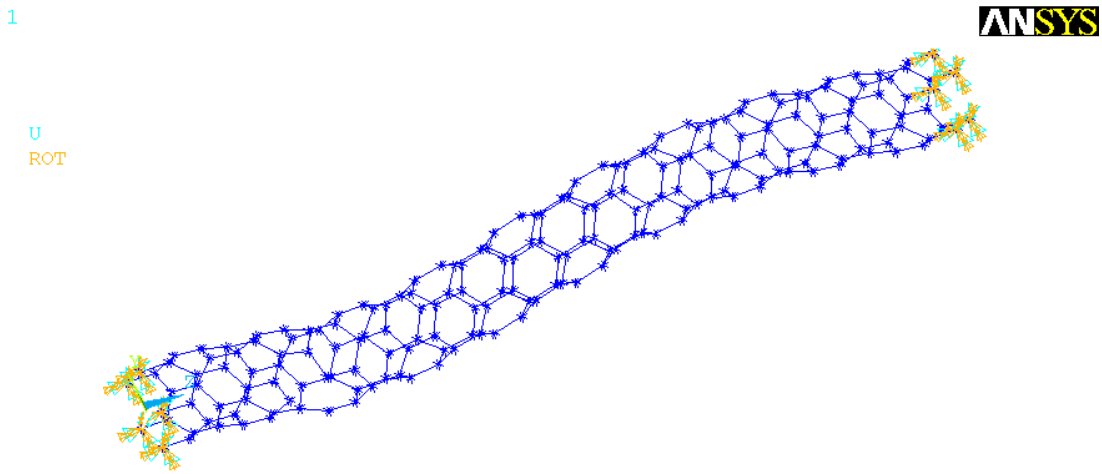

Figure 4.5 Mode Shape of a Bridged Configuration CNT

Since the effect of vacancies on Young's Modulus was investigated, the verification was also done by ANSYS by applying tensile forces on one end of the nanotube.

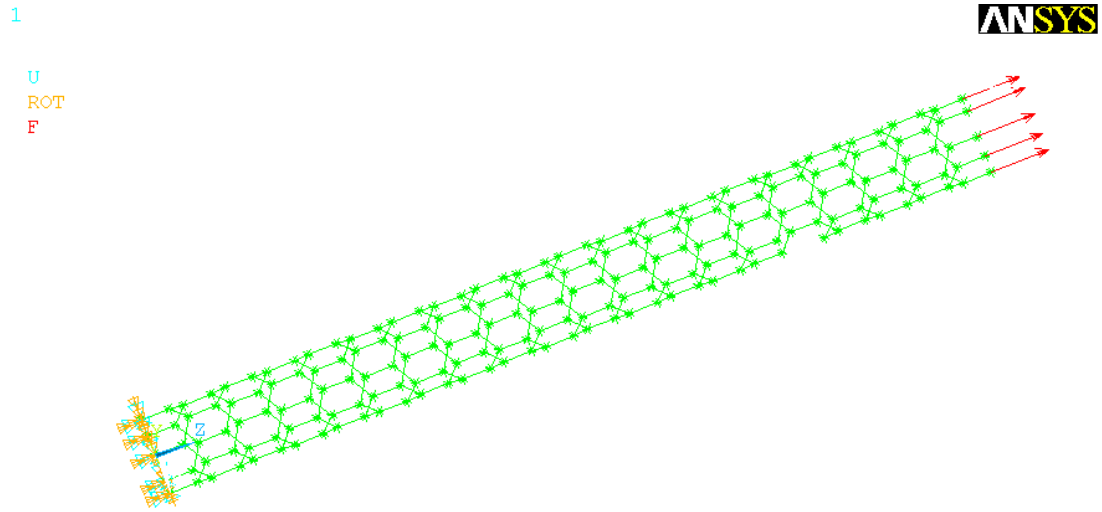

Figure 4.6 Tensile Force Applied CNT

In the post processing phase, the displacements of each node are obtained from ANSYS and used to verify the data obtained with the source code.

CHAPTER 5

RESULTS AND DISCUSSION

In this chapter the results obtained from numerical analyzes will be presented and discussed in detail.

5.1 Effects of Randomly Positioned Atom-Vacancies on First Bridged and Cantilevered Natural Frequencies of Zigzag CNT

The effect of increasing-amount of vacancies in randomly chosen position on fundamental frequencies of various kinds of nanotubes is investigated and plotted. In the first part, a set of zigzag nanotubes varying from (4-0) to (9-0) chirality were implemented with equal percentages of vacancies and reduction in the first cantilevered and bridged natural frequencies are plotted.

For any percentage of vacancies applied, 100 iterations were carried out and the maximum, minimum and average values are stored. The analyses were conducted on the same length and different chiralities of CNT for both zigzag and armchair configuration. Figure 5.1 is the graph of average values of percent reductions on First bridged natural frequencies of zigzag nanotube against different amount of vacancies. Results of different chiralities are designated with chiralities shown in forms of (n, 0) and (nun) on the right sides of the plots.

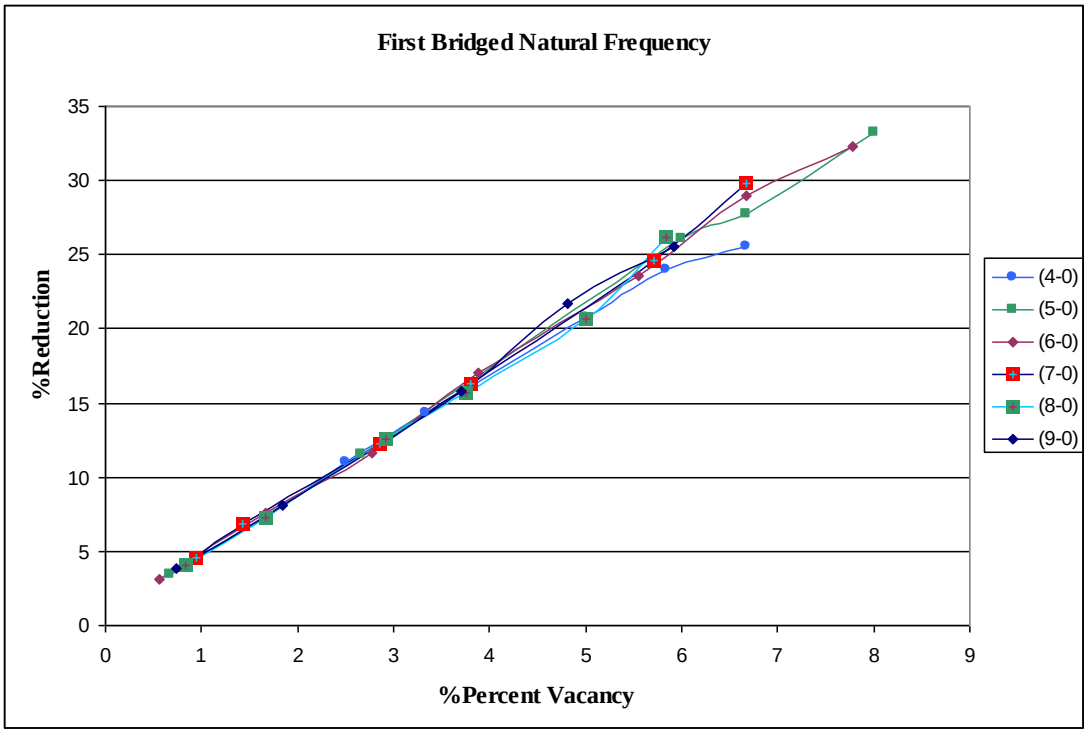

Figure 5.1 Percent Reduction in First Bridged Natural Frequency of Zigzag Nanotubes versus Percent Vacancy

As can be seen even with an amount of 100 iterations at each percentage of all chirality, the reduction is almost linear with vacancies. Also chirality is not a major parameter determining the defected CNT natural frequencies. For any type of zigzag configuration CNT, at about %8 percentage of vacancy among the total number of atoms can decrease the first bridged natural frequency about %33.

Second set of results show the percent reduction in the first cantilevered natural frequencies of zigzag nanotubes. As can be seen, the chirality is not a major parameter affecting the strength of the nanotube against vacancies. Based on average values of percent reduction cantilevered natural frequencies seemed to be affected more with imperfections. For the same length of nanotube with the same percentage

of vacancies CNT tend to be more affected and the first cantilevered natural frequencies decrease more.

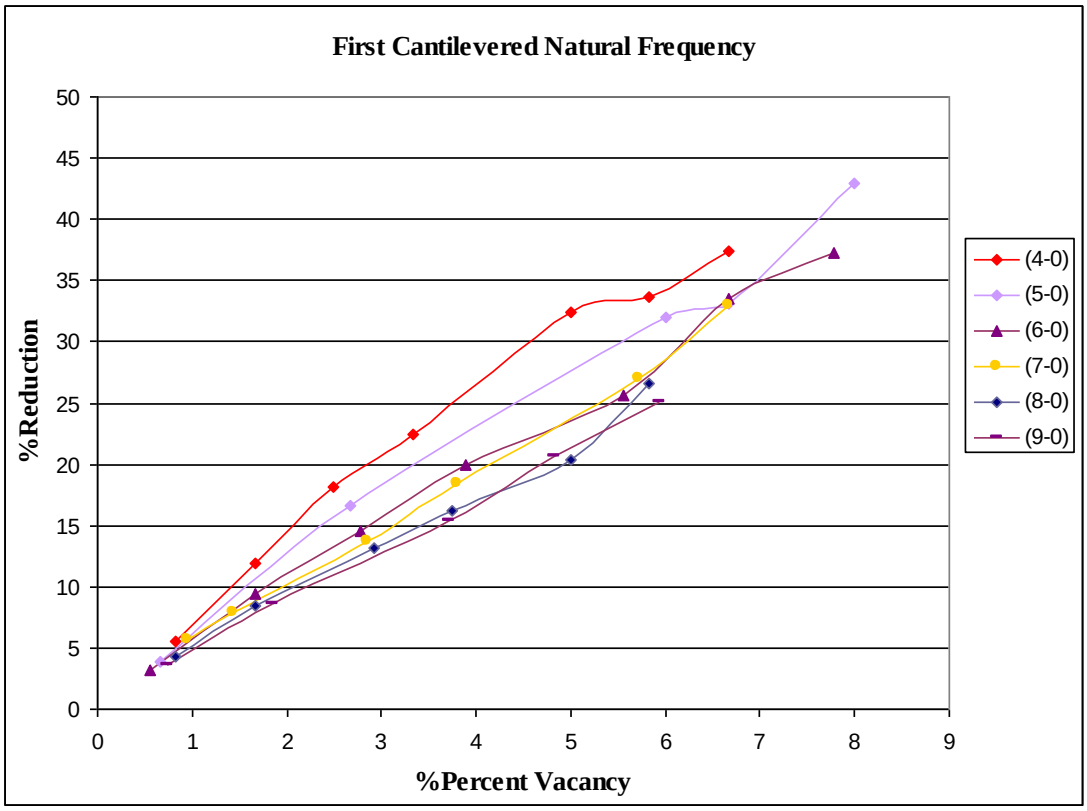

Figure 5.2 Percent Reduction in First Cantilevered Natural Frequency of Zigzag Nanotubes versus Percent Vacancy

5.2 Effects of Randomly Positioned Atom-Vacancies on First Bridged and Cantilevered Natural Frequencies of Armchair CNT

Since the zigzag and armchair configurations differ in bonding structure, the effect of vacancies on armchair configuration is also investigated and the reduction in first bridged natural frequency is plotted in Figure 5.3. The analyses were completed on the same length of armchair nanotubes from (4-4) to (9-9).

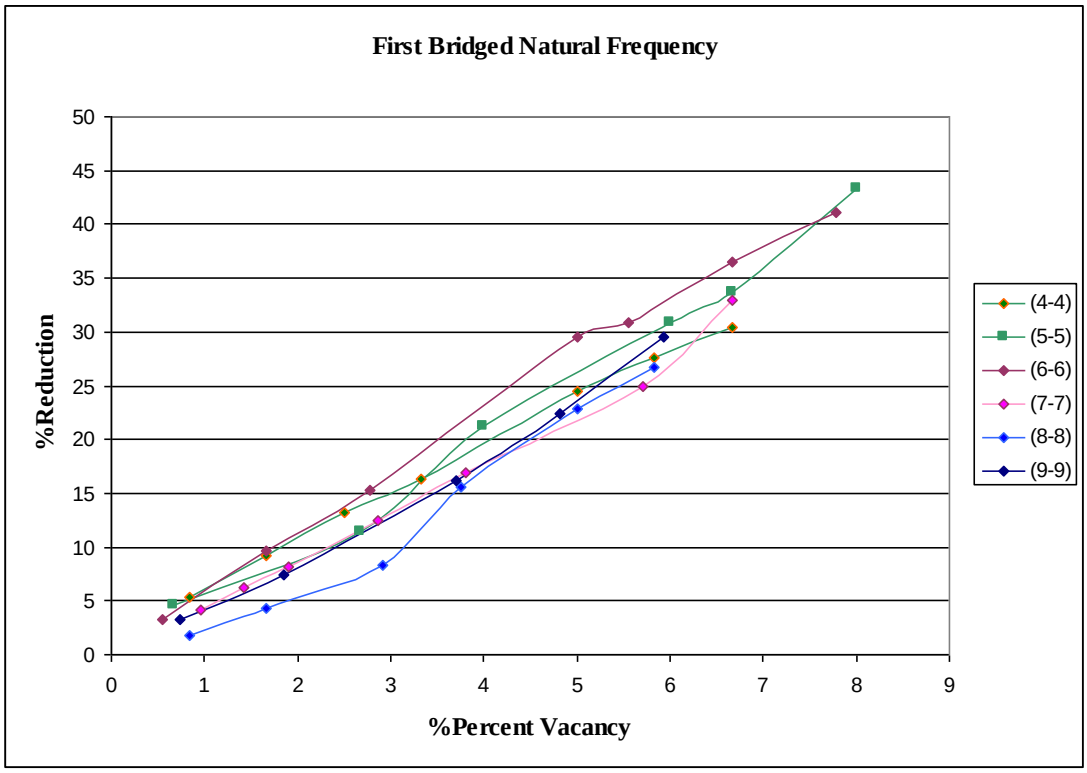

Figure 5.3 Percent Reduction in First Bridged Natural Frequency of Armchair Nanotubes versus Percent Vacancy

Regarding the different type of chirality and bonding network, slight offsets exist between each set. Each trend between percent reduction in natural frequency and percent vacancy can be approximated to be linear.

The graph of effect on vacancies on the cantilevered natural frequencies of armchair configuration with different amount of vacancies is given in Figure 5.4. Similar trends can be observed in the reduction amounts for each nanotube.

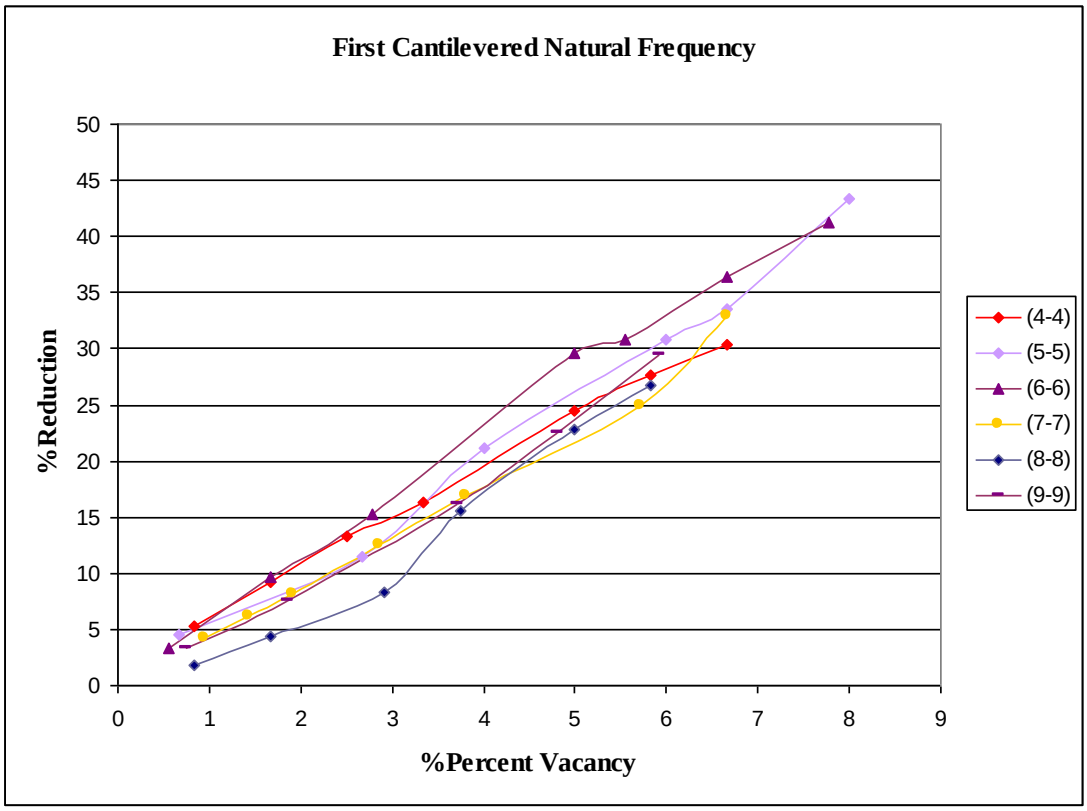

Figure 5.4 Percent Reduction in First Cantilevered Natural Frequency of Armchair Nanotubes versus Percent Vacancy

5.3 Effects of Randomly Positioned Atom-Vacancies on Second Bridged and Cantilevered Natural Frequencies of Zigzag CNT

Second part of the study mainly investigates the effect of boundary conditions on natural frequencies. To find out whether vacancies are that effective on other modes, same amount of analyses were carried out on the second natural frequencies of SWCNT.

Figure 5.5 is the graph of average values of percent reductions on second bridged natural frequencies of zigzag nanotube against different amount of randomly positioned vacancies.

Also as an interesting finding the amount of reduction of any chirality reaches only up to %25 for a vacancy amount of %8. Second modes are less affected than first mode of any type of boundary constraint.

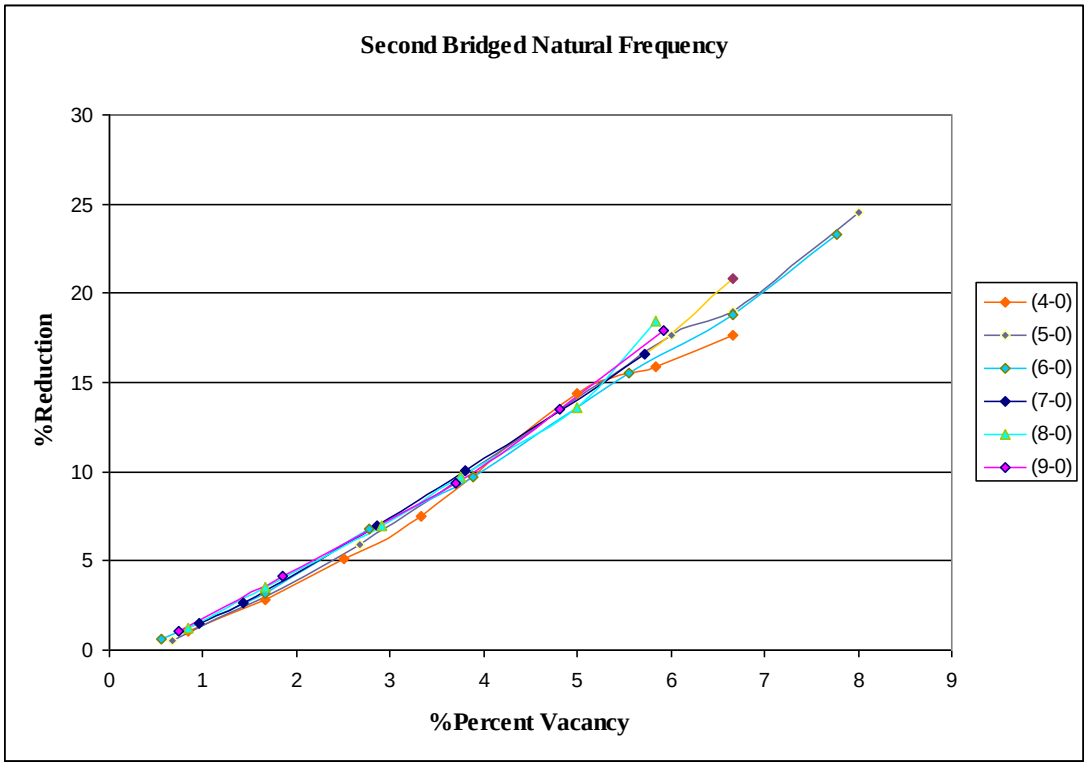

Figure 5.5 Percent Reduction in Second Bridged Natural Frequency of Zigzag Nanotubes versus Percent Vacancy

Figure 5.6 is showing the reduction effect on the second cantilevered natural frequency of zigzag configuration of nanotubes.

As compared to the first modes, second modes are less affected against vacancies and the amount of reduction is approximately the same as the bridged configuration. In addition to these, slight parabolic trends observed and the chirality does not affect the amount of reduction in natural frequencies.

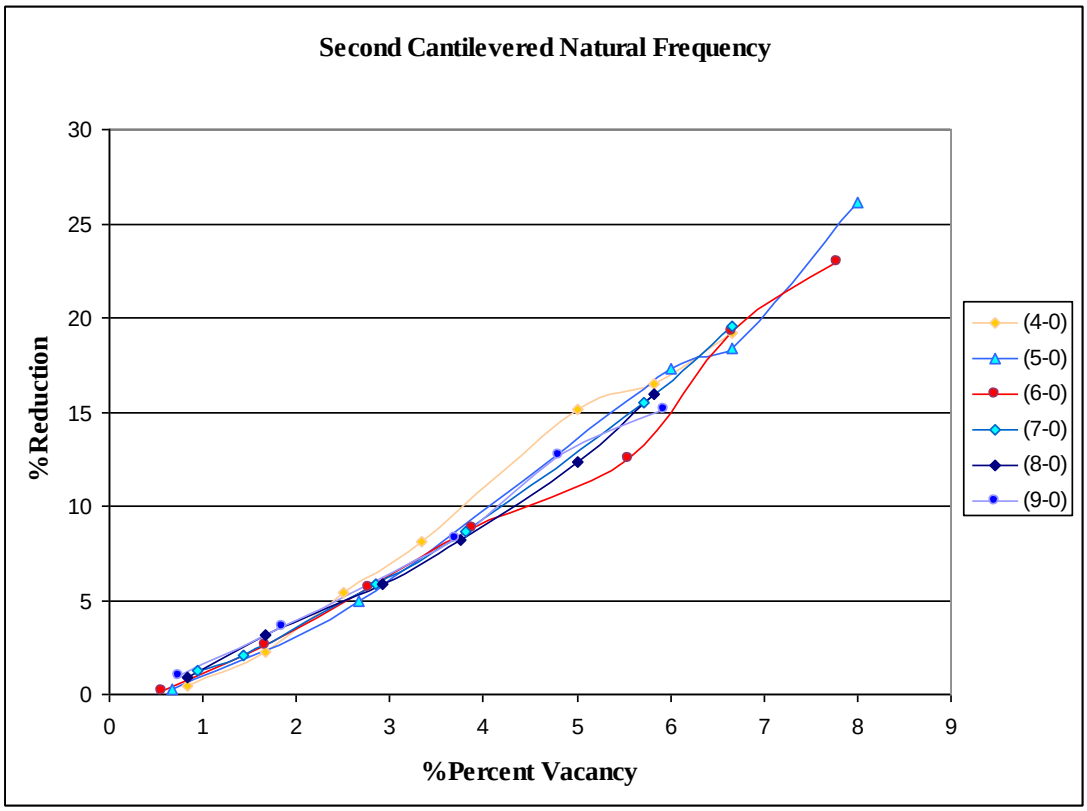

Figure 5.6 Percent Reduction in Second Cantilevered Natural Frequency of Zigzag Nanotubes versus Percent Vacancy

5.4 Effects of Randomly Positioned Atom-Vacancies on Second Bridged and Cantilevered Natural Frequencies of Armchair CNT

Also the effect of vacancies on second mode of armchair configuration is also presented in Figure 5.7 and Figure 5.8 for bridged and cantilevered conditions respectively.

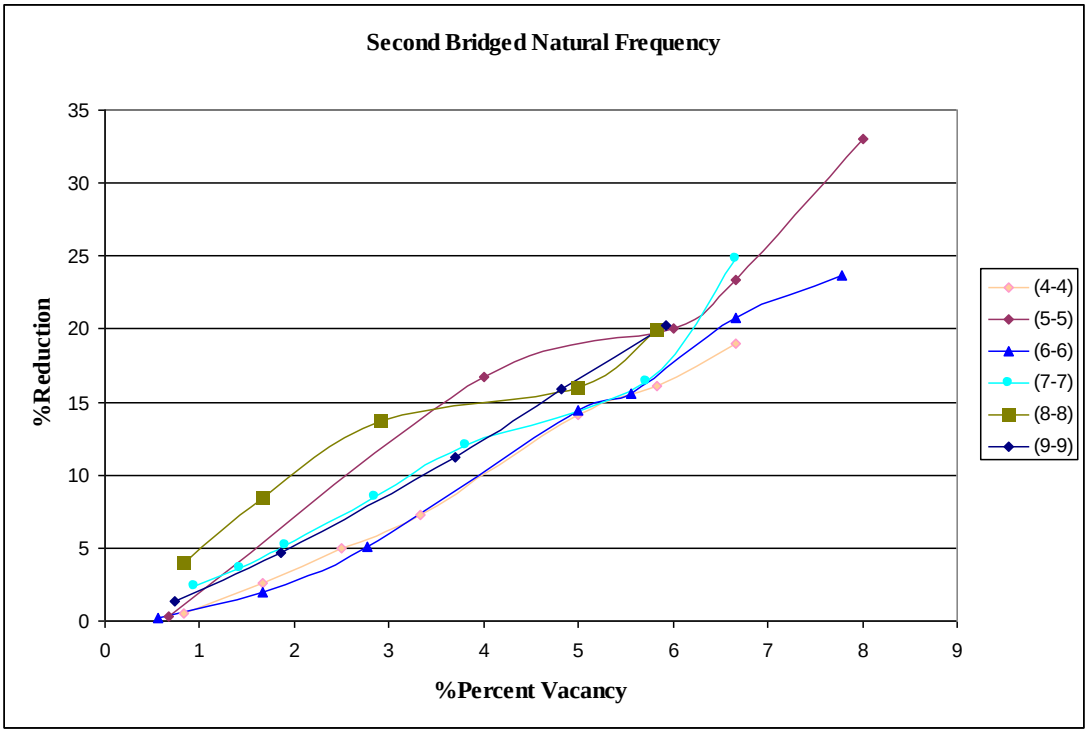

Figure 5.7 Percent Reduction in Second Bridged Natural Frequency of Armchair Nanotubes versus Percent Vacancy

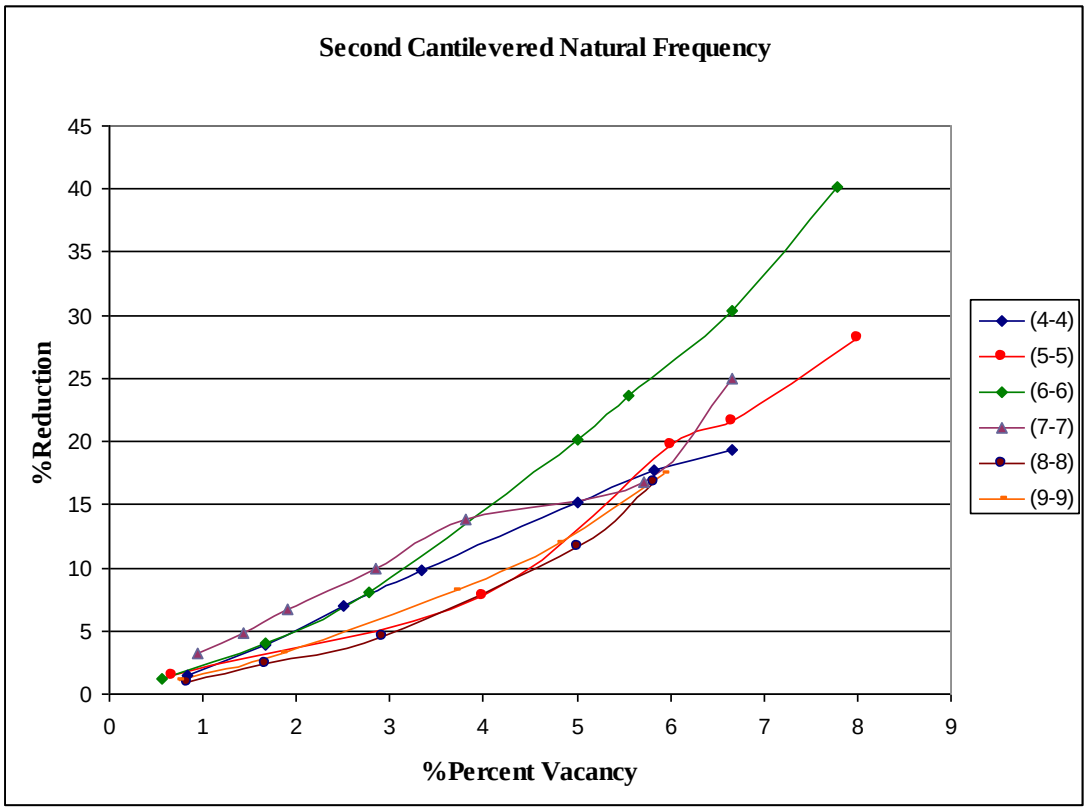

Figure 5.8 Percent Reduction in Second Cantilevered Natural Frequency of Armchair Nanotubes versus Percent Vacancy

5.5 Variations in Effects of Randomly Positioned Atom-Vacancies on First Bridged and Cantilevered Natural Frequencies of Zigzag CNT

Previous investigations were necessary to visualize the significant effect of vacancies on nanotubes. So at this point it is also beneficial to plot the variations of reductions as a result of different amount of vacancies and closeness to each other.

Every vertical bar represents the maximum and minimum reductions of 100 iterations of random positioning. The line around the middle of the lines is the average values of the reduction. Figure 5.9 and Figure 5.10 show the average, the

maximum and minimum values of reduction amount on a (4,0) zigzag configuration of nanotube. These variations show that specific positions of vacancies or accumulation of any amount may vary the resulting natural frequency of the defected nanotube.

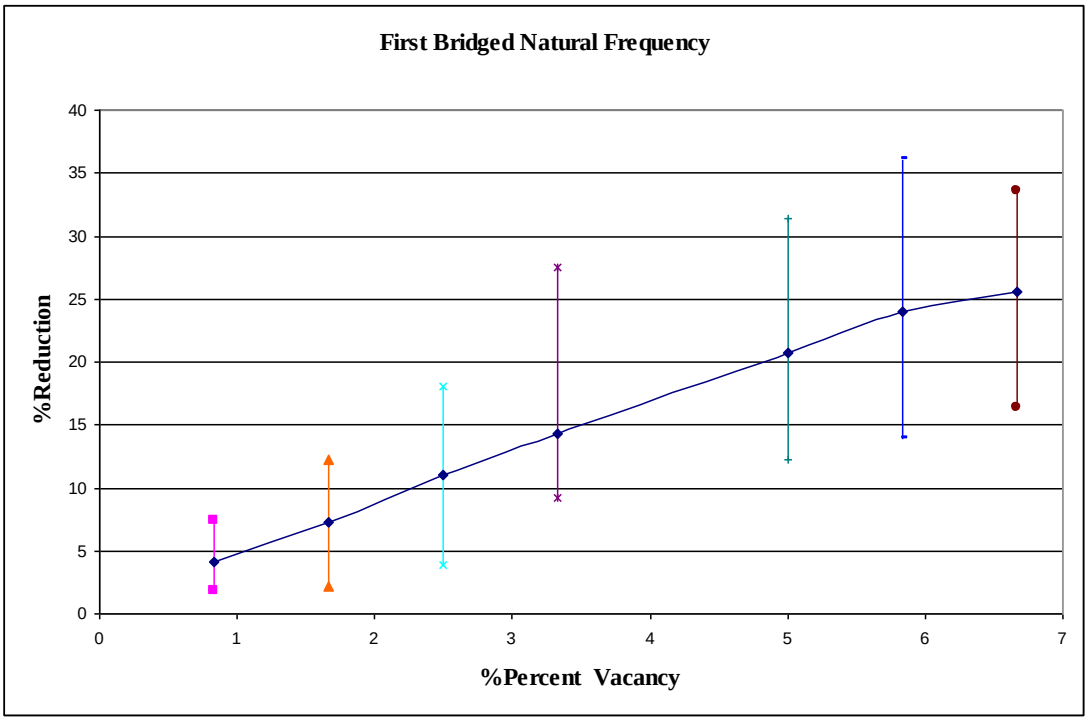

Figure 5.9 Maximum, Minimum and Average Values of Effects of Randomly Positioned Atom-Vacancies on First Bridged Natural Frequency

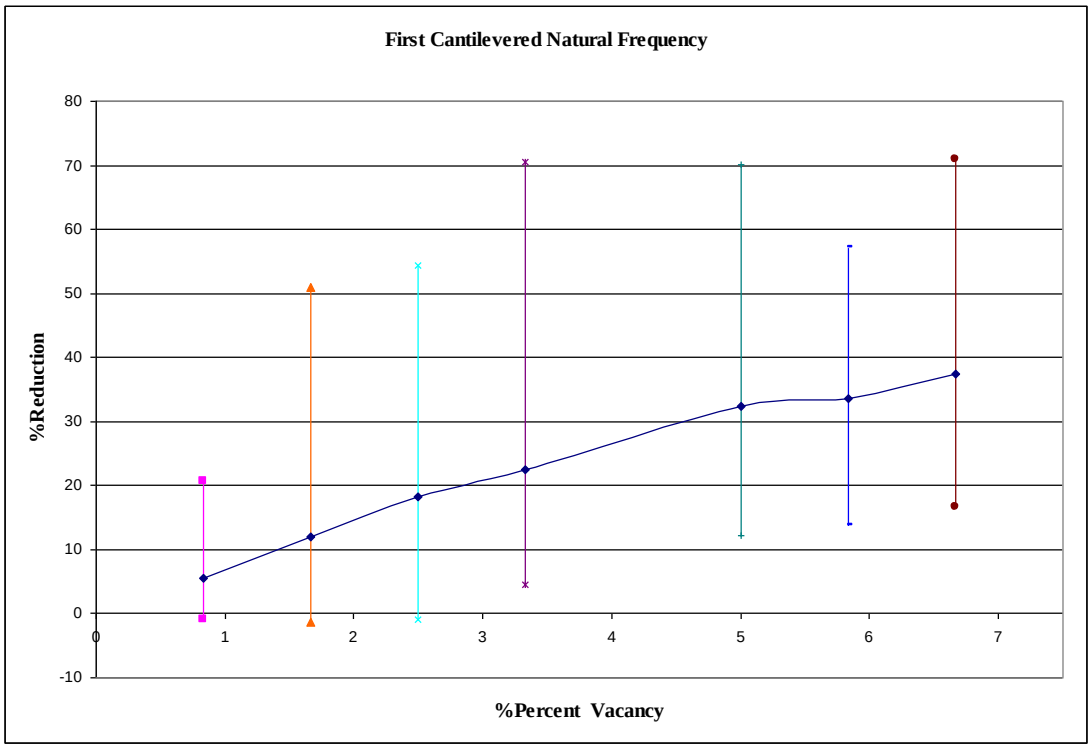

Figure 5.10 Maximum, Minimum and Average Values of Effects of Randomly Positioned Atom-Vacancies on First Cantilevered Natural Frequency

5.6 Variations in Effects of Randomly Positioned Atom-Vacancies on First Bridged and Cantilevered Natural Frequencies of Armchair CNT

Similar analyses were conducted on a (4-4) armchair configuration and the effect of vacancies on bridged and cantilevered natural frequencies in Figure 5.11 and Figure 5.12.

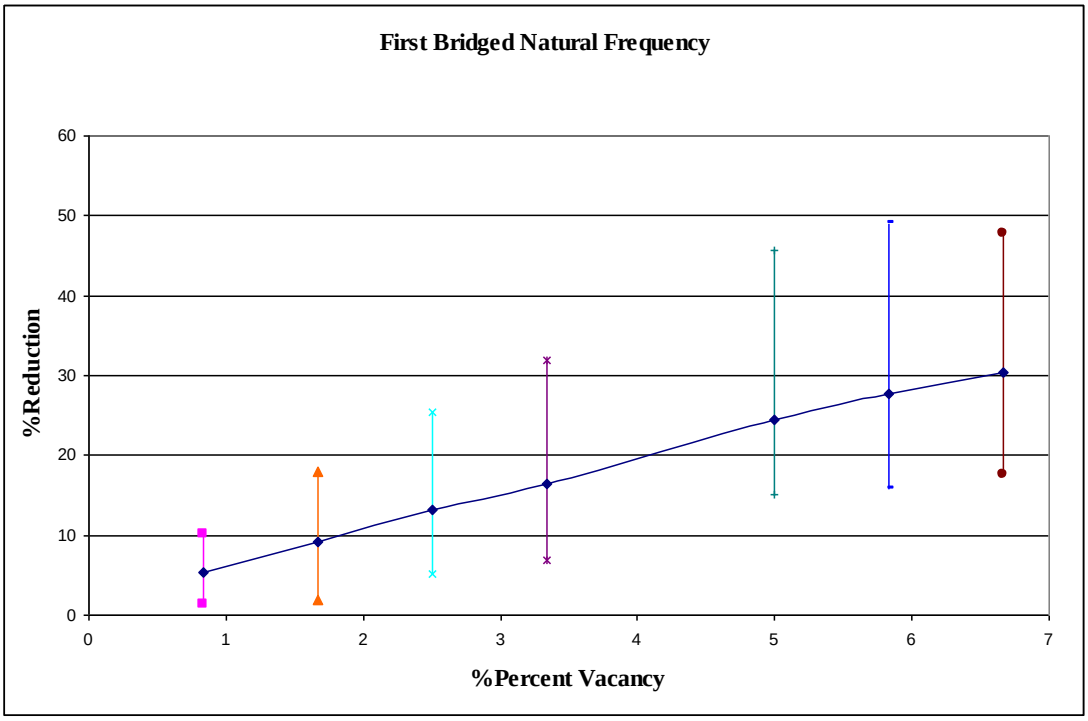

Figure 5.11 Maximum, Minimum and Average Values of Effects of Randomly Positioned Atom-Vacancies on First Bridged Natural Frequency for Armchair Nanotubes

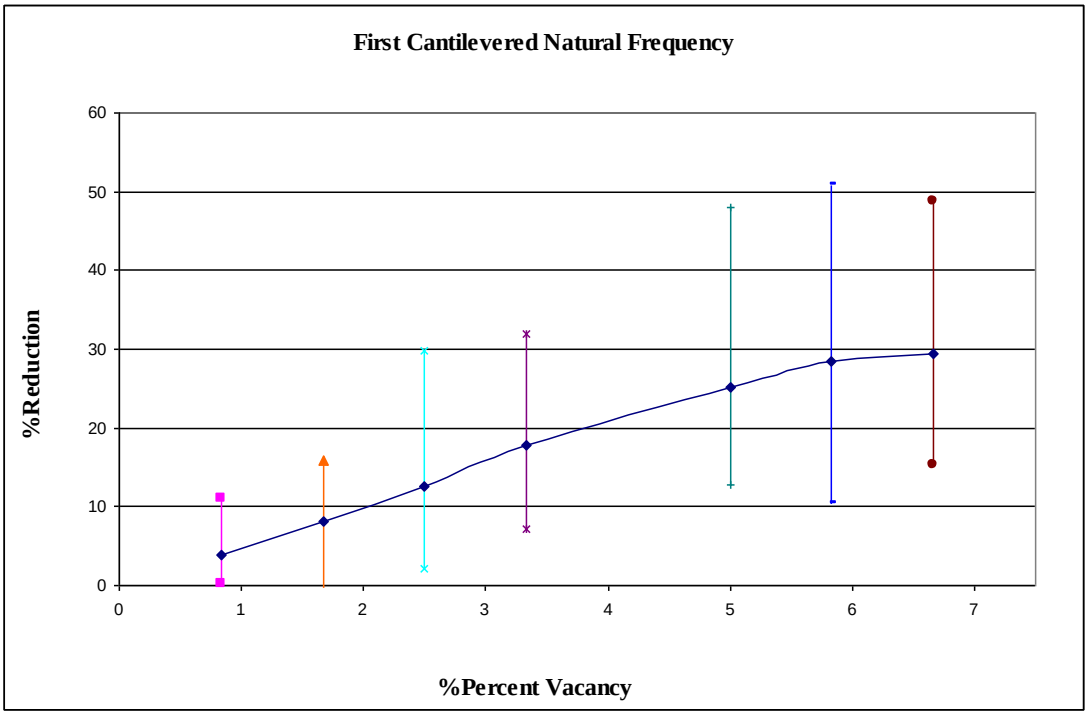

Figure 5.12 Maximum, Minimum and Average Values of Effects of Randomly Positioned Atom-Vacancies on First Cantilevered Natural Frequency for Armchair Nanotubes

5.7 Bridged Natural Frequencies of Zigzag CNT with Consecutively Positioned Atom-vacancies in Axial Direction of Nanotube

It is concluded that the position of atom vacancy is a major parameter for the resulting nanotube characteristics. As a third study, the effect of one atom vacancy being consecutively positioned at each layer of a 30 layer zigzag nanotube is investigated. The offset-type of discrepancies between nanotubes from (4-0) to (9-0) are coming from the percentage of the vacant atom among the total number of nodes. Since the total length of the CNT fixed to be same to obtain a controlled set of results, the percentages of amount of nodes are changing with the chirality

accordingly. This explains the offset between each consecutive set of results like in between (4,0) and (5,0).

Looking at the mode shapes and corresponding variations of natural frequencies, the amount of changes seemed reasonable. Extraction of atoms at points which have zero or near to zero displacements at that particular mode shape may reduce the resulting natural frequency even same amount as the end points.

Also for particular mode shapes, extraction of one atom may affect the nanotube as removal of mass rather than a stiffness element. Hence it is interesting that the resulting fundamental frequency may increase at those situations.

In addition to those, removal of atoms at the location of maximum displacements of mode shapes may lower the natural frequency more, since the corresponding bonds are the critical frame-supports at those mode shapes.

Figures given in pairs in this section show the effect of vacant atoms in first five bridged natural frequencies of zigzag nanotubes and the graphs of deflected nanotube following each graph show that particular mode shape of nanotubes. Again, results of different chiralities are designated with chiralities shown in forms of (n,0) and (n,n) on the right sides of the plots.

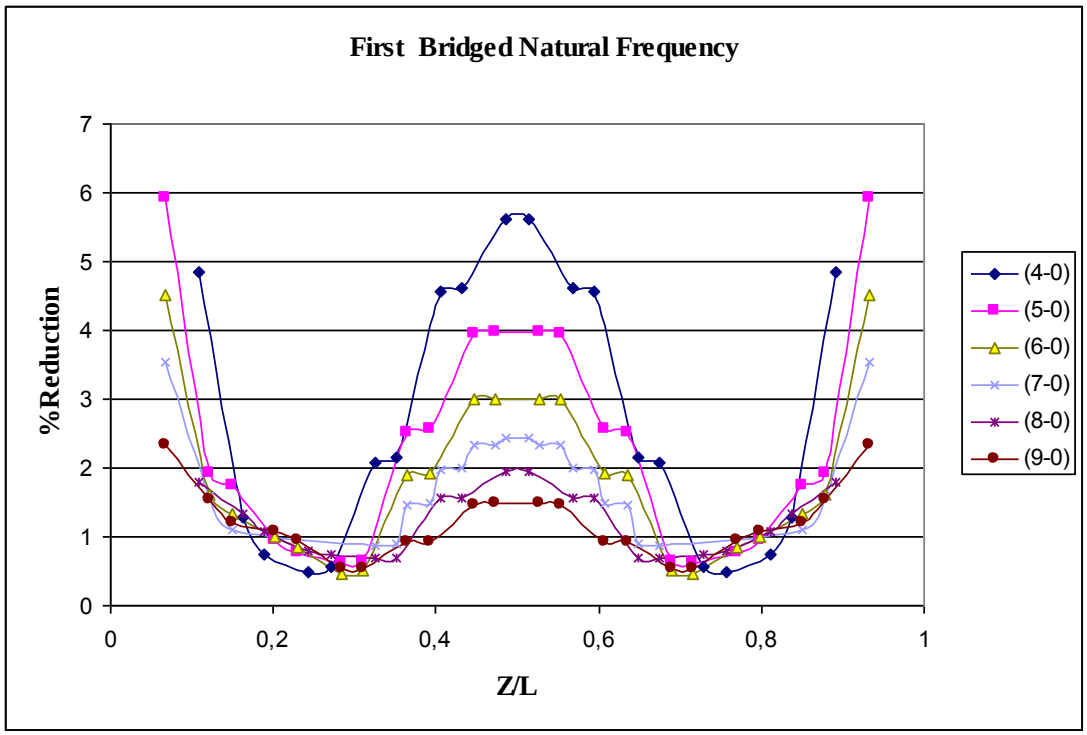

Figure 5.13 Effects of one Atom-Vacancy in Consecutive Positions, on First Bridged Natural Frequencies of Zigzag Nanotubes

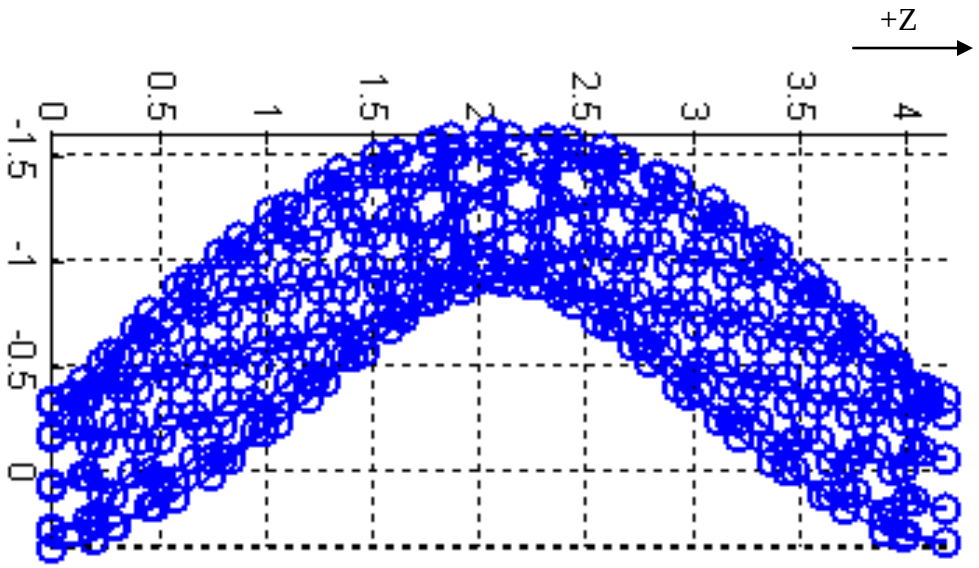

Figure 5.14 First Bridged Mode Shape of a Zigzag nanotube

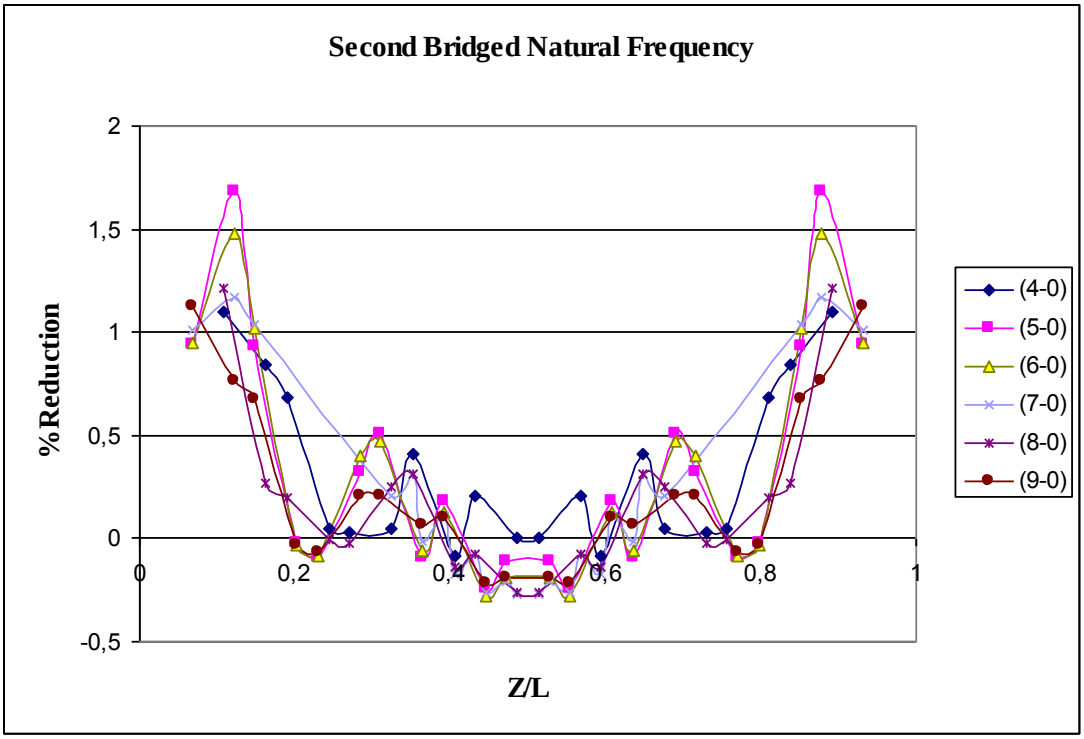

Figure 5.15 Effects of one Atom-Vacancy in Consecutive Positions, on Second Bridged Natural Frequencies of Zigzag Nanotubes

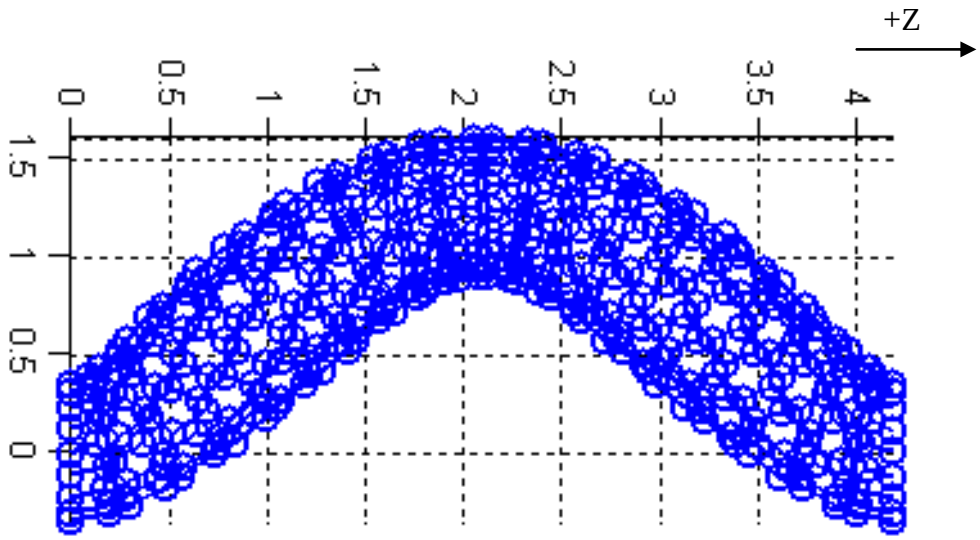

Figure 5.16 Second Bridged Mode Shape of a Zigzag nanotube

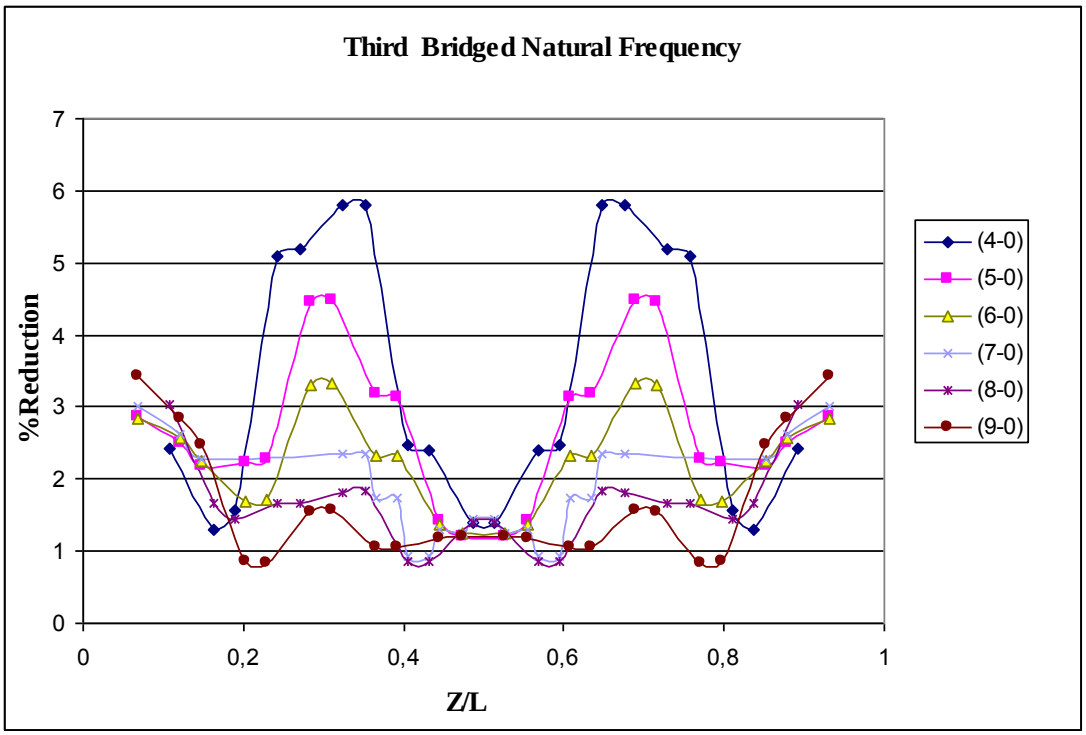

Figure 5.17 Effects of one Atom-Vacancy in Consecutive Positions, on Third Bridged Natural Frequencies of Zigzag Nanotubes

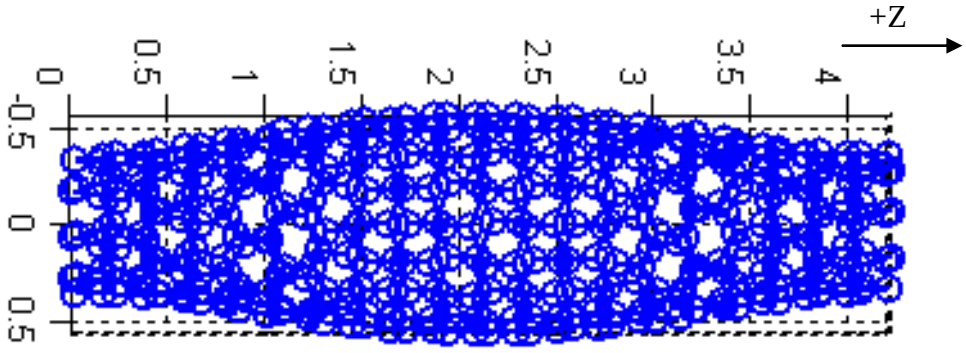

Figure 5.18 Third Bridged Mode Shape of a Zigzag nanotube

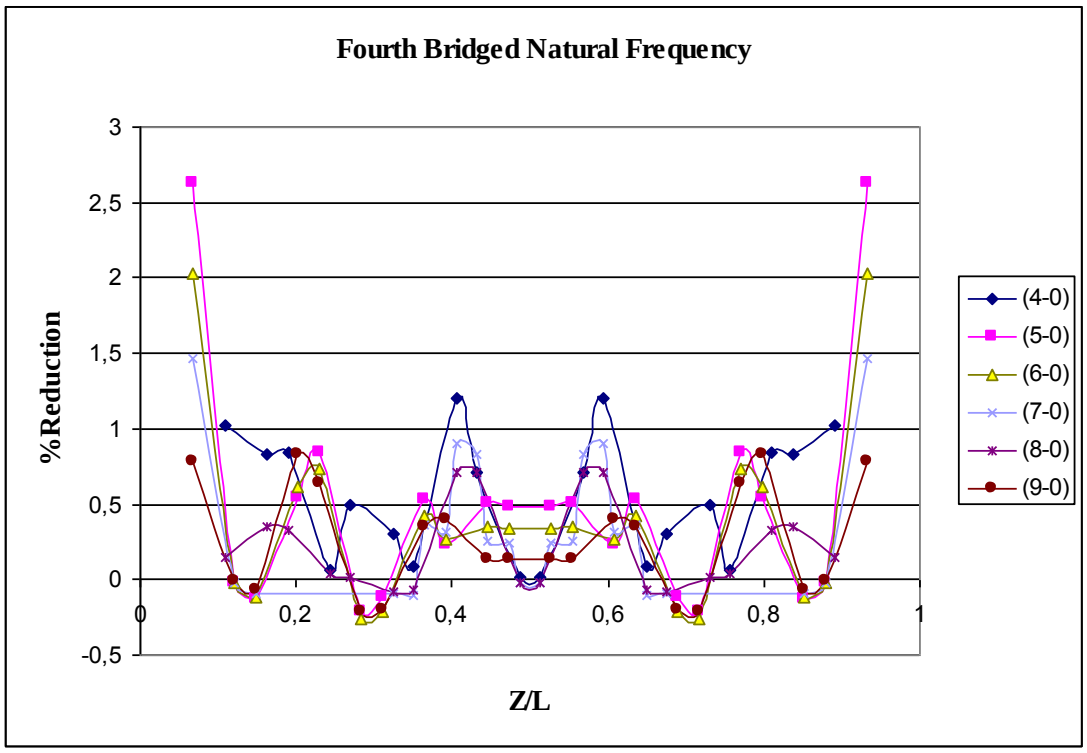

Figure 5.19 Effects of one Atom-Vacancy in Consecutive Positions, on Fourth Bridged Natural Frequencies of Zigzag Nanotubes

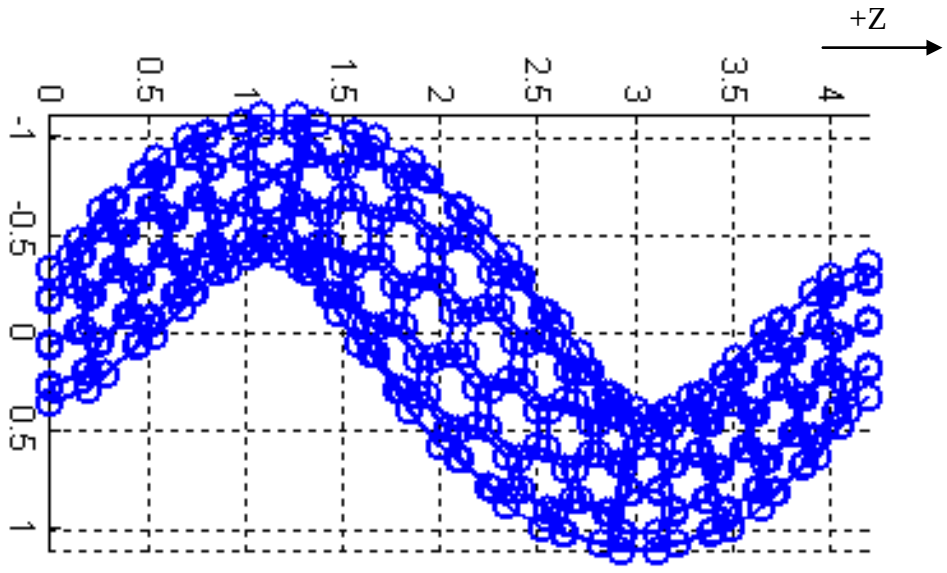

Figure 5.20 Fourth Bridged Mode Shape of a Zigzag nanotube

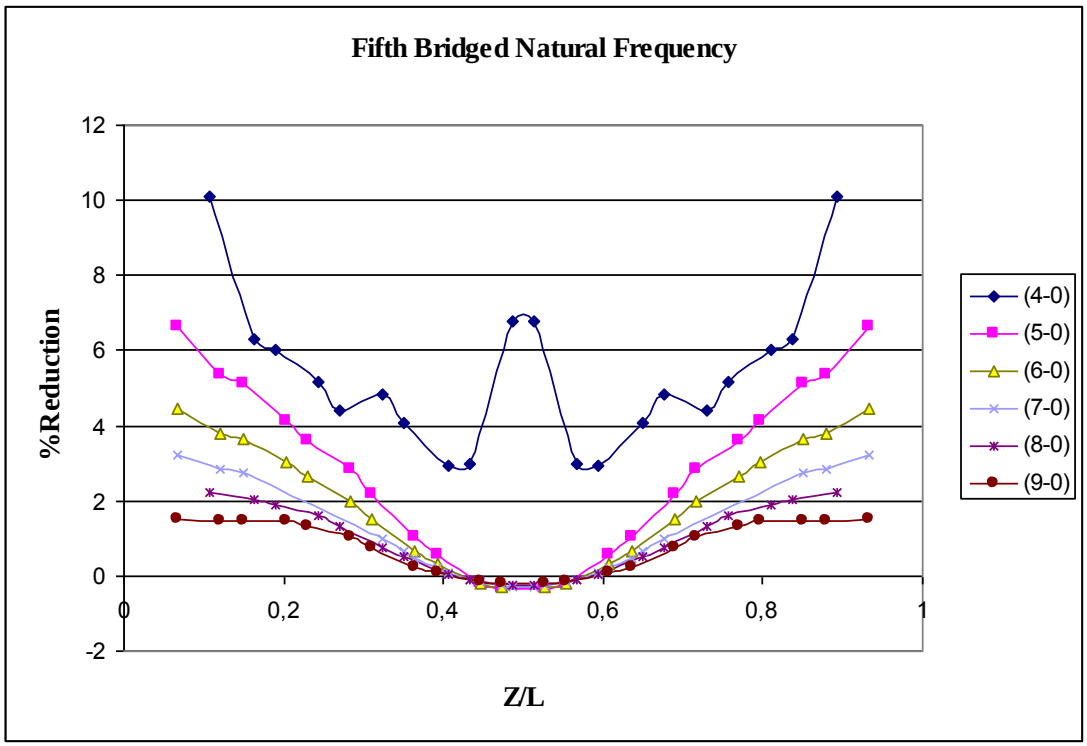

Figure 5.21 Effects of one Atom-Vacancy in Consecutive Positions, on Fifth Bridged Natural Frequencies of Zigzag Nanotubes

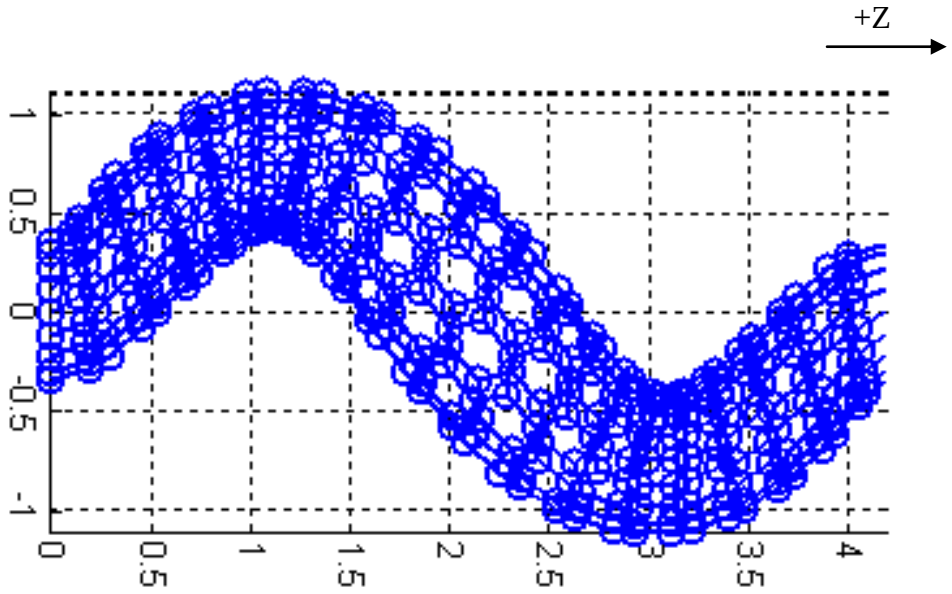

Figure 5.22 Fifth Bridged Mode Shape of a Zigzag nanotube

5.8 Cantilevered Natural Frequencies of Zigzag CNT with Consecutively Positioned Atom-vacancies in Axial Direction of Nanotube

In this section the effect of the positioned atom-vacancies on the cantilevered natural frequencies is investigated. It can be observed and found surprising that for any kind of nanotube in cantilevered support the amount of reduction becomes negative (i.e. percent increase happens) in all five modes. That occurs when the atomic-vacancies happen to be close to the free end of nanotube. It is reasonable since that kind of extraction is mainly acting as removal of mass rather than removal of a spring.

The rigidity of cantilevered nanotubes is mainly governed by the atoms on or close to the fixed end. That is why higher values of reduction are found when the unitless parameter $\frac{Z}{L}$ is around or close to the fixed end.

Again the different amount of reductions for the same amount of vacancies stems from the percentage of the vacant-atom among the total number of atoms. Also the mode shapes are formed in pairs, in which the nanotube deflects to two principal axis directions.

Following that a different set of analyses has been carried out to investigate the effect of vacant nodes in consecutive order on vibrational properties of Armchair nanotubes. In both armchair and zigzag configurations, the reductions in cantilevered fundamental frequencies are higher than bridged configurations as expectedly.

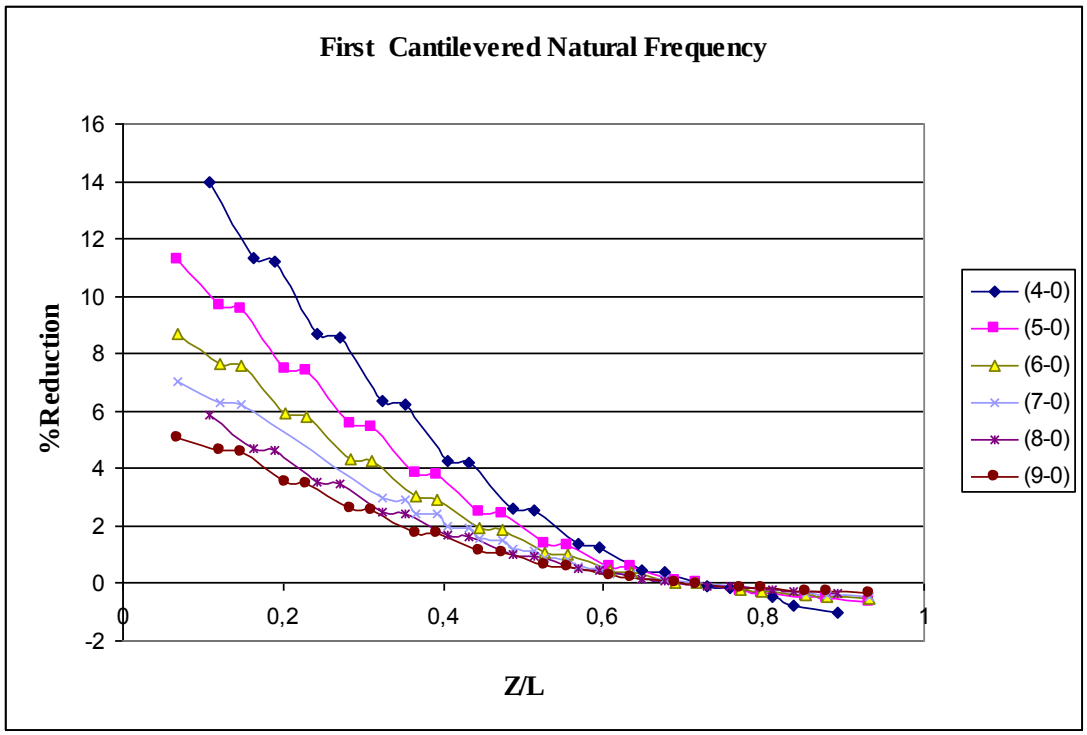

Figure 5.23 Effects of one Atom-Vacancy in Consecutive Positions, on First Cantilevered Natural Frequencies of Zigzag Nanotubes

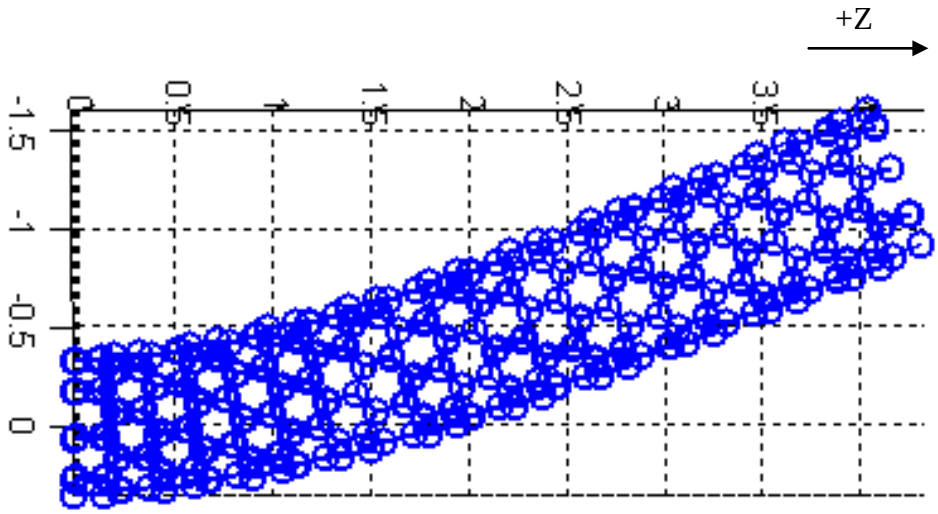

Figure 5.24 First Cantilevered Mode Shape of a Zigzag nanotube

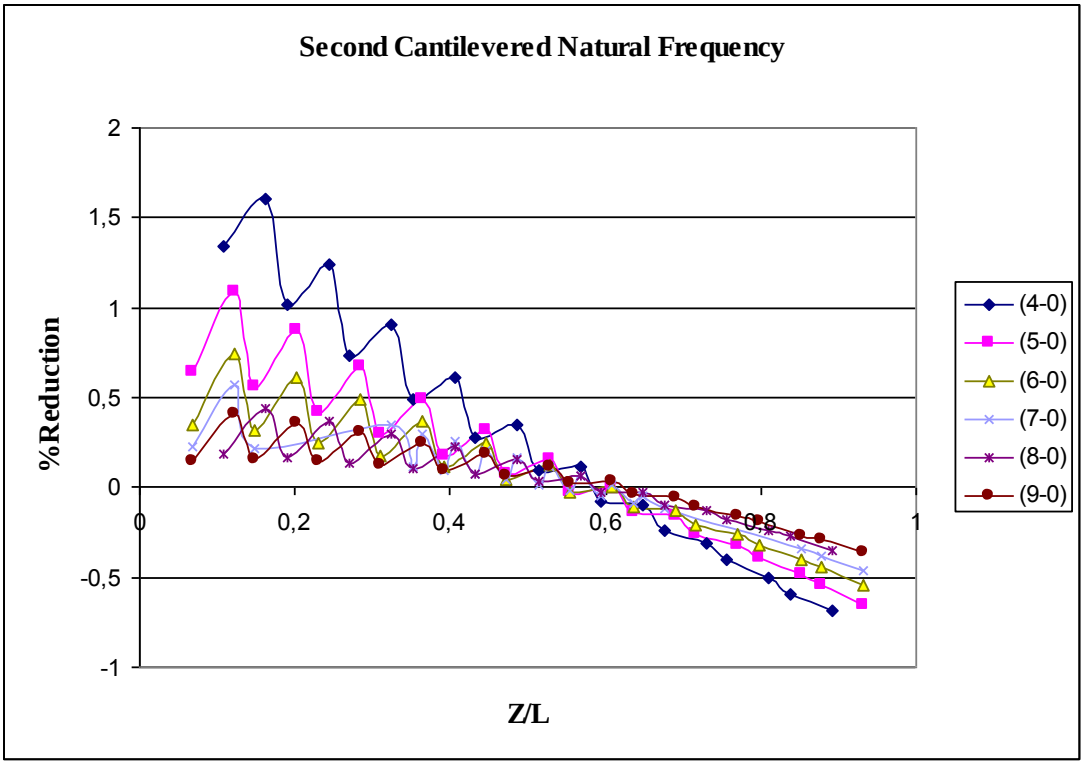

Figure 5.25 Effects of one Atom-Vacancy in Consecutive Positions, on Second Cantilevered Natural Frequencies of Zigzag Nanotubes

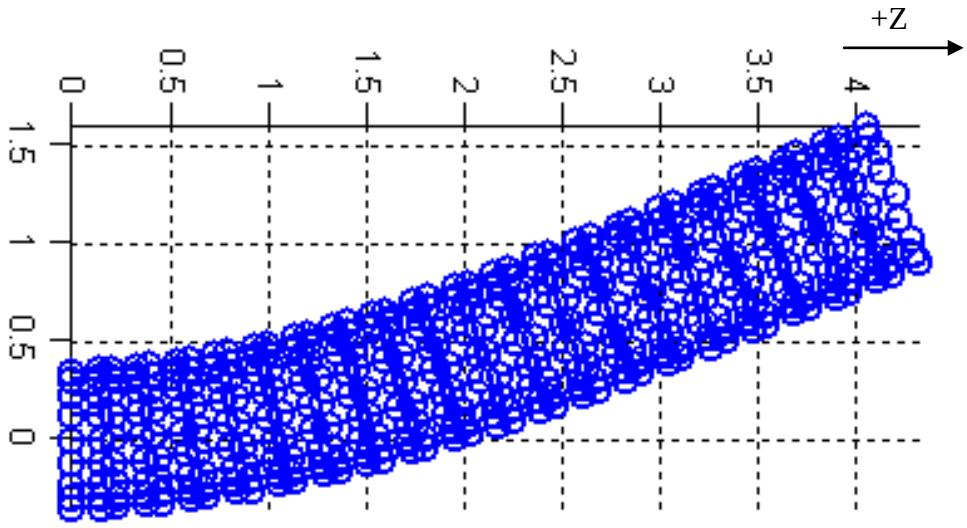

Figure 5.26 Second Cantilevered Mode Shape of a Zigzag nanotube

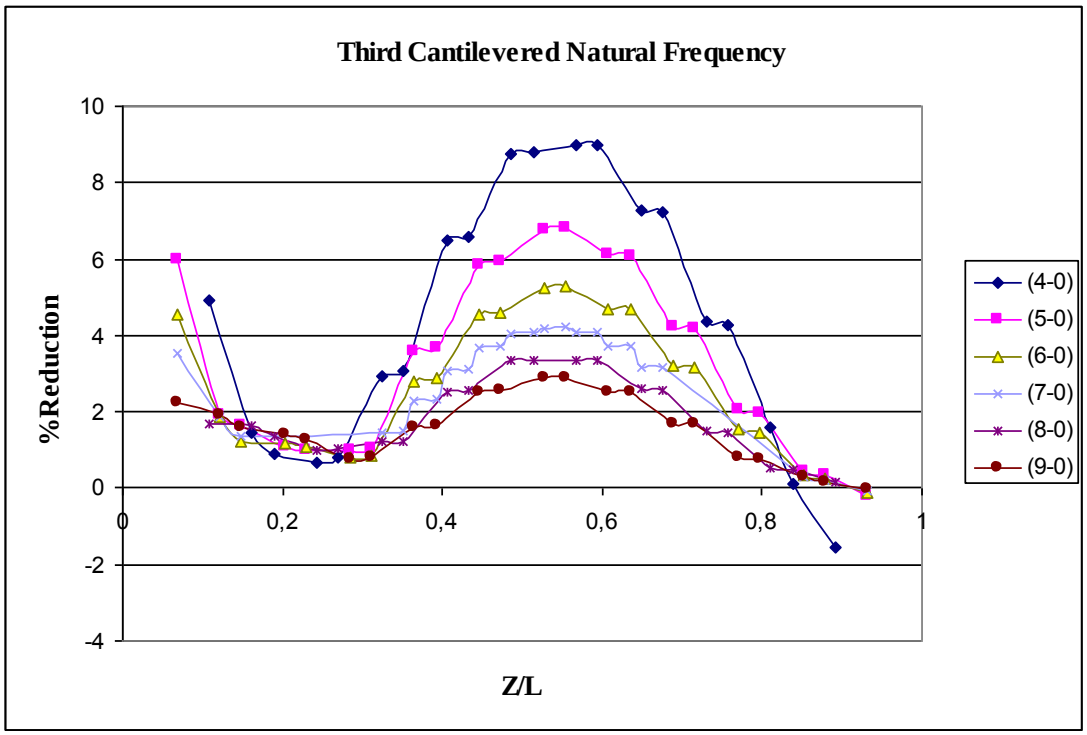

Figure 5.27 Effects of one Atom-Vacancy in Consecutive Positions, on Third Cantilevered Natural Frequencies of Zigzag Nanotubes

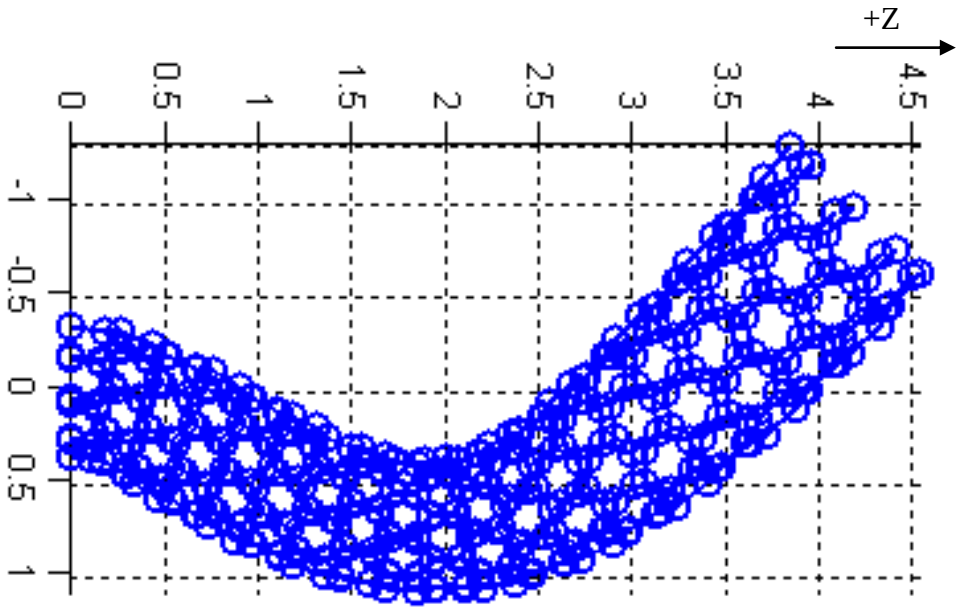

Figure 5.28 Third Cantilevered Mode Shape of a Zigzag nanotube

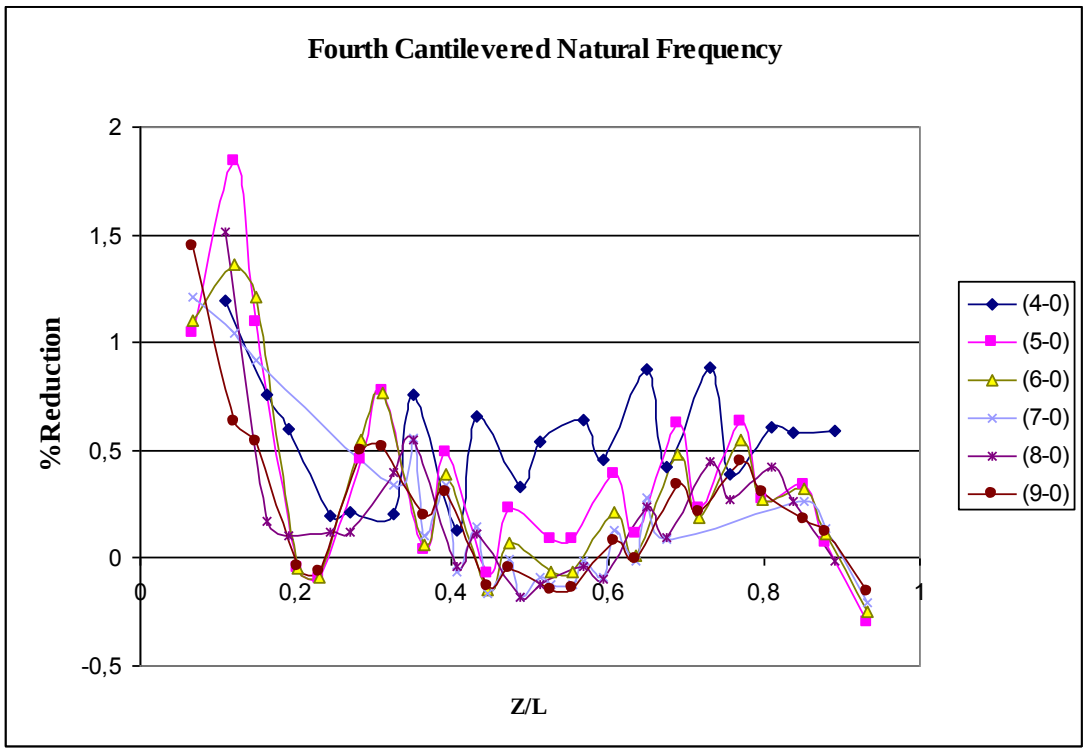

Figure 5.29 Effects of one Atom-Vacancy in Consecutive Positions, on Fourth Cantilevered Natural Frequencies of Zigzag Nanotubes

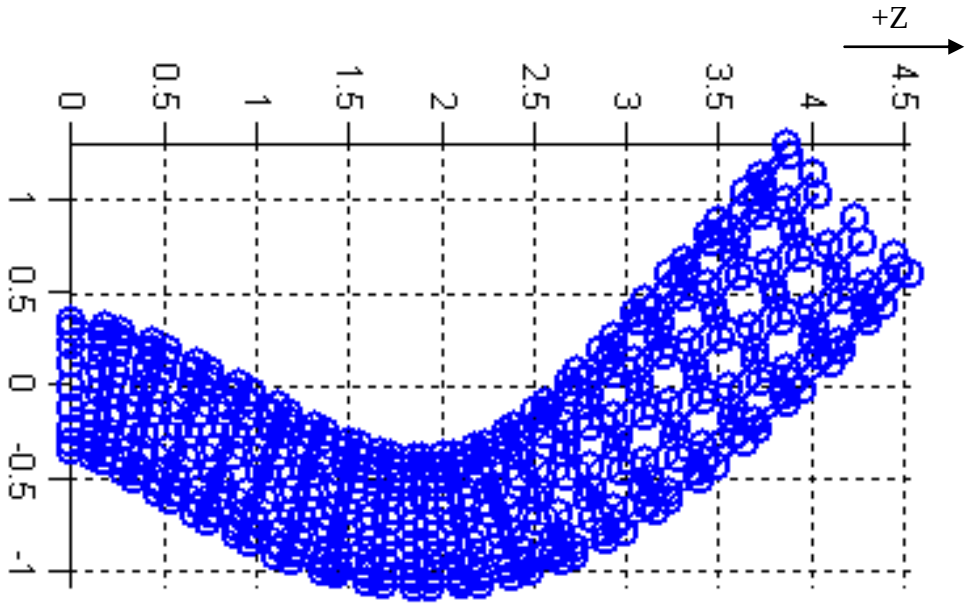

Figure 5.30 Fourth Cantilevered Mode Shape of a Zigzag nanotube

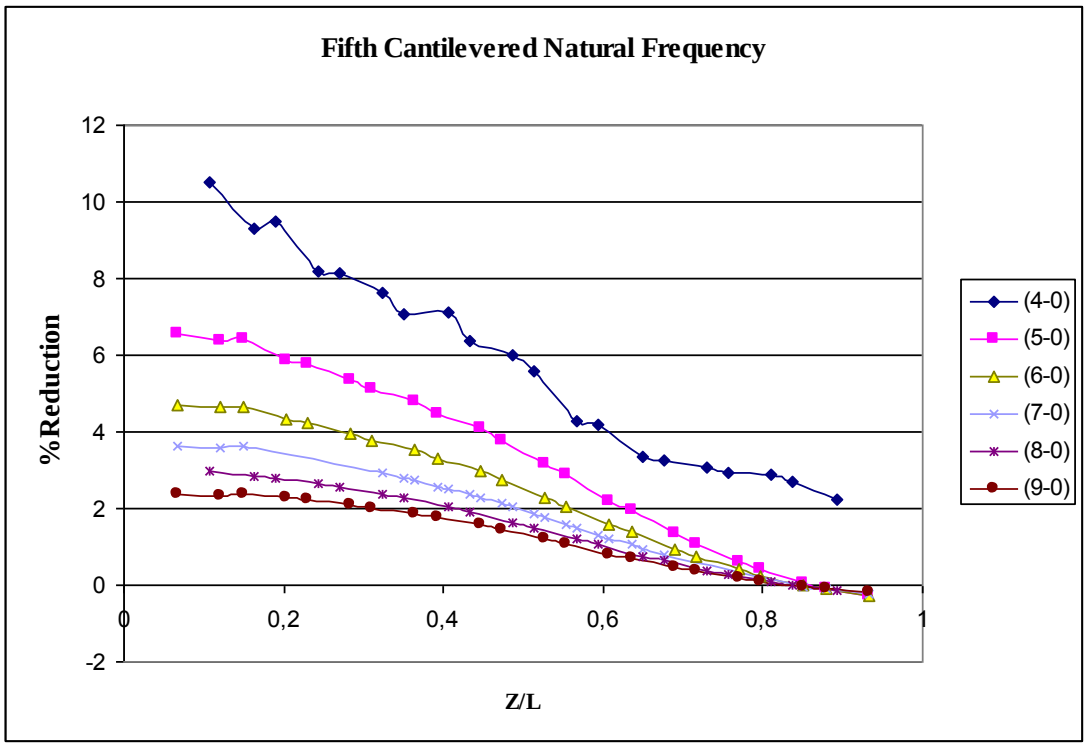

Figure 5.31 Effects of one Atom-Vacancy in Consecutive Positions, on Fifth Cantilevered Natural Frequencies of Zigzag Nanotubes

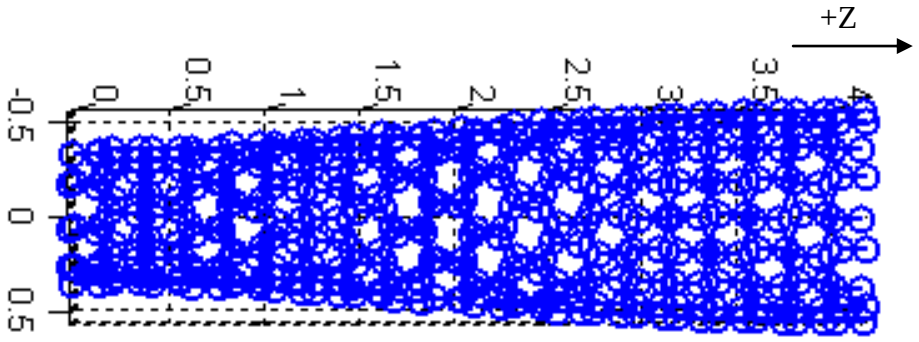

Figure 5.32 Fifth Cantilevered Mode Shape of a Zigzag nanotube

5.9 Bridged and Cantilevered Natural Frequencies of Armchair CNT with Consecutively Positioned Atom-vacancies in Axial Direction of Nanotube

In this section, a brief investigation is presented on the effect of consecutively positioned atom-vacancies on the first three natural frequencies of armchair nanotubes.

Looking at the mode shapes and corresponding variations of natural frequencies, the amount of changes seemed reasonable. Also percent increases were repeated in many cases if the atomic-vacancy is more like the extraction of a mass.

Figures given in pairs in this section show the effect of vacant atoms in first three bridged and cantilevered natural frequencies of armchair nanotubes and the graphs of deflected nanotube following each graph show that particular mode shape of nanotubes.

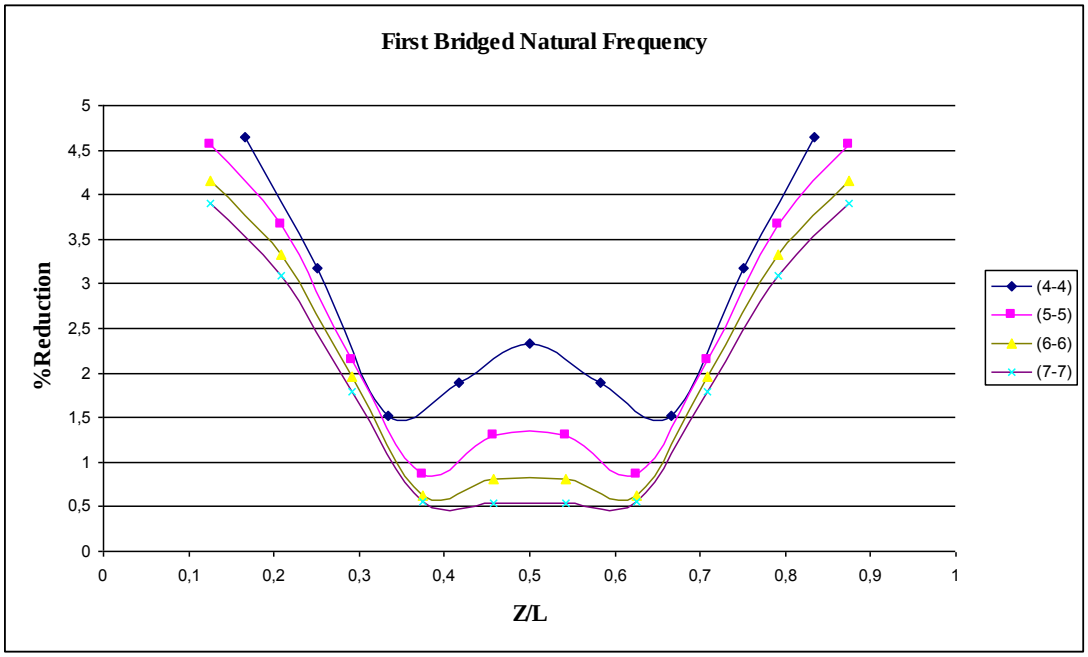

Figure 5.33 Effects of one Atom-Vacancy in Consecutive Positions, on First Bridged Natural Frequencies of Armchair Nanotubes

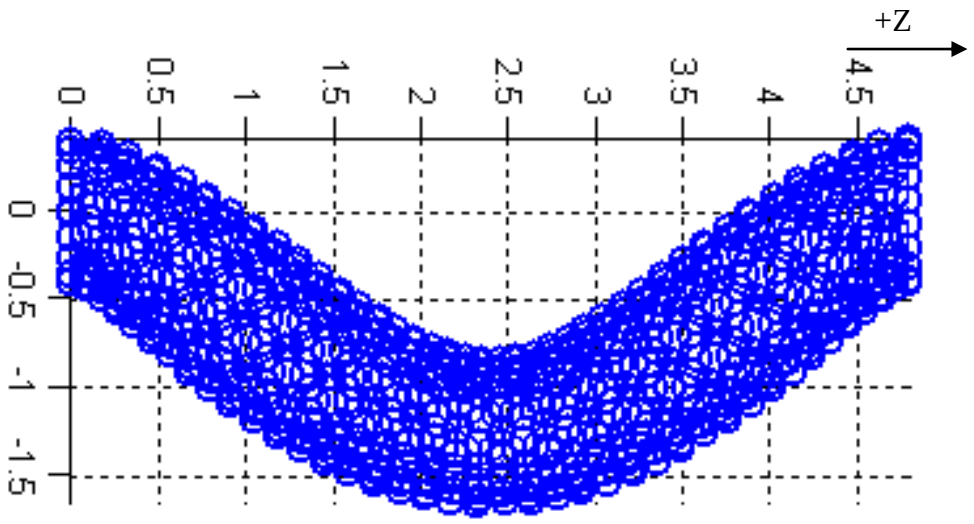

Figure 5.34 First Bridged Mode Shape of an Armchair nanotube

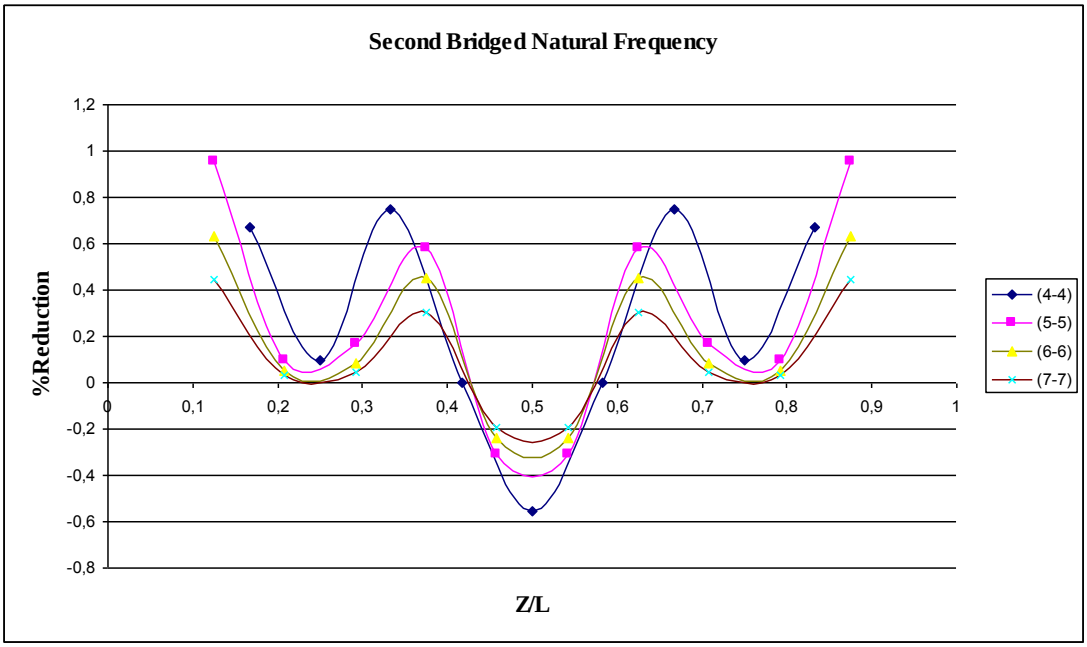

Figure 5.35 Effects of one Atom-Vacancy in Consecutive Positions, on Second Bridged Natural Frequencies of Armchair Nanotubes

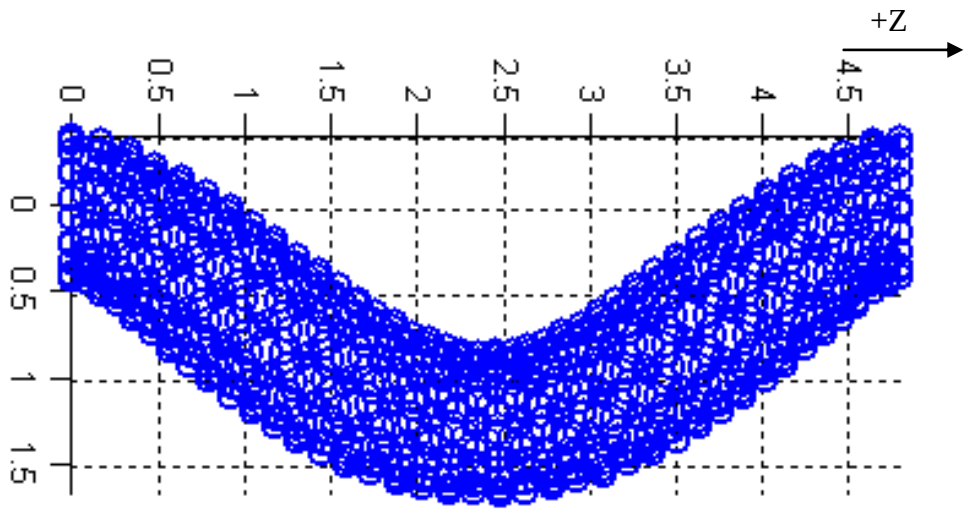

Figure 5.36 Second Bridged Mode Shape of an Armchair nanotube

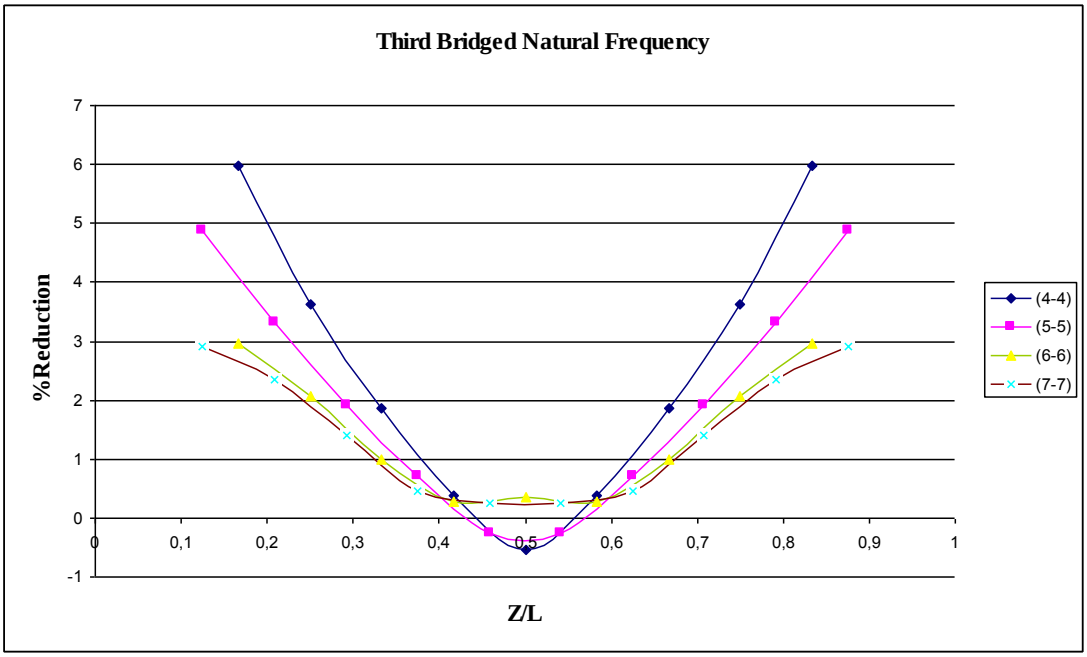

Figure 5.37 Effects of one Atom-Vacancy in Consecutive Positions, on Third Bridged Natural Frequencies of Armchair Nanotubes

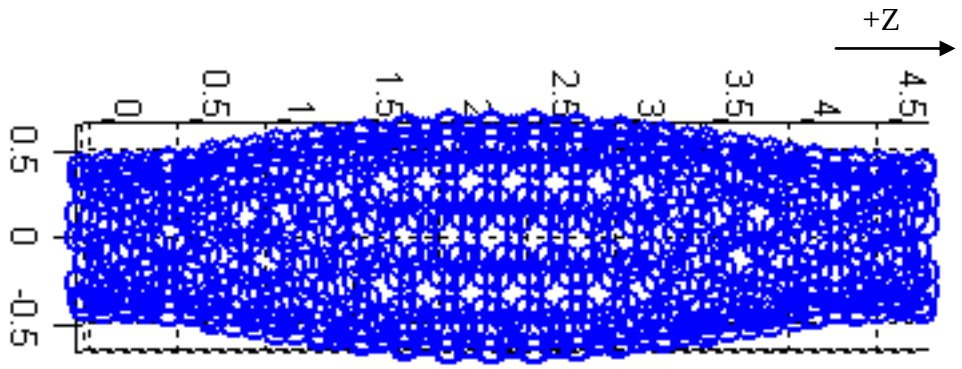

Figure 5.38 Third Bridged Mode Shape of an Armchair nanotube

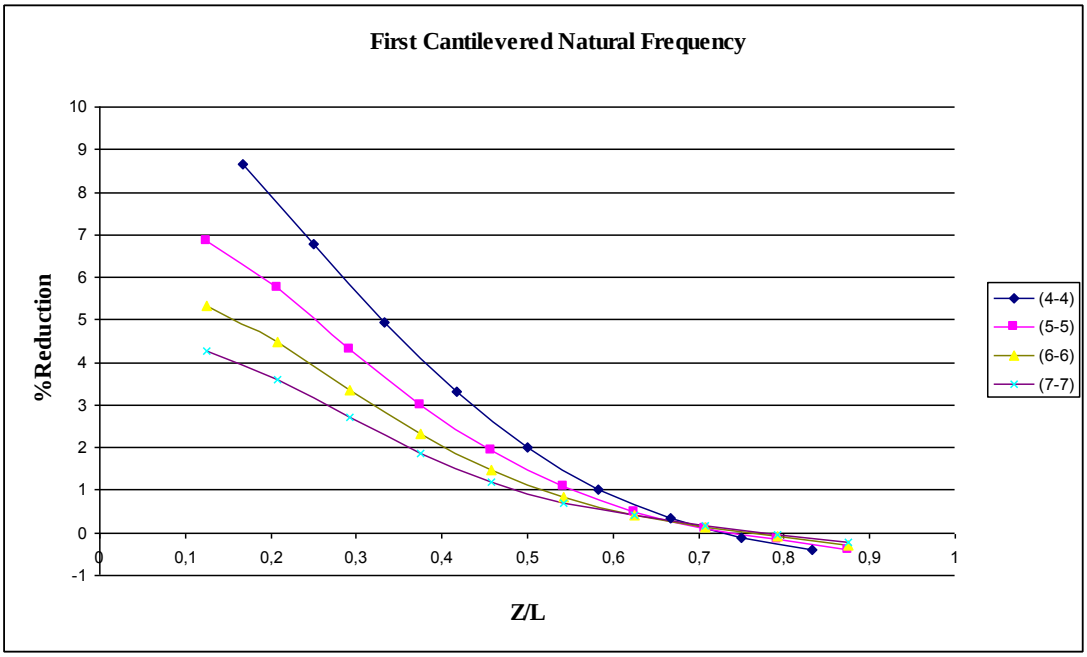

Figure 5.39 Effects of one Atom-Vacancy in Consecutive Positions, on First Cantilevered Natural Frequencies of Armchair Nanotubes

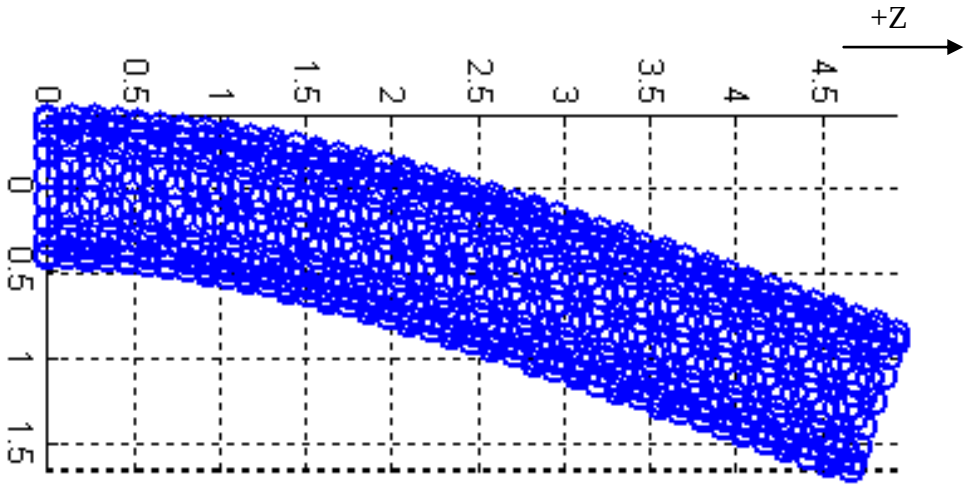

Figure 5.40 First Cantilevered Mode Shape of an Armchair nanotube

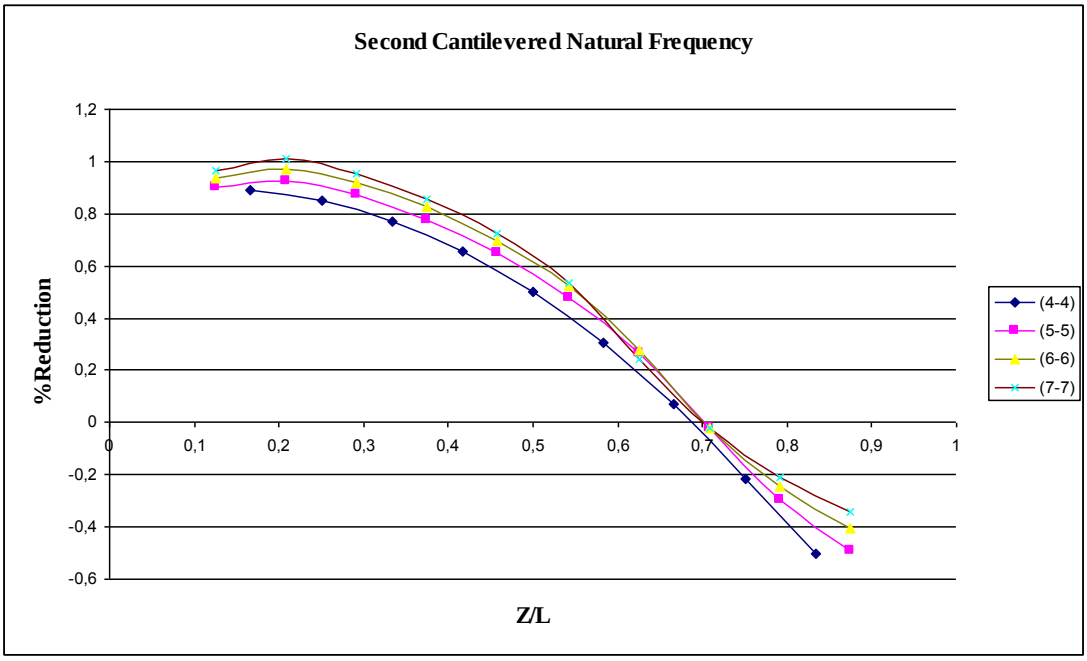

Figure 5.41 Effects of one Atom-Vacancy in Consecutive Positions, on Second Cantilevered Natural Frequencies of Armchair Nanotubes

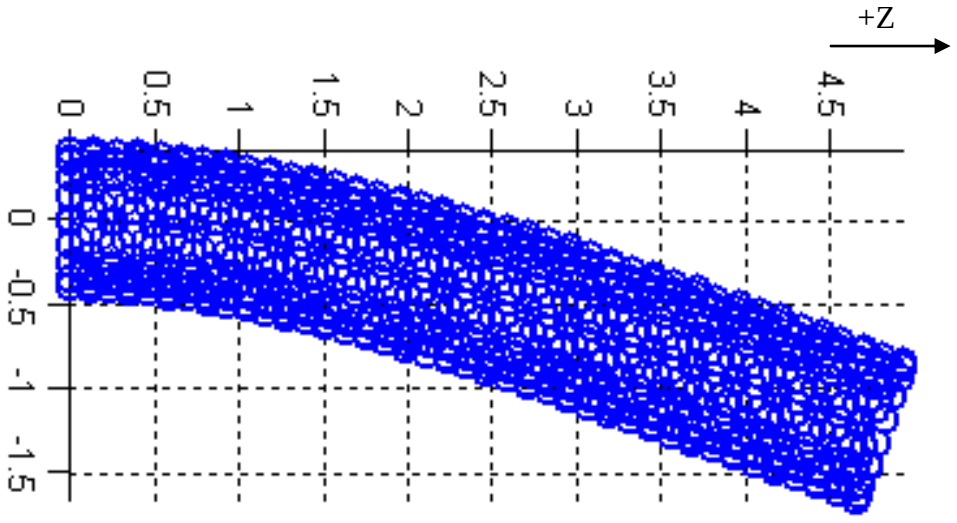

Figure 5.42 Second Cantilevered Mode Shape of an Armchair nanotube

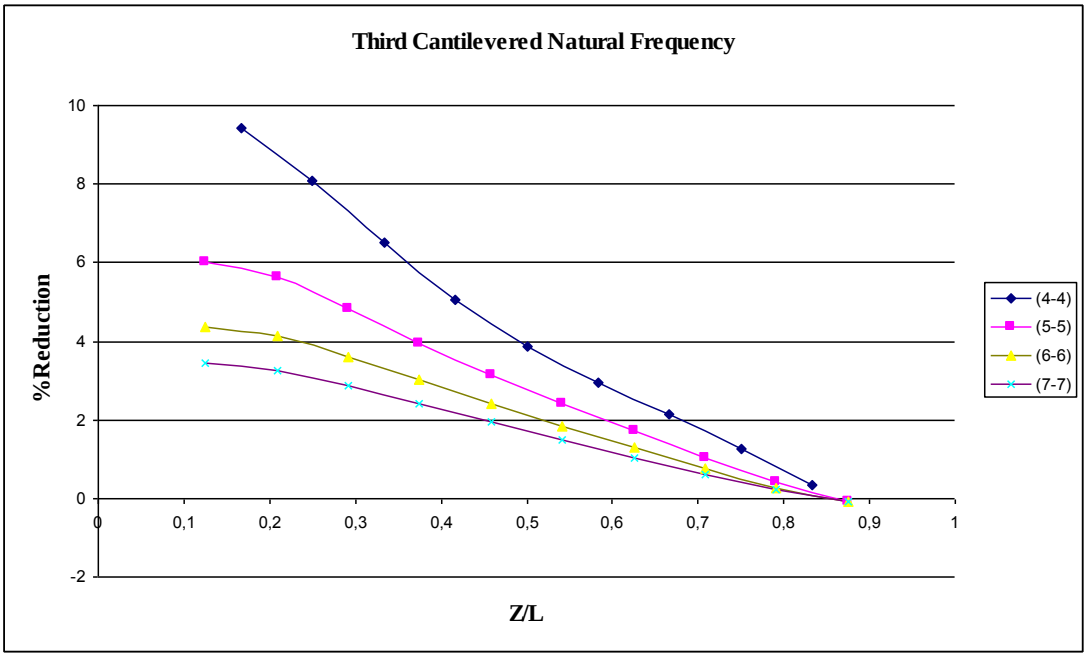

Figure 5.43 Effects of one Atom-Vacancy in Consecutive Positions, on Third Cantilevered Natural Frequencies of Armchair Nanotubes

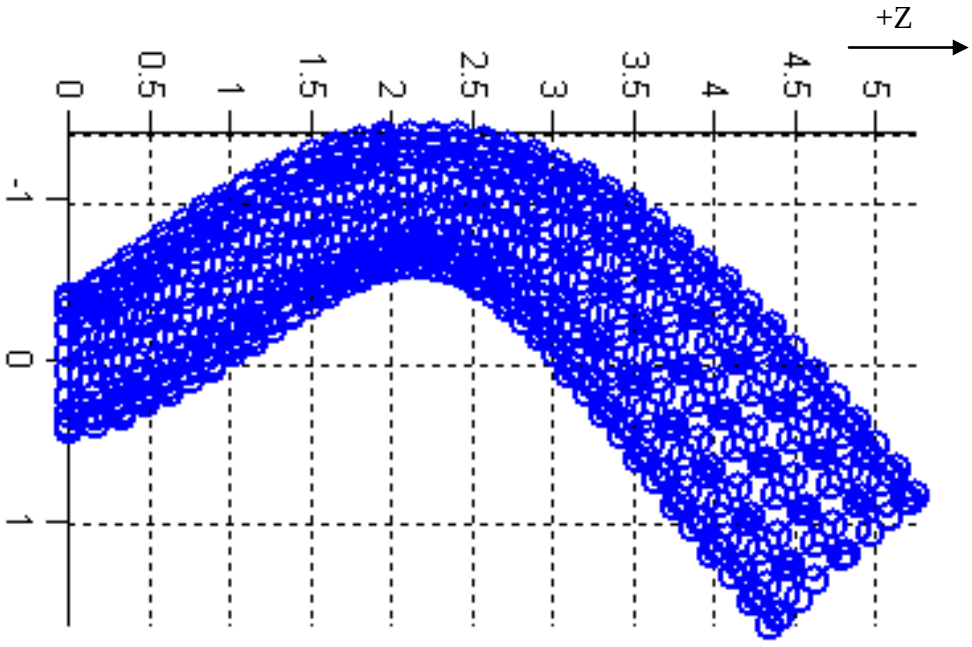

Figure 5.44 Third Cantilevered Mode Shape of an Armchair nanotube

5.10 Effects of one Atom-vacancy on Mode Shapes of Nanotube

In this section, the source code is used to investigate the resulting mode shapes of nanotube when a vacancy is implemented. Since the defect free nanotubes are axi-symmetric, natural frequencies are found to be mostly in pairs in which the mode shapes are perpendicular to each other and the frequencies are found to be almost the same. The paired mode shapes, also known as degenerate modes, occurs in perpendicular planes for any specific frequency.

An investigation is necessary to find out the effect of vacancies on the mode shape of the nanotube. It turns out that the position of one vacancy determines the preferred mode shape plane and the favored mode shape frequency is lower than its pair.

Table 5.1 and Table 5.2 are given to show the lowering effect of vacant atom on bridged and cantilevered natural frequencies for a (4,0) 80 atom CNT.

Table 5.1 Reductions in First Five Bridged Natural Frequencies of a (4,0) Nanotube with one Atom-vacancy Implemented

[Hz]	**Defectless Bridged**	**One Vacancy Bridged**	**%Reduction**
1. Natural Frequency	1,6398E+12	1,5012E+12	8,45
2. Natural Frequency	1,6398E+12	1,6372E+12	0,16
3. Natural Frequency	3,6544E+12	3,2329E+12	11,53
4. Natural Frequency	3,9028E+12	3,6030E+12	7,68
5. Natural Frequency	3,9028E+12	3,8487E+12	1,39

Table 5.2 Reductions in First Five Cantilevered Natural Frequencies of a (4,0) Nanotube with one Atom-vacancy Implemented

[Hz]	**Defectless Cantilevered**	**One Vacancy Cantilevered**	**%Reduction**
1. Natural Frequency	2,7690E+11	2,2224E+11	19,74
2. Natural Frequency	2,7690E+11	2,6143E+11	5,59
3. Natural Frequency	1,5482E+12	1,2648E+12	18,31
4. Natural Frequency	1,5482E+12	1,5435E+12	0,31
5. Natural Frequency	1,7666E+12	1,6456E+12	6,85

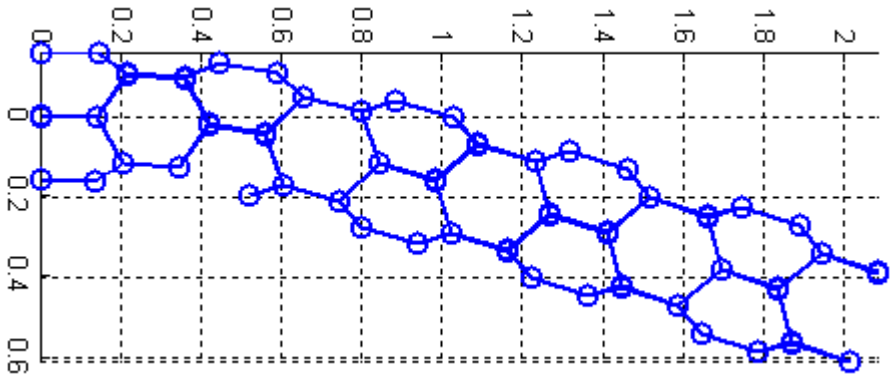

Figure 5.45 First Cantilevered Mode of (4,0) Nanotube with one Atom-Vacancy

Looking at Figure 5.45, it can be seen that the first cantilevered mode shape occurred in the plane of vacant atom and decrease from 0,277 THz to 0,222 THz. On the other hand the second natural frequency occurs in the other plane where the frequency reduced from 0,277 to 0,261 THz.

This shows that not only the position of the vacancy along the axis of the nanotube is important but also the position on that particular distance decides the first mode in both bridged and cantilevered nanotube.

5.11 Effects of Atomic-Vacancies on Young's Modulus of Nanotubes

As discussed before, the source code is developed with in a highly flexible form such that investigation of the effect of vacancies on Young's Modulus of nanotubes is also possible. In the given figures, for each percentage of vacancy and for each kind of chirality, about 100 of iterations made with having randomly positioned vacant atoms. Obvious that any amount of imperfection in this uniformly positioned network reduces the overall strength substantially.

Figure 5.46 and Figure 5.47 show the percent reduction in Young's Modulus with different percentage of vacancies for zigzag and armchair configuration of nanotubes.

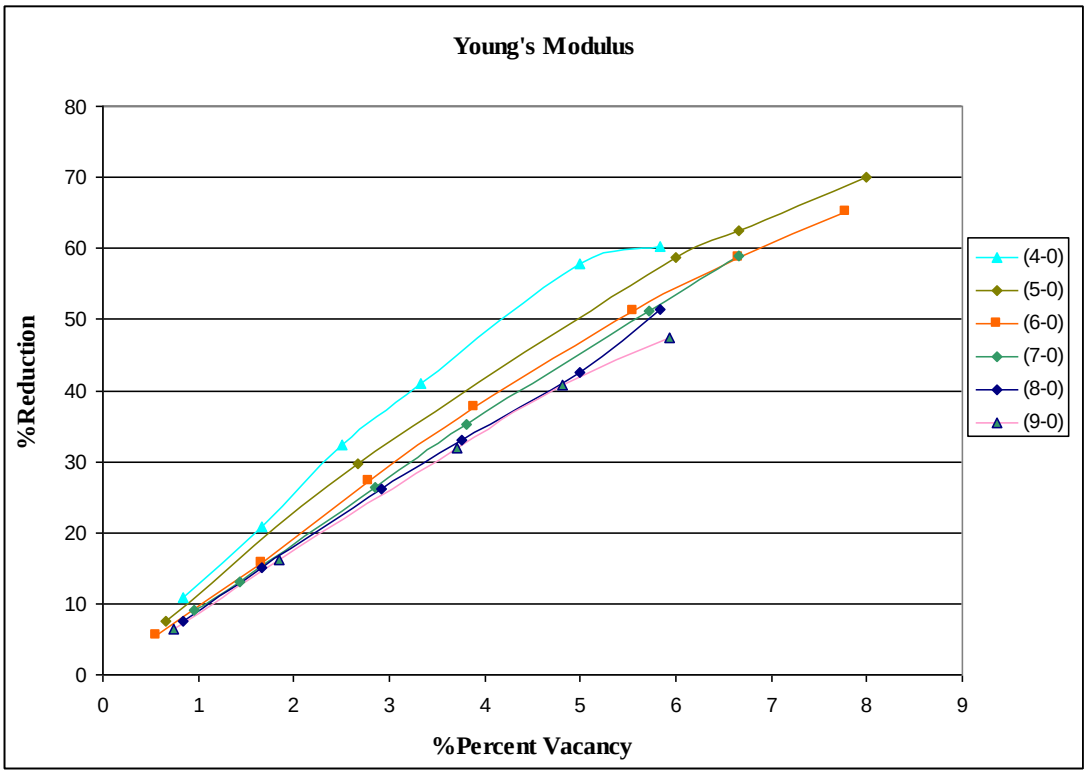

Figure 5.46 Reductions in Young's Modulus of Zigzag Nanotubes with Different Percentage of Vacancies

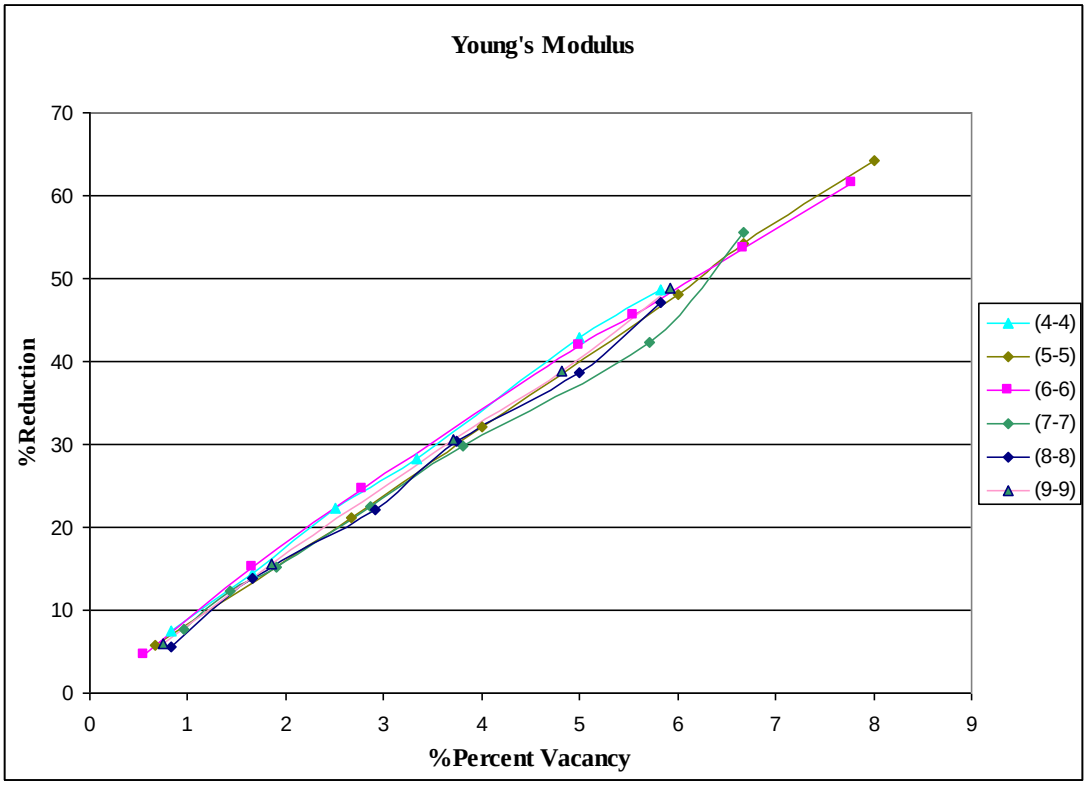

Figure 5.47 Reductions in Young's Modulus of Armchair Nanotubes with Different Percentage of Vacancies

To make a comparison, it can be seen that the same amount of vacancies have slightly more reduction in Young's Modulus of zigzag nanotubes than armchair nanotubes. This shows the importance of bond arrangement in nanotube structure.

In zigzag configuration $\frac{1}{3}$ of total bonds are aligned with the axis of the nanotube. When a vacancy implemented, at least one of the vertical bonds is extracted so the strength against tensile forces is reduced more in zigzag nanotubes. In armchair nanotube all bonds are constructed with an angle.

Also an interesting finding is that effect of vacancy is almost linear for any kind of chirality. Slight non-linearities exist since in some cases the vacancies can dense around some local points. In those cases the nanotubes may lean to a side which inevitably leads to a miscalculation of elongation in +z direction.

Another conclusion is that even though the Young's moduli of different chirality defect free nanotubes are different, their responses to the same amount of vacancies are approximately the same.

CHAPTER 6

SUMMARY, CONCLUSIONS AND RECOMMENDATIONS FOR FUTURE WORK

This study focused on the effects of atomic-vacancies on natural frequencies of SWNT. Investigations are properly divided into subsections in which randomly or consecutively positioned vacancies are implemented to bridged and cantilevered configuration nanotubes.

Main computational work was to have randomly positioned atomic-vacancies in different amounts. The trends of the average values show the significant and almost linear effects on the resulting nanotubes. About 100 iterations with random positioning of atomic-vacancies were conducted for each chirality and that particular percentage of vacancy.

If the range of analyses set to cover both various lengths of armchair and zigzag nanotubes with cantilevered and bridged configuration the computational matrix would be infinite. Hence it is decided that the analyses should be conducted with fixed length of CNT and up to about %10 amount vacancy of overall number of nanotube atoms. Since it is impossible to cover for all length and all chirality of CNT, the analyses were limited to up to (9,0) in zigzag and (9,9) in armchair configuration which are not only theoretical types but also available in commercial production. The aim of the developed code is to have a tool that can be used to predict the natural frequencies of any CNT with or without any vacancies also the code allows the user to monitor the mode shapes of the CNT.

It can be said that the reduction is almost linear with increasing amount vacancies. Also chirality is not a major parameter determining the vacancy induced natural frequencies. For any type of zigzag or armchair configuration CNT, even with about %8 percent of vacancy the nanotubes first natural frequency can be reduced about %30.

Also based on average values of percent reduction cantilevered natural frequencies seemed to be more affected against imperfections as compared to bridged nanotubes. For the same length of nanotube with about the same amount of vacancies in percentage, cantilevered CNT tend to be more affected and the first natural frequencies are reduced more.

Since it is not possible to have exactly same diameter of zigzag and armchair nanotube making comparison between those two families of nanotube will not give reliable conclusions. But analyses were also completed with armchair nanotubes from (4-4) to (9-9) in order to investigate the trends of the reduction in natural frequencies. Expectedly the linearity is repeated and also chirality is not a critical parameter of the amount of reduction in the frequencies.

Also it is presented the variations of the randomly positioned atom-vacancies and observed that significant variations occur even with about 100 iterations. It is understood that if the higher number of iterations were used, the average values that construct the trend line will be at exact mean values of maximum and minimum values. But this subsection was valuable since it pointed out that the position of the vacancy is also a critical parameter and it was necessary to examine the resulting characteristics with properly located vacancies.

So in the next section the study focused on precisely positioned atomic vacancies throughout the length of the CNT. The z-coordinate of the vacancy is divided by the

total length in order to have a non-dimensional position of the vacancy. Valuable conclusions have been accomplished.

It is interesting that the resulting fundamental frequency may increase at some situations and removal of atoms at maximum displacements of mode shapes may lower the natural frequency more.

Since the source code allows the user to monitor mode shapes of the nanotube with or without vacancy, it is decided to examine the resulting mode shape plane if one atom vacancy is implemented. It is observed that the first mode shape of nanotube occurred in the plane of vacant atom and the natural frequency is reduced abruptly On the other hand the pair of that specific mode shape occurs in the other plane where the reduction in the natural frequency is comparatively smaller than the previous one. That is a valuable conclusion since one of the objectives of this study is to modify the vibrational characteristics of nanotube by implementing a vacant atom. So after vacancy is implemented the nanotube will have its first mode shape in a certain vibration plane and hence should be properly known if the modal plane is important for application in which that tuned CNT will be used.

Utilizing an assumption to determine the amount of elongation in the defected nanotube, the effect of atomic-vacancy on its Young's Modulus is also investigated as a case study. Variations were expected and encountered more with higher amount of vacancies since in the deformed shape the end points were not deflected with same amount. Even though this is an atomic scale study, the results are beneficial to obtain an estimation of the effect.
It is concluded that more reduction occurs in Young's Modulus of zigzag nanotubes than armchair nanotubes. This is reasoned with the bond angles in zigzag and armchair configurations. Also effect of vacancy is linear for all CNT. Interestingly even though the Young's moduli of different chirality defect-free nanotubes are different, their responses to same amount of vacancies are approximately same.

To conduct these analyses, some assumptions were needed. The vacancy implementation is an important part of the study but that method leaves dangling atoms with missing bonds. But since given in literature, these kinds of non-reconstructed models gives very close results to reconstructed studies, it can be said that this assumption did not cause critical errors and false conclusions.

The base of this study assumes linear elastic model that is proposed by Li and Chou [30] for the bonds. A number of previous works were based on and published with this assumption and the certainty of the results is approved since it gives valuable data for understanding these outstanding materials.

To mention possible future work, it can be proposed that atomic-interaction programs in physics can be highly beneficial to predict the final positions of the dangling atoms and the recalculated force constant the model can be used to improve the stiffness of the beam elements for later studies. The source code is developed in such a way that the coordinates of the after-vacancy stage can be fed directly into the code in order to complete the rest of the analysis.

Also experimental work can be done to irradiate a nanotube to verify the resulting natural frequencies of the CNT with the data obtained in this work. Atomic force microscopes can be used to monitor the mode shape of the defected CNT with the conclusions made in this report.

Comparatively higher amount of effort is needed to add Van-der Waals bonds to model MWCNT to investigate its vibrational characteristics if a vacancy is implemented on outer or any inner nested layers.

The information gathered in this study is beneficial in some aspect since it can be used to predict the amount of vacancy and the quality of the produced CNT just by observing the natural frequencies. This can be a part of standard procedure of the

CNT qualification process. Secondly, results shows that this kind of effect allows the producer to implement vacancy in order to tune the vibrational properties of any CNT that will be used in sensor applications.

Also this study shows that since the CNT are used as strengthening element in composites, their standalone strength can be highly reduced if the production phase is not completed properly.

In summary, this study was helpful to understand the basics of CNT. Also investigating the previous studies and literature, valuable knowledge had been acquired about the interactions between electrical, optical and mechanical fields. Extending this work at atomistic scale, research can be focused on understanding these interactions. It may be possible to tune optical or electrical properties just by inducing a vacancy to the CNT.

REFERENCES

[1] Iijima, Sumio. "Helical Microtubules of Graphitic Carbon." Nature 354 (1991): 56-58.

[2] Iijima, S. and Ichihashi T. "Single-Shell Carbon Nanotubes of 1-nm Diameter". Nature 363 (1993): 603-605

[3] Guo T., Nikolaev P., et al. "Catalytic Growth of Single-Walled Nanotubes by Laser Vaporization." Chemical Physics Letters 243 (1995): 49-54

[4] José-Yacamán M., Miki-Yoshida M., et al. "Catalytic Growth of Carbon Nanotubes with Fullerene Structure" Appl.Phys. 62 (1993) : 657

[5] Salvetat J., Bonard J., et al. "Mechanical Properties of Carbon Nanotubes." Appl. Phys. A 69 (1999):255–260

[6] Belluci, S. "Carbon Nanotubes: Physics An Applications". Phys. Stat. Sol Vol 2 (2005): 34

[7] Chae, H.G.,et al " Rigid Rod Polymeric Fibers" Journal of Applied Polymer Science Vol 100 (2006) : 791-802

[8] Meo M., Rossi M " Prediction of Young's Modulus of Single Wall Carbon Nanotubes By Molecular-Mechanics Based Finite Element Modeling" Composites Science and Technology Vol 66 (2006): 1597-1605

[9] Popov M., Kyotani M., et al. “Super hard Phase Composed of Single-Wall Carbon Nanotubes” Physical Review B Vol. 65 (2002) : 79-82

[10] Hong S., Myung S., “ Nanotube Electronics : A flexible approach to mobility” Nature Nanotechnology Vol.2 (2007) : 207-208

[11] Pop E., Mann D., et al. “Thermal Conductance of an Individual Single-Wall Carbon Nanotube above Room Temperature” Nano Letters Vol.6 No.1 (2006): 96-100

[12] Kim P., Shi L., et al. “Thermal Transport Measurements of Individual Multiwalled Nanotubes” Physical Review Letters Vol.87 No. 21 (2001): 1-4

[13] Yang Z., Ci L., et al. “Experimental Observation of an Extremely Dark Material Made by a Low-Density Nanotube Array” Nano Letters Vol. 8 No. 2 (2008): 446-451

[14] Hierold C. , Jungen A., et al. “Nano Electromechanical Sensors Based on Carbon Nanotubes”.Sensors and Actuators A 136 (2007): 51–61

[15] Baughman R H., Cui C. et al. “Carbon Nanotube Actuators” Science 284 (1999): 1340-1344

[16] Kim P. and Lieber C. M. “Nanotube Nanotweezers” Science 286 (1999): 2148-2150

[17] Fennimore A. M., Yuzvinsky T. D., et al. “Rotational Actuators Based on Carbon Nanotubes.” Nature Vol 424 (2003): 408-410

[18] Nishio M., Sawaya S., and Akita S. “Carbon Nanotube Oscillators toward Zeptogram Detection”. Applied Physics Letters 86 (2005):133111

[19] Chen J., Perebeinos V. “Bright Infrared Emission from Electrically Induced Excitons in Carbon Nanotubes” Science Vol 310 (2005)

[20] Stewart D. A. and Leonard F. “Energy Conversion Efficiency in Nanotube Optoelectronics” Nano Letters Vol. 5 No 2 (2005): 219-222

[21] Xu J.M. “Highly Ordered Carbon Nanotube Arrays and IR Detection” Infrared Physics and Technology Vol 42 (2001): 485-491

[22] Tans S. J., Verschueren A. R. M. “Room-Temperature Transistor Based on A Single Carbon Nanotube” Nature Vol 393 (1998): 49-52

[23] Demczyk B.G., Wang Y.M., et al. “Direct Mechanical Measurement of the Tensile Strength and Elastic Modulus of Multiwalled Carbon Nanotubes” Materials Science and Engineering A 334 (2002): 173–178

[24] Wong Eric W., Sheehan Paul E., et al. “Nanobeam Mechanics: Elasticity, Strength, and Toughness of Nanorods and Nanotubes” Science Vol. 277 (1997): 1971-1975

[25] Tersoff J. “Energies of Fullerenes” Physical Review B Vol.46 No.23 (1992): 15546-15549

[26] Ru C. Q. “Elastic Buckling of Single-Walled Carbon Nanotube Ropes Under High Pressure” Physical Review B Vol.62 No.15 (2000): 10405-10408

[27] Lu W. B., Liu B. “Continuum Modeling Of Van der Waals Interactions Between Carbon Nanotube Walls” Applied Physics Letters Vol.94 (2009): 101917

[28] Van Lier G., Van Alsenoy C. et al. “Ab Initio Study of the Elastic Properties of Single-Walled Carbon Nanotubes and Graphene” Chemical Physics Letters 326 (2000):181–185

[29] Duan W.H., Wang Q. et al. “Molecular Mechanics Modeling of Carbon Nanotube Fracture” Carbon Vol. 45 (2007): 1769–1776

[30] Li C., Chou T. “A Structural Mechanics Approach For The Analysis of Carbon Nanotubes” International Journal of Solids and Structures Vol. 40 (2003): 2487–2499

[31] Li C., Chou T. “Elastic Moduli of Multi-Walled Carbon Nanotubes And The Effect Of Van der Waals Forces” Composites Science and Technology 63 (2003): 1517–1524

[32] Li C., Chou T. “Single-Walled Carbon Nanotubes As Ultrahigh Frequency Nanomechanical Resonators” Physical Review B Vol.68 (2003):073405

[33] Li C., Chou T. “Vibrational Behaviors of Multiwalled-Carbon-Nanotube-Based Nanomechanical Resonators” Applied Physics Letters Vol.84 No.1 (2004): 121-123

[34] Li C., Chou T. “An Atomistic Modeling of Carbon Nanotube Tensile Strength” AIAA 2002 : 1520

[35] Tserpes K.I., Papanikos P. “Finite Element Modeling of Single-Walled Carbon Nanotubes” Composites: Part B 36 (2005): 468–477

[36] Lu Q. and Bhattacharya B. “Effect of Randomly Occurring Stone–Wales Defects On Mechanical Properties of Carbon Nanotubes Using Atomistic Simulation” Nanotechnology 16 (2005): 555–566

[37] Mielke S., Troya D. et al. “The Role Of Vacancy Defects And Holes in The Fracture Of Carbon Nanotubes” Chemical Physics Letters 390 (2004) : 413–420

[38] Sammalkorpi M., Krasheninnikov A. et al. “Mechanical Properties of Carbon Nanotubes With Vacancies And Related Defects” Physical Review B 70, (2004) : 245416

[39] Pirmoradian M., “Effect of Vacancy Defects on the Fundamental Frequency of Carbon Nanotubes” Nano/Micro Engineered and Molecular Systems (2008) : 1000-1004

[40] Gomez-Navarro C., de Pablo P.J., et al. “Tuning the conductance of single walled carbon nanotubes by ion irradiation in the Anderson localization regime” Materials Science (2005) : 480 - 492

[41] Zheng L.X et al., “Ultra long Single-Wall Carbon Nanotubes” Nature Vol 10 (2004) : 673-676

[42] Dresselhaus M.S., et al “Physics of Carbon Nanotubes” Pergamon Vol 33 (1995) : 883-891

[43] Singiresu S.Rao., “The Finite Element Method in Engineering” Elsevier 4th Edition 2005.

[44] Tserpes K.I., Papanikos P., “Finite element modeling of single-walled carbon nanotubes” Elsevier 2005 : 468-477

[45] MATLAB R2007b Help Manual.

[46] Kattan P.I., “MATLAB Guide to Finite Elements” Springer (2002)

APPENDIX A

MATLAB CODE

In this section, important sections of the code will be presented in order to understand the methodology to do the necessary analyses. MATLAB r2007b version is used to develop the code and complete the analyses.

A.1 Main Code

```
clear,clc,close ALL HIDDEN ;
%% Inputs defining CNT and Defect amount
tic
numThreads=4;           % Multiprocessor
NN=[8];                 % n parameter of the Chirality Vector
Armchair=0;             % if set to 1 Ch=(NN,NN) else Ch=(NN,0)

Nmodes=5;               % Number of modes to be calculated
Dfct=0.01;              % Vacancy percentage from overall atoms
Ftz=0.5;                % Input Force in +Z direction for Young's
Modulus Analysis

Randomizer=1;
LCNT=[30];              % Number of Layers in the CNT

DrawTubes=0;            % Drawing the CNT Geometry is set to 1
DrawModeShapes=1;       % Drawing mode shapes for defect-free CNT if
                          set to 1
DrawDefectedModeShapes=0; % Drawing mode shapes for the defected CNT
                            if set to 1
DrawGraphs=0;           % Drawing other graphs if set to 1
DrawElongatedShapes=0; % Drawing elongated shapes if set to 1
Vibration=1;            % Activating Vibrational Analyses
YoungModulus=0;         % Activating Young's Modulus Analyses

ModeShape2Draw=[1 2 3 4 5]; % Selection of the mode shape to draw
DrawScale=0.5;          % Mode shape drawing scale
FigNo=0;
ANSYS=1;                % 1 for creating ANSYS file for the
                          verification
```

```
Bridged=0;              % If 0 cantilevered; else bridged
                          configuration created in ANSYS file

%% SUBSCRIPT "_DEF" BELONGS TO VARIABLES OF DEFECTED TUBE
for iter=1 : length(LCNT)
    Coor=0; K_GLOB=0; M_GLOB=0 K_GLOB_CANT=0; M_GLOB_CANT=0;
    K_GLOB_BRID=0; M_GLOB_BRID=0; U_CANT=0; A_CANT=0; F_CANT=0;
    Coor_Def=0; K_GLOB_DEF=0; M_GLOB_DEF=0 K_GLOB_CANT_DEF=0;
    M_GLOB_CANT_DEF=0; K_GLOB_BRID_DEF=0 M_GLOB_BRID_DEF=0;
    U_CANT_DEF=0; A_CANT=0; F_CANT_DEF=0;
    MS_NCANT=0; MS_NCANT_DEF=0; MS_NBRID=0; MS_NBRID_DEF=0;
    Deformed_Coor=0; Deformed_Coor_Def=0; MODE_BRID=0;
    MODE_BRID_DEF=0; MODE_CANT=0, MODE_CANT_DEF=0;
    N_BRID=0, N_BRID_DEF=0, N_CANT=0, N_CANT_DEF=0;
    Ncoor=0; Beam=0; Beam_all=0;
    Ncoor_Def=0; Beam_Def=0; Beam_all_Def=0;
    Nnodes=LCNT(iter)*NN(1);            % Number of nodes
    n=NN(1);
    if Armchair==1;
        m=n;
    else
        m=0;
    end
    %%
    a=0.1421;                           % C-C bond length : nm
    zcount=0;                           % counter for layers
    d2r=pi/180;                         % degree to radian converter
    xycount=0;                          % counter of rotation
    if Armchair==0
        thetaxy=-360/n;                 % angle offset
        zheight=-a/2;                   % initial z axis value
    end
    if Armchair==1
        arm_thetaxy=-360/(3*n) ;        % angle offset
        arm_height=-a*(3^(1/2))/2;      % initial z axis value
        arm_initial_theta=360/(6*n);
        arm_zlayer_count=0;
    end
    Dcnt=a*sqrt(3*(n^2+m^2+n*m))/pi;    % Diameter of CNT
    Diameter(iter,1)=Dcnt;
    Rcnt=Dcnt/2;                        % Radius of CNT
    i=1;j=1;k=1;h=1;r=0;                % Multiuse Counters

    %% Defining Cross sectional Parameters
    d=0.340;                    % nm diameter of X sec of bonds
    E=1.02*10^3;                % 5.49*10^-6 N/nm^2 :    5.49 TPa
    G=1.63*10^2;                % N/nm^2    : TPa
    A=pi*d^2 /4;                % area of C-C bond beam X-sec
    I=1.21*10^-4;
    J=I*2;
    mc=1.9943*[10^-26];         % mass of a carbon atom in kg s
    rc=2.75*10^-6;              % radius of C

    %% Randomizing the vacant nodes
      Def=0;
```

```
  if Randomizer==1
    ii =1;
    while ii ==1
        Repeated_def=0;
        if Armchair==0
            Def=floor((1+3*n)+(Nnodes-(1+3*n)-
(1+3*n))*rand(floor(Nnodes*Dfct),1));
        end
        if Armchair==1
            Def=floor((1+5*n)+(Nnodes-(1+5*n)-
(1+5*n))*rand(floor(Nnodes*Dfct),1));
        end
        for i= 1 : length(Def)
            for j=1 : i-1
                if Def(i,1)==Def(j,1)
                    Repeated_def=1;
                end
            end
        end
        if Repeated_def ~= 1
            ii=0;
            break
        end
    end
  end
    Defiter(1:length(Def),iter)=Def(1:length(Def),1);

        %% Distributing the tensile forces to the upper end
    if YoungModulus==1
        if Armchair==0
            F=zeros(6*Nnodes,1);
            for i= Nnodes-n+1 : Nnodes
                F(6*i-3,1)=Ftz/n;
            end
        end
        if Armchair==1
            F=zeros(6*Nnodes,1);
            for i= Nnodes-2*n+1 : Nnodes
                F(6*i-3,1)=Ftz/(2*n);
            end
        end
        if Armchair==0
            F_DEF=zeros(6*(Nnodes-length(Def)),1);
            for i= Nnodes-length(Def)-n : Nnodes-length(Def)-1;
                F_DEF(6*i+3,1)=Ftz/n;
            end
        end
        if Armchair==1
            F_DEF=zeros(6*(Nnodes-length(Def)),1);
            for i= Nnodes-length(Def)-2*n : Nnodes-length(Def)-1;
                F_DEF(6*i+3,1)=Ftz/(2*n);
            end
        end
    end
```

```
%% Coordinates of nodes
for i = 1 : Nnodes
    if Armchair==0
        if rem(i-1,n)==0
            if rem(xycount,2)==0
                thetaxy= thetaxy+360/n;
            end
            xycount=xycount+1;
        end
   Coor(i,1)=Rcnt*cos(mod(i,n)*(360/n*pi/180)+thetaxy*d2r/2);
   Coor(i,2)=Rcnt*sin(mod(i,n)*(360/n*pi/180)+thetaxy*d2r/2);
        if rem((i-1),n)==0
            if rem(zcount,2)==0
                zheight= zheight+a/2;
            elseif rem(zcount,2)==1
                zheight= zheight+a;
            end
            zcount=zcount+1;
        end
        Coor(i,3)=zheight;

    end
    if Armchair==1
        h=h+1;
        if rem(i-1,2*n)==0
            arm_height=arm_height+a*(3^(1/2))/2;
            arm_zlayer_count=arm_zlayer_count+1;
            j=0;
            h=0;
            if rem(arm_zlayer_count,2)==1
                arm_initial_theta=0;
            end
            if rem(arm_zlayer_count,2)==0
                arm_initial_theta=360/(6*n);
            end
        end
        theta_arm=((h+j)*(360/(3*n))+arm_initial_theta);
  Coor(i,1)=Rcnt*cos(((h+j)*(360/(3*n))+arm_initial_theta)*d2r);
  Coor(i,2)=Rcnt*sin(((h+j)*(360/(3*n))+arm_initial_theta)*d2r);
  Coor(i,3)=arm_height;
        if rem(arm_zlayer_count,2)==1
            if rem(i,2)==1
                j=j+1;
            end
        end
        if rem(arm_zlayer_count,2)==0
            if rem(i+1,2)==1
                j=j+1;
            end
        end
    end
end

j=0;
jj=0;
```

```
    for i=1:Nnodes-length(Def)
        j=j+1;
        jj=jj+1;
        for ii=1:length(Def)
            if i==Def(ii);
                jj=jj+1;
            end
        end
        Coor_Def(j,1)=Coor(jj,1);
        Coor_Def(j,2)=Coor(jj,2);
        Coor_Def(j,3)=Coor(jj,3);
    end
    LoverD(iter,1)=Coor(i,3)/Dcnt;

    %% Determination of adjacent nodes for defectless tube
    for i = 1 : Nnodes
        Ncount=1;
        for j = 1: Nnodes
            dist=sqrt(((Coor(i,1)-Coor(j,1))^2+ (Coor(i,2)-
Coor(j,2))^2 +(Coor(i,3)-Coor(j,3))^2));
            if dist>0.9*a && dist<1.1*a  && i ~=j
                Ncoor(i,Ncount)=j;
                Ncount=Ncount+1;
            end
        end
    end

    %% Connectivity matrix
    for  i = 1 : Nnodes
        for j = 1 : 3
            if Ncoor(i,j)~=0
                Beam_all(k,1)=i;
                Beam_all(k,2)=Ncoor(i,j);
                k=k+1;
            end
        end
    end

    %% Eliminating repeated bonds
    p=k-1;
    for  i = 1 : p
        dupt=0;
        for j= 1:i
%Checking for previous bonds
                  if Beam_all(i,2)==Beam_all(j,1)
                  if Beam_all(i,1)==Beam_all(j,2)
                    dupt=1;
                    p=p-1;
                end
            end
        end

     %%Filtering duplicate bonds(like 1-6 ,6-1)
        if dupt==0;
```

```
            r=r+1;
            Beam(r,1)=Beam_all(i,1);        %Assigning to new matrix
            Beam(r,2)=Beam_all(i,2);
            Nbeams=r;                       %Number of Beams in CNT
        end
    end
    %% Drawing the CNT
    if DrawTubes==1;
        FigNo=FigNo+1;
        i=length(Beam);
        fig=figure(FigNo);
        for f=1:i
            fig=plot3([Coor((Beam(f,1)),1);Coor((Beam(f,2)),1)],...
                [Coor((Beam(f,1)),2);Coor((Beam(f,2)),2)],...
                [Coor((Beam(f,1)),3);Coor((Beam(f,2)),3)],'-
ob','LineWidth',2,'markersize',8);
            hold on
            grid on
            axis equal
        end
    end

    %% Defected Connectivity matrix construction
    k=1;
    r=0;
    for i = 1 : Nnodes-length(Def)
        Ncount=1;
        for j = 1: Nnodes-length(Def)
            dist=sqrt(((Coor_Def(i,1)-Coor_Def(j,1))^2+
(Coor_Def(i,2)-Coor_Def(j,2))^2 +(Coor_Def(i,3)-Coor_Def(j,3))^2));
            if dist>0.9*a && dist<1.1*a  && i ~=j
                Ncoor_Def(i,Ncount)=j;
                Ncount=Ncount+1;
            end
        end
    end
    %% Connectivity matrix
    for  i = 1 : Nnodes-length(Def)
        for j = 1 : 3
            if Ncoor_Def(i,j)~=0
                Beam_all_Def(k,1)=i;
                Beam_all_Def(k,2)=Ncoor_Def(i,j);
                k=k+1;
            end
        end
    end

    %% Eliminating repeated bonds
    p=k-1;
    for  i = 1 : p
        dupt=0;
        for j= 1:i
            if Beam_all_Def(i,2)==Beam_all_Def(j,1)
%Checking for previous bonds
                if Beam_all_Def(i,1)==Beam_all_Def(j,2)
```

```
                    dupt=1;
                    p=p-1;
                end
            end
        end
      %Filtering duplicate bonds (like 1-6, 6-1)
      if dupt==0;
            r=r+1;
      Beam_Def(r,1)=Beam_all_Def(i,1);
      Beam_Def(r,2)=Beam_all_Def(i,2);
            Nbeams_Def=r;
        end
    end
    %% Drawing the defected CNT
    if DrawTubes==1;
        FigNo=FigNo+1;
        i=length(Beam_Def);
        fig(iter)=figure(FigNo);
        for f=1:i

fig(iter)=plot3([Coor_Def((Beam_Def(f,1)),1);Coor_Def((Beam_Def(f,2)
),1)],...

[Coor_Def((Beam_Def(f,1)),2);Coor_Def((Beam_Def(f,2)),2)],...

[Coor_Def((Beam_Def(f,1)),3);Coor_Def((Beam_Def(f,2)),3)],'-
ob','LineWidth',2,'markersize',8);
            hold on
            grid on
            axis equal
        end
    end

    %% Preparing a text file to ANSYS
    if ANSYS==1
        fid = fopen('ANSYS.doc','w+');
        fprintf(fid,'/CLEAR,NOSTART\n');

fprintf(fid,'/NOPR\n/PMETH,OFF,0\nKEYW,PR_SET,1\nKEYW,PR_STRUC,1\nKE
YW,PR_THERM,0\nKEYW,PR_FLUID,0\nKEYW,PR_MULTI,0\n/GO\n/PREP7\n');
        fprintf(fid,'ET,1,BEAM4\nET,2,MASS21\n!SECTYPE,   1, BEAM,
CSOLID, , 0\n!SECOFFSET,
CENT\n!SECDATA,%6.8f,0,0,0,0,0,0,0,0,0\n',d);

fprintf(fid,'MPTEMP,,,,,,,,\nMPTEMP,1,0\nMPDATA,EX,1,,%6.10f\nMPDATA
,EY,1,,%6.10f\nMPDATA,EZ,1,,%6.10f\n',E,E,E);

fprintf(fid,'MPDATA,PRXY,1,,0.3\nMPDATA,PRYZ,1,,0.3\nMPDATA,PRXZ,1,,
0.3\nMPDATA,GXY,1,,%6.8f\nMPDATA,GYZ,1,,%6.8f\nMPDATA,GXZ,1,,%6.8f\n
',G,G,G);
        fprintf(fid,'R,1,%6.10f,%6.10f,%6.10f,,,,\nRMORE, ,%6.10f ,
, , ,\nR,2,1.9943E-26,1.9943E-26,1.9943E-26,0,0,0,\n',A,I,I,J);
        j=1;
        for i=1:Nnodes
```

```
fprintf(fid,'N,%d,%6.8f,%6.8f,%6.8f,,,,\n',i,Coor(i,1),Coor(i,2),Coo
r(i,3));
        end
        fprintf(fid,'TYPE,1\nMAT,1\nREAL,1\nTSHAP,LINE\n');
        for i=1:Nbeams
            fprintf(fid,'E,%d,%d\n',Beam(i,1),Beam(i,2));
        end
        fprintf(fid,'TYPE,2\nMAT,1\nREAL,2\nTSHAP,LINE\n');
        for i=1:Nnodes
            fprintf(fid,'E,    %d\n',i);
        end

fprintf(fid,'EPLOT\nFINISH\n/SOL\nANTYPE,2\nMODOPT,LANB,%d\nEQSLV,SP
AR\nMXPAND,%d, , ,1\nLUMPM,1\n,PSTRES,0\n',Nmodes,Nmodes);
        fprintf(fid,'NSEL,S,LOC,Z,0\n') ;
% Select nodes at Z =0 location
        if Bridged==1
        fprintf(fid,'NSEL,A,LOC,Z,%10.8f\n',Coor(length(Coor),3)) ;
% Also select the upper end nodes
        end
        fprintf(fid,'D,ALL, ,0, , , ,ALL, , , , , \n')  ;
% DOF=0 for all nodes selected above
        fprintf(fid,'ALLSEL,ALL\n')      ;
% Select all
        fprintf(fid,'MODOPT,LANB,%d,0,0,
,OFF,/STATUS,SOLU\nSOLVE\nFINISH\n',Nmodes);
        fprintf(fid,'/POST1\nSET,LIST,2\n');
        fclose(fid);

        %% Preparing a text file to ANSYS for the defected matrix
        fid = fopen('ANSYS_DEFECTED.doc','w+');
        fprintf(fid,'/CLEAR,NOSTART\n');

fprintf(fid,'/NOPR\n/PMETH,OFF,0\nKEYW,PR_SET,1\nKEYW,PR_STRUC,1\nKE
YW,PR_THERM,0\nKEYW,PR_FLUID,0\nKEYW,PR_MULTI,0\n/GO\n/PREP7\n');
        fprintf(fid,'ET,1,BEAM4\nET,2,MASS21\n!SECTYPE,   1, BEAM,
CSOLID, , 0\n!SECOFFSET,
CENT\n!SECDATA,%6.8f,0,0,0,0,0,0,0,0,0\n',d);

fprintf(fid,'MPTEMP,,,,,,,,\nMPTEMP,1,0\nMPDATA,EX,1,,%6.10f\nMPDATA
,EY,1,,%6.10f\nMPDATA,EZ,1,,%6.10f\n',E,E,E);

fprintf(fid,'MPDATA,PRXY,1,,0.3\nMPDATA,PRYZ,1,,0.3\nMPDATA,PRXZ,1,,
0.3\nMPDATA,GXY,1,,%6.8f\nMPDATA,GYZ,1,,%6.8f\nMPDATA,GXZ,1,,%6.8f\n
',G,G,G);
        fprintf(fid,'R,1,%6.10f,%6.10f,%6.10f,,,,\nRMORE, ,%6.10f ,
, , ,\nR,2, 1.9943E-26,1.9943E-26,1.9943E-26,0,0,0,\n',A,I,I,J);
        j=1;
        for i=1:Nnodes-length(Def)

fprintf(fid,'N,%d,%6.8f,%6.8f,%6.8f,,,,\n',i,Coor_Def(i,1),Coor_Def(
i,2),Coor_Def(i,3));
        end
        fprintf(fid,'TYPE,1\nMAT,1\nREAL,1\nTSHAP,LINE\n');
```

```
        for i=1:Nbeams_Def
            fprintf(fid,'E,%d,%d\n',Beam_Def(i,1),Beam_Def(i,2));
        end
        fprintf(fid,'TYPE,2\nMAT,1\nREAL,2\nTSHAP,LINE\n');
        for i=1:Nnodes-length(Def)
            fprintf(fid,'E,    %d\n',i);
        end

fprintf(fid,'EPLOT\nFINISH\n/SOL\nANTYPE,2\nMODOPT,LANB,%d\nEQSLV,SP
AR\nMXPAND,%d, , ,1\nLUMPM,1\n,PSTRES,0\n',Nmodes,Nmodes);
        fprintf(fid,'NSEL,S,LOC,Z,0\n');
% Select nodes at Z =0 location
        if Bridged==1
fprintf(fid,'NSEL,A,LOC,Z,%10.8f\n',Coor_Def(length(Coor_Def),3));
% Also select the upper end nodes
        end
        fprintf(fid,'D,ALL, ,0, , , ,ALL, , , , , \n');
% DOF=0 for all nodes selected above
        fprintf(fid,'ALLSEL,ALL\n');
% Select all
        fprintf(fid,'MODOPT,LANB,%d,0,0,
,OFF,/STATUS,SOLU\nSOLVE\nFINISH\n',Nmodes);
        fprintf(fid,'/POST1\nSET,LIST,2\n');
        fclose(fid);
    end
    %% Constructing elementary stiffness matrices and Assembling
into Global K & M matrix
    K_GLOB=zeros(6*Nnodes,6*Nnodes);
    M_GLOB=zeros(6*Nnodes,6*Nnodes);
    for i=1:6:6*Nnodes

diagM(i:i+5)=[mc;mc;mc;(2/3)*mc*rc^2;(2/3)*mc*rc^2;(2/3)*mc*rc^2];
    end
    M_GLOB=diag(diagM);
    for i=1:Nbeams

K_ELE=SpaceFrameElementStiffness(E,G,A,I,I,J,Coor(Beam(i,1),1),Coor(
Beam(i,1),2),Coor(Beam(i,1),3),Coor(Beam(i,2),1),Coor(Beam(i,2),2),C
oor(Beam(i,2),3));
        K_GLOB=SpaceFrameAssemble(K_GLOB,K_ELE,Beam(i,1),Beam(i,2));
        K_ELE=0;
    End

    %% Constructing fixed end Global matrices
    if Armchair==0
        K_GLOB_CANT=K_GLOB((6*n)+1:6*Nnodes,(6*n)+1:6*Nnodes);
        M_GLOB_CANT=M_GLOB((6*n)+1:6*Nnodes,(6*n)+1:6*Nnodes);

        K_GLOB_BRID=K_GLOB((6*n)+1:6*Nnodes-6*n,(6*n)+1:6*Nnodes-
6*n);
        M_GLOB_BRID=M_GLOB((6*n)+1:6*Nnodes-6*n,(6*n)+1:6*Nnodes-
6*n);
    end
    if Armchair==1
        K_GLOB_CANT=K_GLOB((12*n)+1:6*Nnodes,(12*n)+1:6*Nnodes);
```

```
        M_GLOB_CANT=M_GLOB((12*n)+1:6*Nnodes,(12*n)+1:6*Nnodes);

        K_GLOB_BRID=K_GLOB((12*n)+1:6*Nnodes-12*n,(12*n)+1:6*Nnodes-
12*n);
        M_GLOB_BRID=M_GLOB((12*n)+1:6*Nnodes-12*n,(12*n)+1:6*Nnodes-
12*n);
    end
    %% Constructing Defected Global K & M matrix
    K_GLOB_DEF=zeros(6*(Nnodes-length(Def)),6*(Nnodes-length(Def)));
    M_GLOB_DEF=zeros(6*(Nnodes-length(Def)),6*(Nnodes-length(Def)));
    j=length(Beam_Def);
    K_ELE=0;
    for i= 1: j

K_ELE=SpaceFrameElementStiffness(E,G,A,I,I,J,Coor_Def(Beam_Def(i,1),
1),Coor_Def(Beam_Def(i,1),2),Coor_Def(Beam_Def(i,1),3),Coor_Def(Beam
_Def(i,2),1),Coor_Def(Beam_Def(i,2),2),Coor_Def(Beam_Def(i,2),3));

K_GLOB_DEF=SpaceFrameAssemble(K_GLOB_DEF,K_ELE,Beam_Def(i,1),Beam_De
f(i,2));
        K_ELE=0;
    end
    for i=1:6:6*(Nnodes-length(Def))

M_DIAG(i:i+5)=[mc;mc;mc;(2/3)*mc*rc^2;(2/3)*mc*rc^2;(2/3)*mc*rc^2];
    end
    M_GLOB_DEF=diag(M_DIAG);

    %% Constructing fixed end Global matrices for defected matrices
    if Armchair==0
        K_GLOB_CANT_DEF=K_GLOB_DEF((6*n)+1:6*(Nnodes-
length(Def)),(6*n)+1:6*(Nnodes-length(Def)));
        M_GLOB_CANT_DEF=M_GLOB_DEF((6*n)+1:6*(Nnodes-
length(Def)),(6*n)+1:6*(Nnodes-length(Def)));
        K_GLOB_BRID_DEF=K_GLOB_DEF((6*n)+1:6*(Nnodes-length(Def))-
6*n,(6*n)+1:6*(Nnodes-length(Def))-6*n);
        M_GLOB_BRID_DEF=M_GLOB_DEF((6*n)+1:6*(Nnodes-length(Def))-
6*n,(6*n)+1:6*(Nnodes-length(Def))-6*n);
    end
    if Armchair==1
        K_GLOB_CANT_DEF=K_GLOB_DEF((12*n)+1:6*(Nnodes-
length(Def)),(12*n)+1:6*(Nnodes-length(Def)));
        M_GLOB_CANT_DEF=M_GLOB_DEF((12*n)+1:6*(Nnodes-
length(Def)),(12*n)+1:6*(Nnodes-length(Def)));
        K_GLOB_BRID_DEF=K_GLOB_DEF((12*n)+1:6*(Nnodes-length(Def))-
12*n,(12*n)+1:6*(Nnodes-length(Def))-12*n);
        M_GLOB_BRID_DEF=M_GLOB_DEF((12*n)+1:6*(Nnodes-length(Def))-
12*n,(12*n)+1:6*(Nnodes-length(Def))-12*n);
    end

    if YoungModulus==1
        if Armchair==0
            F_CANT=F((6*n)+1:6*Nnodes,1);
        end
        if Armchair==1
```

```
            F_CANT=F((12*n)+1:6*Nnodes,1);
        end
    end

    %% Tensile force calculation
    if YoungModulus==1
        U_CANT=inv(K_GLOB_CANT)*F_CANT;
        A_CANT=pi*((Dcnt/2+d/2)^2-(Dcnt/2-d/2)^2)*10^-8;
        Young_CANT(iter,1)=(Ftz/A_CANT)/(U_CANT(length(U_CANT)-
3,1)/Coor(length(Coor),3));
        if DrawGraphs==1
            FigNo=FigNo+1;
            fig=figure(FigNo);
            fig=plot(Diameter,Young_CANT);
        end
    end
    %% Young modulus calculation
    if YoungModulus==1
        if Armchair==0
            F_CANT_DEF=F_DEF((6*n)+1:6*(Nnodes-length(Def)),1);
        end
        if Armchair==1
            F_CANT_DEF=F_DEF((12*n)+1:6*(Nnodes-length(Def)),1);
        end

        U_CANT_DEF=inv(K_GLOB_CANT_DEF)*F_CANT_DEF;
        Max_elong_in_z=0;
        if Armchair==0
            for i=1 : n

Max_elong_in_z=Max_elong_in_z+abs(U_CANT_DEF(length(U_CANT_DEF)-
6*i+3,1));
            end
            Max_elong_in_z=Max_elong_in_z/n;
        end

        if Armchair==1
            for i=1 : 2*n

Max_elong_in_z=Max_elong_in_z+abs(U_CANT_DEF(length(U_CANT_DEF)-
6*i+3,1));
            end
            Max_elong_in_z=Max_elong_in_z/(2*n);
        end
        A_CANT=pi*((Dcnt/2+d/2)^2-(Dcnt/2-d/2)^2)*10^-8;

Young_CANT_DEF(iter,1)=(Ftz/A_CANT)/(Max_elong_in_z/Coor_Def(length(
Coor_Def),3));
        if DrawGraphs==1
            FigNo=FigNo+1;
            fig=figure(FigNo);
            fig=plot(Diameter,Young_CANT_DEF);
        end
```

```
        Young_CANT_REDUCED(iter,1)=100*(Young_CANT(iter,1)-
Young_CANT_DEF(iter,1))/Young_CANT(iter,1);
    End

    %% Solving Eigenvalue problem & Natural Frequency analysis
    if Vibration==1
        [MODE_CANT,D] = eig(K_GLOB_CANT,M_GLOB_CANT);
        NF_CANT=diag(D);
        N_CANT=sort(NF_CANT);
        for i=1:Nmodes
            NAT_FREQ_CANT(i,iter)=(sqrt(N_CANT(i,1)))/(2*pi);
        end
        if DrawModeShapes==1
            for j=1:Nmodes
                for i=1: length(NF_CANT);
                    if N_CANT(j)==NF_CANT(i);
                        MS_NCANT(j)=i;
                    end
                end
            end
        end

        [MODE_BRID,D] = eig(K_GLOB_BRID,M_GLOB_BRID);
        NF_BRID=diag(D);
        N_BRID=sort(NF_BRID);
        for i=1:Nmodes
            NAT_FREQ_BRID(i,iter)=(sqrt(N_BRID(i,1)))/(2*pi);
        end
        if DrawModeShapes==1
            for j=1:Nmodes
                for i=1: length(NF_BRID);
                    if N_BRID(j)==NF_BRID(i);
                        MS_NBRID(j)=i;
                    end
                end
            end
        end

        [MODE_CANT_DEF,D] = eig(K_GLOB_CANT_DEF,M_GLOB_CANT_DEF);
        NF_CANT_DEF=diag(D);
        N_CANT_DEF=sort(NF_CANT_DEF);
        for i=1:Nmodes

            NAT_FREQ_CANT_DEF(i,iter)=(sqrt(N_CANT_DEF(i,1)))/(2*pi)
        end
        if DrawDefectedModeShapes==1
            for j=1:Nmodes
                for i=1: length(NF_CANT_DEF);
                    if N_CANT_DEF(j)==NF_CANT_DEF(i);
                        MS_NCANT_DEF(j)=i;
                    end
                end
            end
        end
```

```
        [MODE_BRID_DEF,D] = eig(K_GLOB_BRID_DEF,M_GLOB_BRID_DEF);
        NF_BRID_DEF=diag(D);
        N_BRID_DEF=sort(NF_BRID_DEF);
        if DrawDefectedModeShapes==1
            for j=1:Nmodes
                for i=1: length(NF_BRID_DEF);
                    if N_BRID_DEF(j)==NF_BRID_DEF(i);
                        MS_NBRID_DEF(j)=i;
                    end
                end
            end
        end
        for i=1:Nmodes

      NAT_FREQ_BRID_DEF(i,iter)=(sqrt(N_BRID_DEF(i,1)))/(2*pi);
        end


      NAT_FREQ_CANT_REDUCED(1,iter)=100*(NAT_FREQ_CANT(1,iter)-
      NAT_FREQ_CANT_DEF(1,iter))/NAT_FREQ_CANT(1,iter);
      NAT_FREQ_BRID_REDUCED(1,iter)=100*(NAT_FREQ_BRID(1,iter)-
      NAT_FREQ_BRID_DEF(1,iter))/NAT_FREQ_BRID(1,iter);

    end
      %% Calculating the node positions after young modulus and
      vibration analysis

for iter2=1:length(ModeShape2Draw)
    if Armchair==0
        j=1;
        if YoungModulus==1
            Deformed_Coor(1:n,1:3)=Coor(1:n,1:3);
        end
        if Vibration==1
            ModeShape_Coor_CANT(1:n,1:3)=Coor(1:n,1:3);
            ModeShape_Coor_BRID(1:n,1:3)=Coor(1:n,1:3);
            ModeShape_Coor_BRID(length(Coor)-
n+1:length(Coor),1:3)=Coor(length(Coor)-n+1:length(Coor),1:3);
        end
        for i=(n+1):length(Coor)
            if YoungModulus==1 && DrawElongatedShapes==1;
                Deformed_Coor(i,1)=Coor(i,1)+U_CANT(j);
                Deformed_Coor(i,2)=Coor(i,2)+U_CANT(j+1);
                Deformed_Coor(i,3)=Coor(i,3)+U_CANT(j+2);
            end
            if Vibration==1 &&DrawModeShapes==1

ModeShape_Coor_CANT(i,1)=Coor(i,1)+DrawScale*MODE_CANT(j,MS_NCANT(Mo
deShape2Draw(iter2)));

ModeShape_Coor_CANT(i,2)=Coor(i,2)+DrawScale*MODE_CANT(j+1,MS_NCANT(
ModeShape2Draw(iter2)));
```

```
ModeShape_Coor_CANT(i,3)=Coor(i,3)+DrawScale*MODE_CANT(j+2,MS_NCANT(
ModeShape2Draw(iter2)));
            end
            j=j+6;
        end
        j=1;
        for i=(n+1):length(Coor)-n
            if Vibration==1 &&DrawModeShapes==1

ModeShape_Coor_BRID(i,1)=Coor(i,1)+DrawScale*MODE_BRID(j,MS_NBRID(Mo
deShape2Draw(iter2)));

ModeShape_Coor_BRID(i,2)=Coor(i,2)+DrawScale*MODE_BRID(j+1,MS_NBRID(
ModeShape2Draw(iter2)));

ModeShape_Coor_BRID(i,3)=Coor(i,3)+DrawScale*MODE_BRID(j+2,MS_NBRID(
ModeShape2Draw(iter2)));
            end
            j=j+6;
        end



        j=1;
        if YoungModulus==1
            Deformed_Coor_Def(1:n,1:3)=Coor_Def(1:n,1:3);
        end
        if Vibration==1
            ModeShape_Coor_CANT_Def(1:n,1:3)=Coor_Def(1:n,1:3);
            ModeShape_Coor_BRID_Def(1:n,1:3)=Coor_Def(1:n,1:3);
            ModeShape_Coor_BRID_Def(length(Coor_Def)-
n+1:length(Coor_Def),1:3)=Coor(length(Coor_Def)-
n+1:length(Coor_Def),1:3);
        end
        for i=(n+1):length(Coor_Def)
            if YoungModulus==1 && DrawElongatedShapes==1;
                Deformed_Coor_Def(i,1)=Coor_Def(i,1)+U_CANT_DEF(j);

Deformed_Coor_Def(i,2)=Coor_Def(i,2)+U_CANT_DEF(j+1);

Deformed_Coor_Def(i,3)=Coor_Def(i,3)+U_CANT_DEF(j+2);
            end
            if Vibration==1 &&DrawDefectedModeShapes==1


ModeShape_Coor_CANT_Def(i,1)=Coor_Def(i,1)+DrawScale*MODE_CANT_DEF(j
,MS_NCANT_DEF(ModeShape2Draw(iter2)));

ModeShape_Coor_CANT_Def(i,2)=Coor_Def(i,2)+DrawScale*MODE_CANT_DEF(j
+1,MS_NCANT_DEF(ModeShape2Draw(iter2)));

ModeShape_Coor_CANT_Def(i,3)=Coor_Def(i,3)+DrawScale*MODE_CANT_DEF(j
+2,MS_NCANT_DEF(ModeShape2Draw(iter2)));
```

```
            end
            j=j+6;
        end
        j=1;
        for i=(n+1):length(Coor_Def)-n
            if Vibration==1 &&DrawDefectedModeShapes==1

ModeShape_Coor_BRID_Def(i,1)=Coor_Def(i,1)+DrawScale*MODE_BRID_DEF(j
,MS_NBRID_DEF(ModeShape2Draw(iter2)));

ModeShape_Coor_BRID_Def(i,2)=Coor_Def(i,2)+DrawScale*MODE_BRID_DEF(j
+1,MS_NBRID_DEF(ModeShape2Draw(iter2)));

ModeShape_Coor_BRID_Def(i,3)=Coor_Def(i,3)+DrawScale*MODE_BRID_DEF(j
+2,MS_NBRID_DEF(ModeShape2Draw(iter2)));
            end
            j=j+6;
        end
    end

    if Armchair==1
        j=1;
        if YoungModulus==1
            Deformed_Coor(1:(2*n),1:3)=Coor(1:(2*n),1:3);
        end
        if Vibration==1
            ModeShape_Coor_CANT(1:(2*n),1:3)=Coor(1:(2*n),1:3);
            ModeShape_Coor_BRID(1:(2*n),1:3)=Coor(1:(2*n),1:3);
            ModeShape_Coor_BRID(length(Coor)-
2*n+1:length(Coor),1:3)=Coor(length(Coor)-2*n+1:length(Coor),1:3);
        end
        for i=(2*n+1):length(Coor)
            if YoungModulus==1 && DrawElongatedShapes==1;
                Deformed_Coor(i,1)=Coor(i,1)+U_CANT(j);
                Deformed_Coor(i,2)=Coor(i,2)+U_CANT(j+1);
                Deformed_Coor(i,3)=Coor(i,3)+U_CANT(j+2);
            end
            if Vibration==1 &&DrawModeShapes==1

ModeShape_Coor_CANT(i,1)=Coor(i,1)+DrawScale*MODE_CANT(j,MS_NCANT(Mo
deShape2Draw(iter2)));

ModeShape_Coor_CANT(i,2)=Coor(i,2)+DrawScale*MODE_CANT(j+1,MS_NCANT(
ModeShape2Draw(iter2)));

ModeShape_Coor_CANT(i,3)=Coor(i,3)+DrawScale*MODE_CANT(j+2,MS_NCANT(
ModeShape2Draw(iter2)));
            end
            j=j+6;
        end
        j=1;
        for i=(2*n+1):length(Coor)-2*n
            if Vibration==1 &&DrawModeShapes==1
```

```
ModeShape_Coor_BRID(i,1)=Coor(i,1)+DrawScale*MODE_BRID(j,MS_NBRID(Mo
deShape2Draw(iter2)));

ModeShape_Coor_BRID(i,2)=Coor(i,2)+DrawScale*MODE_BRID(j+1,MS_NBRID(
ModeShape2Draw(iter2)));

ModeShape_Coor_BRID(i,3)=Coor(i,3)+DrawScale*MODE_BRID(j+2,MS_NBRID(
ModeShape2Draw(iter2)));
            end
            j=j+6;
        end

        j=1;
        if YoungModulus==1
            Deformed_Coor_Def(1:(2*n),1:3)=Coor_Def(1:(2*n),1:3);
        end
        if Vibration==1

ModeShape_Coor_CANT_Def(1:(2*n),1:3)=Coor_Def(1:(2*n),1:3);

ModeShape_Coor_BRID_Def(1:(2*n),1:3)=Coor_Def(1:(2*n),1:3);
            ModeShape_Coor_BRID_Def(length(Coor_Def)-
2*n+1:length(Coor_Def),1:3)=Coor_Def(length(Coor_Def)-
2*n+1:length(Coor_Def),1:3);
        end
        for i=(2*n+1):length(Coor_Def)
            if YoungModulus==1&& DrawElongatedShapes==1;
                Deformed_Coor_Def(i,1)=Coor_Def(i,1)+U_CANT_DEF(j);

Deformed_Coor_Def(i,2)=Coor_Def(i,2)+U_CANT_DEF(j+1);

Deformed_Coor_Def(i,3)=Coor_Def(i,3)+U_CANT_DEF(j+2);
            end
            if Vibration==1 &&DrawDefectedModeShapes==1

ModeShape_Coor_CANT_Def(i,1)=Coor_Def(i,1)+DrawScale*MODE_CANT_DEF(j
,MS_NCANT_DEF(ModeShape2Draw(iter2)));

ModeShape_Coor_CANT_Def(i,2)=Coor_Def(i,2)+DrawScale*MODE_CANT_DEF(j
+1,MS_NCANT_DEF(ModeShape2Draw(iter2)));

ModeShape_Coor_CANT_Def(i,3)=Coor_Def(i,3)+DrawScale*MODE_CANT_DEF(j
+2,MS_NCANT_DEF(ModeShape2Draw(iter2)));
            end
            j=j+6;
        end
        j=1;
        for i=(2*n+1):length(Coor)-2*n
            if Vibration==1 &&DrawDefectedModeShapes==1

ModeShape_Coor_BRID_Def(i,1)=Coor_Def(i,1)+DrawScale*MODE_BRID_DEF(j
,MS_NBRID_DEF(ModeShape2Draw(iter2)));
```

```
ModeShape_Coor_BRID_Def(i,2)=Coor_Def(i,2)+DrawScale*MODE_BRID_DEF(j
+1,MS_NBRID_DEF(ModeShape2Draw(iter2)));

ModeShape_Coor_BRID_Def(i,3)=Coor_Def(i,3)+DrawScale*MODE_BRID_DEF(j
+2,MS_NBRID_DEF(ModeShape2Draw(iter2)));
            end
            j=j+6;
        end
    end

    %% Drawing the CNT with its deformation under tensile force
    if YoungModulus==1 && DrawElongatedShapes==1;
        FigNo=FigNo+1;
        i=length(Beam);
        fig=figure(FigNo);
           for f=1:i

fig=plot3([Deformed_Coor((Beam(f,1)),1);Deformed_Coor((Beam(f,2)),1)
],...

[Deformed_Coor((Beam(f,1)),2);Deformed_Coor((Beam(f,2)),2)],...
[Deformed_Coor((Beam(f,1)),3);Deformed_Coor((Beam(f,2)),3)],'-
.or','LineWidth',2,'markersize',8);
            hold on
            grid on
            axis equal
            title('Plot of CNT under Tensile Force')
        end
    end
    %% Drawing the defected CNT with its deformation under tensile
    if YoungModulus==1 && DrawElongatedShapes==1;
        FigNo=FigNo+1;
        i=length(Beam_Def);
        fig(iter)=figure(FigNo);
        for f=1:i

fig(iter)=plot3([Deformed_Coor_Def((Beam_Def(f,1)),1);Deformed_Coor_
Def((Beam_Def(f,2)),1)],...

[Deformed_Coor_Def((Beam_Def(f,1)),2);Deformed_Coor_Def((Beam_Def(f,
2)),2)],...

[Deformed_Coor_Def((Beam_Def(f,1)),3);Deformed_Coor_Def((Beam_Def(f,
2)),3)],'-.or','LineWidth',2,'markersize',8);
            hold on
            grid on
            axis equal
            title('Plot of defected CNT under Tensile Force')
        end
    end
    %% Drawing the CNT 's modal shape
    if Vibration==1 && DrawModeShapes==1;
        FigNo=FigNo+1;
```

```
        i=length(Beam);
        fig(iter)=figure(FigNo);
        for f=1:i

fig(iter)=plot3([ModeShape_Coor_CANT((Beam(f,1)),1);ModeShape_Coor_C
ANT((Beam(f,2)),1)],...
[ModeShape_Coor_CANT((Beam(f,1)),2);ModeShape_Coor_CANT((Beam(f,2)),
2)],...
[ModeShape_Coor_CANT((Beam(f,1)),3);ModeShape_Coor_CANT((Beam(f,2)),
3)],'-ob','LineWidth',2,'markersize',8);
            hold on
            grid on
            axis equal
            title('Mode Shape of Defectless CNT')
        end
    end

    %% Drawing the defected CNT's modal shape
    if Vibration==1 && DrawDefectedModeShapes==1;
        FigNo=FigNo+1;
        i=length(Beam_Def);
        fig(iter)=figure(FigNo);
        for f=1:i

fig(iter)=plot3([ModeShape_Coor_CANT_Def((Beam_Def(f,1)),1);ModeShap
e_Coor_CANT_Def((Beam_Def(f,2)),1)],...

[ModeShape_Coor_CANT_Def((Beam_Def(f,1)),2);ModeShape_Coor_CANT_Def(
(Beam_Def(f,2)),2)],...

[ModeShape_Coor_CANT_Def((Beam_Def(f,1)),3);ModeShape_Coor_CANT_Def(
(Beam_Def(f,2)),3)],'-ob','LineWidth',2,'markersize',8);
            hold on
            grid on
            axis equal
            title('iter2')
        end
    end
        if Vibration==1 && DrawDefectedModeShapes==1;
        FigNo=FigNo+1;
        i=length(Beam_Def);
        fig(iter)=figure(FigNo);
        for f=1:i

fig(iter)=plot3([ModeShape_Coor_BRID_Def((Beam_Def(f,1)),1);ModeShap
e_Coor_BRID_Def((Beam_Def(f,2)),1)],...

[ModeShape_Coor_BRID_Def((Beam_Def(f,1)),2);ModeShape_Coor_BRID_Def(
(Beam_Def(f,2)),2)],...

[ModeShape_Coor_BRID_Def((Beam_Def(f,1)),3);ModeShape_Coor_BRID_Def(
(Beam_Def(f,2)),3)],'-ob','LineWidth',2,'markersize',8);
            hold on
            grid on
            axis equal
```

```
            title('iter2')
        end
    end
end
end

t=toc;
```

A.2 Elemental Stiffness Matrix Sub-Function

```
function y =
SpaceFrameElementStiffness(E,G,A,Iy,Iz,J,x1,y1,z1,x2,y2,z2)
%SpaceFrameElementStiffness   This function returns the element
%                             stiffness matrix for a space frame
%                             element with modulus of elasticity E,
%                             shear modulus of elasticity G, cross-
%                             sectional area A, moments of inertia
%                             Iy and Iz, torsional constant J,
%                             coordinates (x1,y1,z1) for the first
%                             node and coordinates (x2,y2,z2) for
%                             second node.
%                             The size of the element stiffness
%                             matrix is 12 x 12.
L = sqrt((x2-x1)*(x2-x1) + (y2-y1)*(y2-y1) + (z2-z1)*(z2-z1));
w1 = E*A/L;
w2 = 12*E*Iz/(L*L*L);
w3 = 6*E*Iz/(L*L);
w4 = 4*E*Iz/L;
w5 = 2*E*Iz/L;
w6 = 12*E*Iy/(L*L*L);
w7 = 6*E*Iy/(L*L);
w8 = 4*E*Iy/L;
w9 = 2*E*Iy/L;
w10 = G*J/L;
kprime = [w1 0 0 0 0 0 -w1 0 0 0 0 0 ;
          0 w2 0 0 0 w3 0 -w2 0 0 0 w3 ;
          0 0 w6 0 -w7 0 0 0 -w6 0 -w7 0 ;
          0 0 0 w10 0 0 0 0 0 -w10 0 0 ;
          0 0 -w7 0 w8 0 0 0 w7 0 w9 0 ;
          0 w3 0 0 0 w4 0 -w3 0 0 0 w5 ;
          -w1 0 0 0 0 0 w1 0 0 0 0 0 ;
          0 -w2 0 0 0 -w3 0 w2 0 0 0 -w3 ;
          0 0 -w6 0 w7 0 0 0 w6 0 w7 0 ;
          0 0 0 -w10 0 0 0 0 0 w10 0 0 ;
          0 0 -w7 0 w9 0 0 0 w7 0 w8 0 ;
          0 w3 0 0 0 w5 0 -w3 0 0 0 w4];
if x1 == x2 & y1 == y2
   if z2 > z1
      Lambda = [0 0 1 ; 0 1 0 ; -1 0 0];
   else
      Lambda = [0 0 -1 ; 0 1 0 ; 1 0 0];
   end
```

```
else
   CXx = (x2-x1)/L;
    CYx = (y2-y1)/L;
    CZx = (z2-z1)/L;
    D = sqrt(CXx*CXx + CYx*CYx);
    CXy = -CYx/D;
    CYy = CXx/D;
    CZy = 0;
    CXz = -CXx*CZx/D;
    CYz = -CYx*CZx/D;
    CZz = D;
    Lambda = [CXx CYx CZx ; CXy CYy CZy ; CXz CYz CZz];
end
R = [Lambda zeros(3) zeros(3) zeros(3) ;
   zeros(3) Lambda zeros(3) zeros(3) ;
   zeros(3) zeros(3) Lambda zeros(3) ;
   zeros(3) zeros(3) zeros(3) Lambda];
y = R'*kprime*R;
```

A.3 Assemble into Global Matrix Sub-Function

```
function y = SpaceFrameAssemble(K,k,i,j)
%SpaceFrameAssemble   This function assembles the element stiffness
%                     matrix k of the space frame element with nodes
%                     i and j into the global stiffness matrix K.
%                     This function returns the global stiffness
%                     matrix K after the element stiffness matrix
%                     k is assembled.
K(6*i-5,6*i-5) = K(6*i-5,6*i-5) + k(1,1);
K(6*i-5,6*i-4) = K(6*i-5,6*i-4) + k(1,2);
K(6*i-5,6*i-3) = K(6*i-5,6*i-3) + k(1,3);
K(6*i-5,6*i-2) = K(6*i-5,6*i-2) + k(1,4);
K(6*i-5,6*i-1) = K(6*i-5,6*i-1) + k(1,5);
K(6*i-5,6*i) = K(6*i-5,6*i) + k(1,6);
K(6*i-5,6*j-5) = K(6*i-5,6*j-5) + k(1,7);
K(6*i-5,6*j-4) = K(6*i-5,6*j-4) + k(1,8);
K(6*i-5,6*j-3) = K(6*i-5,6*j-3) + k(1,9);
K(6*i-5,6*j-2) = K(6*i-5,6*j-2) + k(1,10);
K(6*i-5,6*j-1) = K(6*i-5,6*j-1) + k(1,11);
K(6*i-5,6*j) = K(6*i-5,6*j) + k(1,12);
K(6*i-4,6*i-5) = K(6*i-4,6*i-5) + k(2,1);
K(6*i-4,6*i-4) = K(6*i-4,6*i-4) + k(2,2);
K(6*i-4,6*i-3) = K(6*i-4,6*i-3) + k(2,3);
K(6*i-4,6*i-2) = K(6*i-4,6*i-2) + k(2,4);
K(6*i-4,6*i-1) = K(6*i-4,6*i-1) + k(2,5);
K(6*i-4,6*i) = K(6*i-4,6*i) + k(2,6);
K(6*i-4,6*j-5) = K(6*i-4,6*j-5) + k(2,7);
K(6*i-4,6*j-4) = K(6*i-4,6*j-4) + k(2,8);
K(6*i-4,6*j-3) = K(6*i-4,6*j-3) + k(2,9);
K(6*i-4,6*j-2) = K(6*i-4,6*j-2) + k(2,10);
K(6*i-4,6*j-1) = K(6*i-4,6*j-1) + k(2,11);
K(6*i-4,6*j) = K(6*i-4,6*j) + k(2,12);
```

```
K(6*i-3,6*i-5) = K(6*i-3,6*i-5) + k(3,1);
K(6*i-3,6*i-4) = K(6*i-3,6*i-4) + k(3,2);
K(6*i-3,6*i-3) = K(6*i-3,6*i-3) + k(3,3);
K(6*i-3,6*i-2) = K(6*i-3,6*i-2) + k(3,4);
K(6*i-3,6*i-1) = K(6*i-3,6*i-1) + k(3,5);
K(6*i-3,6*i) = K(6*i-3,6*i) + k(3,6);
K(6*i-3,6*j-5) = K(6*i-3,6*j-5) + k(3,7);
K(6*i-3,6*j-4) = K(6*i-3,6*j-4) + k(3,8);
K(6*i-3,6*j-3) = K(6*i-3,6*j-3) + k(3,9);
K(6*i-3,6*j-2) = K(6*i-3,6*j-2) + k(3,10);
K(6*i-3,6*j-1) = K(6*i-3,6*j-1) + k(3,11);
K(6*i-3,6*j) = K(6*i-3,6*j) + k(3,12);
K(6*i-2,6*i-5) = K(6*i-2,6*i-5) + k(4,1);
K(6*i-2,6*i-4) = K(6*i-2,6*i-4) + k(4,2);
K(6*i-2,6*i-3) = K(6*i-2,6*i-3) + k(4,3);
K(6*i-2,6*i-2) = K(6*i-2,6*i-2) + k(4,4);
K(6*i-2,6*i-1) = K(6*i-2,6*i-1) + k(4,5);
K(6*i-2,6*i) = K(6*i-2,6*i) + k(4,6);
K(6*i-2,6*j-5) = K(6*i-2,6*j-5) + k(4,7);
K(6*i-2,6*j-4) = K(6*i-2,6*j-4) + k(4,8);
K(6*i-2,6*j-3) = K(6*i-2,6*j-3) + k(4,9);
K(6*i-2,6*j-2) = K(6*i-2,6*j-2) + k(4,10);
K(6*i-2,6*j-1) = K(6*i-2,6*j-1) + k(4,11);
K(6*i-2,6*j) = K(6*i-2,6*j) + k(4,12);
K(6*i-1,6*i-5) = K(6*i-1,6*i-5) + k(5,1);
K(6*i-1,6*i-4) = K(6*i-1,6*i-4) + k(5,2);
K(6*i-1,6*i-3) = K(6*i-1,6*i-3) + k(5,3);
K(6*i-1,6*i-2) = K(6*i-1,6*i-2) + k(5,4);
K(6*i-1,6*i-1) = K(6*i-1,6*i-1) + k(5,5);
K(6*i-1,6*i) = K(6*i-1,6*i) + k(5,6);
K(6*i-1,6*j-5) = K(6*i-1,6*j-5) + k(5,7);
K(6*i-1,6*j-4) = K(6*i-1,6*j-4) + k(5,8);
K(6*i-1,6*j-3) = K(6*i-1,6*j-3) + k(5,9);
K(6*i-1,6*j-2) = K(6*i-1,6*j-2) + k(5,10);
K(6*i-1,6*j-1) = K(6*i-1,6*j-1) + k(5,11);
K(6*i-1,6*j) = K(6*i-1,6*j) + k(5,12);
K(6*i,6*i-5) = K(6*i,6*i-5) + k(6,1);
K(6*i,6*i-4) = K(6*i,6*i-4) + k(6,2);
K(6*i,6*i-3) = K(6*i,6*i-3) + k(6,3);
K(6*i,6*i-2) = K(6*i,6*i-2) + k(6,4);
K(6*i,6*i-1) = K(6*i,6*i-1) + k(6,5);
K(6*i,6*i) = K(6*i,6*i) + k(6,6);
K(6*i,6*j-5) = K(6*i,6*j-5) + k(6,7);
K(6*i,6*j-4) = K(6*i,6*j-4) + k(6,8);
K(6*i,6*j-3) = K(6*i,6*j-3) + k(6,9);
K(6*i,6*j-2) = K(6*i,6*j-2) + k(6,10);
K(6*i,6*j-1) = K(6*i,6*j-1) + k(6,11);
K(6*i,6*j) = K(6*i,6*j) + k(6,12);
K(6*j-5,6*i-5) = K(6*j-5,6*i-5) + k(7,1);
K(6*j-5,6*i-4) = K(6*j-5,6*i-4) + k(7,2);
K(6*j-5,6*i-3) = K(6*j-5,6*i-3) + k(7,3);
K(6*j-5,6*i-2) = K(6*j-5,6*i-2) + k(7,4);
K(6*j-5,6*i-1) = K(6*j-5,6*i-1) + k(7,5);
K(6*j-5,6*i) = K(6*j-5,6*i) + k(7,6);
K(6*j-5,6*j-5) = K(6*j-5,6*j-5) + k(7,7);
```

```
K(6*j-5,6*j-4) = K(6*j-5,6*j-4) + k(7,8);
K(6*j-5,6*j-3) = K(6*j-5,6*j-3) + k(7,9);
K(6*j-5,6*j-2) = K(6*j-5,6*j-2) + k(7,10);
K(6*j-5,6*j-1) = K(6*j-5,6*j-1) + k(7,11);
K(6*j-5,6*j) = K(6*j-5,6*j) + k(7,12);
K(6*j-4,6*i-5) = K(6*j-4,6*i-5) + k(8,1);
K(6*j-4,6*i-4) = K(6*j-4,6*i-4) + k(8,2);
K(6*j-4,6*i-3) = K(6*j-4,6*i-3) + k(8,3);
K(6*j-4,6*i-2) = K(6*j-4,6*i-2) + k(8,4);
K(6*j-4,6*i-1) = K(6*j-4,6*i-1) + k(8,5);
K(6*j-4,6*i) = K(6*j-4,6*i) + k(8,6);
K(6*j-4,6*j-5) = K(6*j-4,6*j-5) + k(8,7);
K(6*j-4,6*j-4) = K(6*j-4,6*j-4) + k(8,8);
K(6*j-4,6*j-3) = K(6*j-4,6*j-3) + k(8,9);
K(6*j-4,6*j-2) = K(6*j-4,6*j-2) + k(8,10);
K(6*j-4,6*j-1) = K(6*j-4,6*j-1) + k(8,11);
K(6*j-4,6*j) = K(6*j-4,6*j) + k(8,12);
K(6*j-3,6*i-5) = K(6*j-3,6*i-5) + k(9,1);
K(6*j-3,6*i-4) = K(6*j-3,6*i-4) + k(9,2);
K(6*j-3,6*i-3) = K(6*j-3,6*i-3) + k(9,3);
K(6*j-3,6*i-2) = K(6*j-3,6*i-2) + k(9,4);
K(6*j-3,6*i-1) = K(6*j-3,6*i-1) + k(9,5);
K(6*j-3,6*i) = K(6*j-3,6*i) + k(9,6);
K(6*j-3,6*j-5) = K(6*j-3,6*j-5) + k(9,7);
K(6*j-3,6*j-4) = K(6*j-3,6*j-4) + k(9,8);
K(6*j-3,6*j-3) = K(6*j-3,6*j-3) + k(9,9);
K(6*j-3,6*j-2) = K(6*j-3,6*j-2) + k(9,10);
K(6*j-3,6*j-1) = K(6*j-3,6*j-1) + k(9,11);
K(6*j-3,6*j) = K(6*j-3,6*j) + k(9,12);
K(6*j-2,6*i-5) = K(6*j-2,6*i-5) + k(10,1);
K(6*j-2,6*i-4) = K(6*j-2,6*i-4) + k(10,2);
K(6*j-2,6*i-3) = K(6*j-2,6*i-3) + k(10,3);
K(6*j-2,6*i-2) = K(6*j-2,6*i-2) + k(10,4);
K(6*j-2,6*i-1) = K(6*j-2,6*i-1) + k(10,5);
K(6*j-2,6*i) = K(6*j-2,6*i) + k(10,6);
K(6*j-2,6*j-5) = K(6*j-2,6*j-5) + k(10,7);
K(6*j-2,6*j-4) = K(6*j-2,6*j-4) + k(10,8);
K(6*j-2,6*j-3) = K(6*j-2,6*j-3) + k(10,9);
K(6*j-2,6*j-2) = K(6*j-2,6*j-2) + k(10,10);
K(6*j-2,6*j-1) = K(6*j-2,6*j-1) + k(10,11);
K(6*j-2,6*j) = K(6*j-2,6*j) + k(10,12);
K(6*j-1,6*i-5) = K(6*j-1,6*i-5) + k(11,1);
K(6*j-1,6*i-4) = K(6*j-1,6*i-4) + k(11,2);
K(6*j-1,6*i-3) = K(6*j-1,6*i-3) + k(11,3);
K(6*j-1,6*i-2) = K(6*j-1,6*i-2) + k(11,4);
K(6*j-1,6*i-1) = K(6*j-1,6*i-1) + k(11,5);
K(6*j-1,6*i) = K(6*j-1,6*i) + k(11,6);
K(6*j-1,6*j-5) = K(6*j-1,6*j-5) + k(11,7);
K(6*j-1,6*j-4) = K(6*j-1,6*j-4) + k(11,8);
K(6*j-1,6*j-3) = K(6*j-1,6*j-3) + k(11,9);
K(6*j-1,6*j-2) = K(6*j-1,6*j-2) + k(11,10);
K(6*j-1,6*j-1) = K(6*j-1,6*j-1) + k(11,11);
K(6*j-1,6*j) = K(6*j-1,6*j) + k(11,12);
K(6*j,6*i-5) = K(6*j,6*i-5) + k(12,1);
K(6*j,6*i-4) = K(6*j,6*i-4) + k(12,2);
```

```
K(6*j,6*i-3) = K(6*j,6*i-3) + k(12,3);
K(6*j,6*i-2) = K(6*j,6*i-2) + k(12,4);
K(6*j,6*i-1) = K(6*j,6*i-1) + k(12,5);
K(6*j,6*i) = K(6*j,6*i) + k(12,6);
K(6*j,6*j-5) = K(6*j,6*j-5) + k(12,7);
K(6*j,6*j-4) = K(6*j,6*j-4) + k(12,8);
K(6*j,6*j-3) = K(6*j,6*j-3) + k(12,9);
K(6*j,6*j-2) = K(6*j,6*j-2) + k(12,10);
K(6*j,6*j-1) = K(6*j,6*j-1) + k(12,11);
K(6*j,6*j) = K(6*j,6*j) + k(12,12);
y = K;
```

APPENDIX B

ANSYS INPUT FILE

In this appendix, a shortened version of the input file created by the source code is given. Dots are used to shorten the text file and represent the whole array for coordinates of nodes, connectivity information and mass locations in order not to give unnecessary amount of detail. The analyses were completed in ANSYS 11 Classic.

```
/CLEAR,NOSTART
/NOPR
/PMETH,OFF,0
KEYW,PR_SET,1
KEYW,PR_STRUC,1
KEYW,PR_THERM,0
KEYW,PR_FLUID,0
KEYW,PR_MULTI,0
/GO
/PREP7
ET,1,BEAM4
ET,2,MASS21
MPTEMP,,,,,,,,
MPTEMP,1,0
MPDATA,EX,1,,1020.0000000000
MPDATA,EY,1,,1020.0000000000
MPDATA,EZ,1,,1020.0000000000
MPDATA,PRXY,1,,0.3
MPDATA,PRYZ,1,,0.3
MPDATA,PRXZ,1,,0.3
MPDATA,GXY,1,,163.00000000
MPDATA,GYZ,1,,163.00000000
MPDATA,GXZ,1,,163.00000000
R,1,0.0907920277,0.0001210000,0.0001210000,,,,
RMORE, ,0.0002420000 , , , ,
```

```
R,2,1.9943E-26,1.9943E-26,1.9943E-26,0,0,0,
N,1,0.06052394,0.18627354,0.00000000,,,,
N,2,-0.15845374,0.11512338,0.00000000,,,,
N,3,-0.15845374,-0.11512338,0.00000000,,,,
N,4,0.06052394,-0.18627354,0.00000000,,,,
.
.
TYPE,1
MAT,1
REAL,1
TSHAP,LINE
E,1,6
E,2,7
E,3,8
E,4,9
.
.
TYPE,2
MAT,1
REAL,2
TSHAP,LINE
E,    1
E,    2
E,    3
E,    4
.
.
EPLOT
FINISH
/SOL
ANTYPE,2
MODOPT,LANB,20
EQSLV,SPAR
MXPAND,20, , ,1
LUMPM,1
,PSTRES,0
NSEL,S,LOC,Z,0
D,ALL, ,0, , , ,ALL, , , , ,
ALLSEL,ALL
MODOPT,LANB,20,0,0, ,OFF,/STATUS,SOLU
SOLVE
FINISH
/POST1
SET,LIST,2
```